DOE/BC/14447-15
(DE92001061)

FLUID DIVERSION AND SWEEP IMPROVEMENT WITH CHEMICAL GELS IN OIL RECOVERY PROCESSES

Final Report

By
Randall S. Seright
F. David Martin

September 1992

Performed Under Contract No. FG22-89BC14447

New Mexico Institute of Mining and Technology
Petroleum Recovery Research Center
Socorro, New Mexico

Bartlesville Project Office
U. S. DEPARTMENT OF ENERGY
Bartlesville, Oklahoma

DISCLAIMER

ABSTRACT

This report describes progress made during the third and final year of the three-year project, "Fluid Diversion and Sweep Improvement with Chemical Gels in Oil Recovery Processes." Our experimental work focused on four types of gels: (1) resorcinol-formaldehyde, (2) colloidal silica, (3) Cr^{3+}(chloride)-xanthan, and (4) Cr^{3+}(acetate)-polyacrylamide. All experiments were performed at 41°C. During injection of gelants that contained Cr^{3+}, chromium propagation was significantly more rapid when the counterion was acetate rather than chloride. For a given counterion, chromium propagation was much more rapid in Berea sandstone cores than in Indiana limestone cores. It is doubtful that unbuffered chromium-chloride gelants can propagate through carbonate reservoirs.

During core experiments, the "strongest" gels reduced the permeability of all cores to about the same value (in the low microdarcy range). For "weaker" gels (i.e., those leaving a significant permeability), residual resistance factors decreased with increased rock permeability in Berea sandstone. Tracer studies indicated that strong gels occupied most of the pore space, while weaker gels occupied a small fraction of the pore space. Experiments revealed that gelation in the porous rock was often far less complete than that in a bottle. For unbuffered gelants in porous rocks, the pH at which gelation occurs may be determined more by rock mineralogy than by the pH of the injected gelant. Thus, the buffering action of reservoir rocks must be considered when evaluating gel performance in the laboratory.

For gel applications in production wells, a critical property is the ability of a gel to reduce water permeability more than oil permeability. Much of our experimental work was directed at understanding why this property occurs. Whereas previous literature reported this phenomenon for polymers and "weak" polymer-based gels, we also observed the disproportionate permeability reduction with a monomer-based gel, as well as with both "weak" and relatively "strong" polymer-based gels. In contrast, a colloidal-silica gel reduced water and oil permeabilities by about the same factor. Residual resistance factors for several gels were found to erode during multiple cycles of oil and water injection. In spite of this erosion, the disproportionate permeability reduction persisted through the cycles for most of the gels. Studies using both oil and water tracers suggested that the strongest gels encapsulated the original residual oil saturation—thus rendering the residual oil inaccessible during subsequent oil flooding.

In part of our experimental program, we examined how different types of gels reduce permeability to water and compressed gasses (CO_2 and N_2). These experiments were performed at pressures of either 900 psi or 1500 psi. All four types of gels that were tested can reduce water permeability in Berea sandstone to a greater extent than CO_2 permeability. All of these gels experienced some breakdown during water-alternating-gas (WAG) cycles. Gel breakdown was more severe during exposure to a WAG cycle than during prolonged injection of either brine or gas. For the polymer-based gels, an apparent shear-thinning behavior was observed during brine injection. However, during gas or oil injection, the apparent rheology in porous media was more or less Newtonian for all gels examined. The behavior observed during N_2 injection was very similar to that during CO_2 injection. Also, the behavior observed during CO_2 injection at 900 psi was similar to that at 1500 psi.

During this three-year project, a number of theoretical analyses were performed to determine where gel treatments are expected to work best and where they are not expected to be effective. The most important predictions from these analyses are listed in the Executive Summary of this report. Undoubtedly, some of these predictions will be controversial. However, they do provide a starting point in establishing guidelines for the selection of field candidates for gel treatments. A logical next step is to seek field data that either confirm or contradict these predictions.

TABLE OF CONTENTS

LIST OF FIGURES

LIST OF TABLES

ACKNOWLEDGEMENTS

This work was financially supported by the U.S. Department of Energy, the New Mexico Department of Energy and Minerals, Conoco, Elf Aquitaine, Marathon Oil Co., Mobil Research and Development Corp., Oryx Energy Co., Phillips Petroleum Co., Shell Development Co., and Texaco. This support is gratefully acknowledged. We greatly appreciate the efforts of those individuals who contributed to this project. Richard Schrader performed the corefloods associated with Sections 2 and 4, and he was invaluable during many of the other experimental portions of the project. John Hagstrom performed the flow visualization experiments in Sections 4 and 5. Dr. Jenn-Tai Liang and Haiwang Sun were principally responsible for performing and reporting the experimental work in Section 3. We also thank Yingli He for her help during the experiments described in Section 3. The authors thank the staff of the New Mexico Petroleum Recovery Research Center (notably Karen Bohlender and Kathy Lambert) for their help in preparing this report. We especially appreciate the thorough review of the manuscript by Julie Ruff and K. Allbritton.

EXECUTIVE SUMMARY

The objectives of this project were to identify the mechanisms by which gel treatments divert fluids in reservoirs and to establish where and how gel treatments are best applied. Several different types of gelants were examined, including polymer-based gelants, a monomer-based gelant, and a colloidal-silica gelant. This research was directed at gel applications in water injection wells, in production wells, and in high-pressure gas floods. The work examined how the flow properties of gels and gelling agents are influenced by permeability, lithology, and wettability. Other goals included determining the proper placement of gelants, the stability of in-place gels, and the types of gels required for the various oil recovery processes and for different scales of reservoir heterogeneity.

SUMMARY OF THEORETICAL PREDICTIONS

During this three-year project, we performed a number of theoretical analyses to determine where gel treatments are expected to work best and where they are not expected to be effective. The most important predictions from these analyses are listed below. Undoubtedly, some of these predictions will be controversial. However, they do provide a starting point in establishing guidelines for the selection of field candidates for gel treatments. A logical next step is to seek field data that either confirm or contradict these predictions.

1. Conventional gel treatments are most likely to be effective if a fracture is the source of the channeling problem, assuming that the proper gelation chemistry is employed.

2. Conventional gel treatments in unfractured injection wells will only be effective if the injected gelant is prevented from entering the oil-productive zones (e.g., by zone isolation during gelant placement).

3. Injectivity changes (measured at the wellhead) do not indicate anything about the selectivity of gelant placement.

4. Injection-profile changes measured at the wellbore do not indicate changes in sweep efficiency for reservoirs with good pressure communication between strata.

5. The degree of gelant penetration into less-permeable zones (relative to that in a high-permeability zone) will be greater when using viscous gelants than when using low-viscosity gelants.

6. Viscous gelants can enter and damage less-permeable zones to a greater extent if crossflow can occur than if crossflow cannot occur.

7. If extensive crossflow can occur, treatments using viscous gelants in unfractured injection wells will be ineffective, regardless of the amount of gelant injected.

8. Capillary pressure and relative permeability effects will not prevent aqueous gelants from penetrating significant distances into reservoir strata with high oil saturations.

9. To minimize damage to oil-productive zones in production wells when zones are not isolated during gelant placement, the gel must be able to reduce k_{rw} much more than k_{ro}, and the productive zones must have high oil saturations.

10. The desired production rate must be less than 3 to 5 times the critical rate in order for gel treatments to be effective in unfractured producers with coning problems.

11. Gel treatments are most likely to suppress water influx in production wells if fractures provide the conduit for the excess water.

12. Gel properties and gel placement are important in fractured wells.

SUMMARY OF IMPORTANT EXPERIMENTAL FINDINGS

Our experimental work focused on four types of gels: (1) resorcinol-formaldehyde, (2) colloidal silica, (3) Cr^{3+}(chloride)-xanthan, and (4) Cr^{3+}(acetate)-polyacrylamide. All experiments were performed at 41°C. The following is a list of the most important conclusions from the three experimental portions of this project.

Impact of Permeability and Lithology on Gel Performance. In most field applications of gel treatments, the gelant penetrates to some extent into low-permeability, oil-productive zones. A gel treatment can either enhance or harm oil production, depending on how the gel's performance in low-permeability rock compares with that in the "thief" zone. Thus, one portion of our experimental program was directed at determining gel performance as a function of rock permeability and lithology. In these experiments, oil and gas were not present. Some important conclusions from this work include:

1. During injection of gelants that contained Cr^{3+}, chromium propagation was significantly more rapid when the counterion was acetate rather than chloride. For a given counterion, chromium propagation was much more rapid in Berea sandstone cores than in Indiana limestone cores. It is doubtful that unbuffered chromium-chloride gelants can propagate through carbonate reservoirs.

2. The "strongest" gels were found to reduce the permeability of all cores to approximately the same value (in the low microdarcy range). Tracer studies indicated that these gels occupied most of the available pore space.

3. Flow experiments performed in rectangular micromodels indicated that the permeabilities (to water) for five gels were less than about 60 μD.

4. For "weaker" gels (i.e., those leaving a significant permeability), residual resistance factors decreased with increased rock permeability in Berea sandstone. Tracer studies indicated that these gels occupied a small fraction of the pore space in a core. Experiments revealed that gelation in the porous rock was often far less complete than that in a bottle. For unbuffered gelants in porous rocks, the pH at which gelation occurs may be determined more by rock mineralogy than by the pH of the injected gelant. Thus, the buffering action of reservoir rocks should be considered when evaluating gel performance in the laboratory.

5. Residual resistance factors for Cr^{3+}-xanthan and Cr^{3+}(acetate)-polyacrylamide gels exhibited a reversible shear-thinning character. In contrast, residual resistance factors for the resorcinol-formaldehyde gels were generally Newtonian.

Reduction of Oil and Water Permeabilities Using Gels. For gel applications in production wells, a critical property is the ability of a gel to reduce water permeability more than oil permeability. Much of our work in this portion of the experimental program was directed at understanding why this property occurs. We do not yet have a clear understanding of why some polymers and gels can reduce water permeability more than oil permeability. However, we have introduced some new tools and clues in this quest. Some relevant findings and conclusions from our work are as follows:

1. Before gel placement in cores, multiple imbibition and drainage cycles were performed in both flow directions. Results from these studies established that hysteresis of oil and water relative permeabilities were not responsible for the behavior observed during our subsequent gel studies.

2. Several gels clearly reduced water permeability significantly more than oil permeability. Whereas previous literature reported this phenomenon for polymers and "weak" polymer-based gels, we also observed the disproportionate permeability reduction with a monomer-based gel (resorcinol-formaldehyde), as well as with both "weak" Cr^{3+}(chloride)-xanthan and relatively "strong" Cr^{3+}(acetate)-HPAM gels (i.e., using 1.39% HPAM with a molecular weight of 2 million daltons). In contrast, a colloidal-silica gel reduced water and oil permeabilities by about the same factor.

3. Residual resistance factors for several gels were found to erode during multiple cycles of oil and water injection. In spite of this erosion, the disproportionate permeability reduction persisted through the cycles for most of the gels.

4. The impact of wettability on gel performance was found to vary with the gel. For a resorcinol-formaldehyde gel, the disproportionate permeability reduction was more pronounced in Berea sandstone with an intermediate wettability than in strongly water-wet Berea sandstone. In contrast, the performance of a Cr^{3+}(chloride)-xanthan gel was less sensitive to wettability.

5. For the Cr^{3+}(acetate)-polyacrylamide gels that were studied, an apparent shear-thinning behavior was observed during brine injection in Berea cores. For other gels, the rheology was more or less Newtonian during brine injection. For all gels investigated, the apparent rheology during oil injection was more or less Newtonian.

6. Studies using both oil and water tracers provided insights into the fraction of the pore volume occupied by gel. The strongest gels appeared to encapsulate the original residual oil saturation—thus rendering the residual oil inaccessible during subsequent oil flooding. For a relatively "strong" Cr^{3+}(acetate)-polyacrylamide gel, the fraction of the original pore volume that remained open to oil flow after gel placement was about the same as that for water flow (16% to 20%). However, the residual resistance factor for oil was substantially less than that for water. Also, an apparent shear-thinning behavior was observed during water injection, but Newtonian behavior was observed during oil injection.

7. In contrast, oil and water residual resistance factors for a colloidal-silica gel were about the same (i.e., no disproportionate permeability reduction), and Newtonian behavior was observed during both oil and water injection. Tracer studies revealed that, during the first water and oil injection after gel treatment, the fraction of the original pore volume that remained open to flow of water or oil (2% to 4%) was significantly less than those values for the Cr^{3+}(acetate)-polyacrylamide gel. Surprisingly, the oil and water residual resistance factors were also less for the colloidal-silica gel than for the Cr^{3+}(acetate)-polyacrylamide gel.

Reduction of Gas and Water Permeabilities Using Gels. The third portion of our experimental program was directed at determining how different types of gels reduce permeability to water and compressed gasses (CO_2 and N_2) in Berea sandstone. These experiments were performed at pressures of either 900 psi or 1500 psi. As in our other studies, we examined four different types of gels, including (1) a resorcinol-formaldehyde gel, (2) a colloidal-silica gel, (3) a Cr^{3+}-xanthan gel, and (4) a Cr^{3+}(acetate)-polyacrylamide gel. The following conclusions were reached:

1. All four types of gels can reduce water permeability in Berea sandstone to a greater extent than CO_2 permeability.

2. All four types of gels experienced some breakdown during water-alternating-gas (WAG) cycles. Gel breakdown was more severe during exposure to a WAG cycle than during prolonged injection of either brine or gas.

3. An apparent shear-thinning behavior was observed for the polymer-based gels during brine injection.

4. The apparent rheology in porous media was more or less Newtonian for all four gels during gas injection.

5. Using a resorcinol-formaldehyde gel that was buffered and formed at pH value 9.0, an experiment was performed at 900 psi using N_2 instead of CO_2. We noted (1) for both compressed CO_2 and compressed N_2, the gel can reduce brine permeability significantly more than gas permeability, and (2) multiple WAG cycles degrade the residual resistance factors to about the same extent for CO_2 as for N_2. The similarity in results suggests that the observed behavior is not sensitive to the type of gas used.

6. Most of our experiments were performed at 900 psi. However, two experiments were performed with CO_2 at 1500 psi—one using a resorcinol-formaldehyde gel (at pH=9) and the other using a Cr^{3+}(acetate)-HPAM gel. From these studies, we conclude that the overall behavior at 1500 psi (where CO_2 density is 0.641 g/cm^3) is not radically different from that at 900 psi (where CO_2 density is 0.156 g/cm^3).

7. No significant macroscopic changes were observed for a resorcinol-formaldehyde gel or a Cr^{3+}(acetate)-HPAM gel when exposed to brine, CO_2, or oil (Soltrol 130®) during high-pressure visualization experiments at 1500 psi.

FUTURE RESEARCH PLANS

A logical next step is to seek field data that either confirm or contradict our theoretical predictions concerning gel treatments. This step will constitute one part of our future plan. We will also continue to examine why some polymers and gels reduce permeability to water more than to oil. We also hope to compare the effectiveness of gels with other fluid-diversion agents (e.g., foams, emulsions, particulates). We may also try to combine portions of different types of fluid-diversion processes to create a superior process.

1. INTRODUCTION

In any oil recovery process, large-scale heterogeneities, such as fractures, channels, or high-permeability streaks, can cause breakthrough of injected fluid that will reduce oil recovery efficiency. In enhanced recovery projects, this problem is particularly acute because of the cost of the injected fluids.

Crosslinked-polymer treatments (gel treatments) were developed to reduce channeling of fluids through fractures and streaks of very high permeability. Although many projects have been very successful, many other gel projects have been technical failures. Even though 20% of all EOR projects during the past decade were gel treatments, they have been responsible for less than 2% of the total EOR production in the United States.[1] In part, the success of gel projects has been sporadic because the science and technology base did not adequately complement the extensive field applications.

This report describes work performed during the third and final year of the project, "Fluid Diversion and Sweep Improvement with Chemical Gels in Oil Recovery Processes." Details concerning work for the first and second years of the project can be found in the first and second annual project reports.[2,3]

Project Objectives

The objectives of this project were to identify the mechanisms by which gel treatments divert fluids in reservoirs and to establish where and how gel treatments are best applied. Several different types of gelants were examined, including polymer-based gelants, a monomer-based gelant, and a colloidal-silica gelant. This research was directed at gel applications in water injection wells, in production wells, and in high-pressure gasfloods. The work examined how the flow properties of gels and gelling agents are influenced by permeability, lithology, and wettability. Other goals included determining the proper placement of gelants, the stability of in-place gels, and the types of gels required for the various oil recovery processes, and for different scales of reservoir heterogeneity.

Project Task Areas

Eight task areas were included in this project. They were as follows:

Task 1: Equipment Design and Construction
Task 2: Screening Tests
Task 3: Gels for Producing Well Applications
Task 4: Chemical Gels in Waterflooding
Task 5: Flow Properties of Gels and Gelling Agents
Task 6: Chemical Gels in High-Pressure Gasflooding
Task 7: Mathematical Modeling
Task 8: Coordination with Other Research Programs

The equipment design and construction (Task 1) and the screening tests (Task 2) were completed in the first year of the project. This work was described in our first annual report.[2]

Task 3 (gels for applications in producing wells) is addressed in Section 3. This section describes an experimental investigation of the reduction of oil and water permeabilities using four different types of gels, including (1) a resorcinol-formaldehyde gel, (2) a Cr^{3+}-xanthan gel, (3) a Cr^{3+}(acetate)-polyacrylamide gel, and (4) a colloidal-silica gel.

Task 4 (gels for waterflood applications) and Task 5 (flow properties of gels and gelling agents) are discussed in Section 2. Section 2 describes the effects of rock permeability and lithology on the performance of the same four types of gels that were studied in Section 3. Three types of rock were used during our core experiments, including (1) a high-permeability Berea sandstone, (2) a low-permeability Berea sandstone, and (3) an Indiana limestone. The dependence of residual resistance factor (F_{rrw}) on brine injection rate was characterized for the gels.

Task 6 (gels in high-pressure gasflooding) is addressed in Section 4. This investigation examines how different types of gels reduce permeability to water, compressed carbon dioxide, and compressed nitrogen in Berea sandstone.

Task 7 (mathematical modeling) is covered in Section 5. Objectives are discussed for gel placement in fractured reservoirs. We also present some results from flow visualization studies that illustrate the importance of fluid properties during gelant placement in fractured systems.

Task 8 (coordination with other research programs) was addressed primarily at professional meetings and through written correspondence.

2. IMPACT OF PERMEABILITY AND LITHOLOGY ON GEL PERFORMANCE

Ideally, gel treatments should reduce channeling of fluids through high-permeability, watered-out flow paths without damaging oil-productive zones. However, in most applications, the gelant penetrates to some extent into low-permeability, oil-productive zones. A gel treatment can either enhance or harm oil production, depending on how the gel's performance in low-permeability rock compares with that in the "thief" zone.[4,5]

Some researchers have attempted to evaluate the effectiveness of fluid diversion processes using porous media with only one permeability.[6-9] Unfortunately, this type of evaluation indicates nothing about the performance of the diversion process in strata with different permeabilities. For example, assume that a diverting agent reduces the flow capacity of a "thief" zone by a factor of ten. If the diverting agent reduces the flow capacity of a nearby oil-productive zone by a factor of two, then the fluid diversion process could improve sweep efficiency. However, if the diverting agent reduces the flow capacity of the oil-productive zone by a factor of twenty, then the diversion process could reduce sweep efficiency substantially. Thus, the effectiveness of a diversion process cannot be assessed by using rock with a single permeability.

Other researchers have used parallel linear corefloods with cores of different permeabilities to evaluate the effectiveness of fluid diversion processes.[10-18] Unfortunately, these studies can be extremely misleading for several reasons.[2-4,19-22] First, the results are not relevant to unfractured wells where the flow geometry is radial. Simple calculations using the Darcy equation reveal that the performance of a diverting agent can be substantially different in a radial geometry than in a linear geometry.[2,4] Second, the short bank of the diverting agent in the less-permeable core can be diluted enough by diffusion and dispersion to deactivate the diverting agent. This situation is much more likely to occur on a laboratory scale than on a field scale.[2,19] Third, depending on the wettability of the system, capillary effects may prevent an aqueous diversion fluid from entering the less-permeable core. This circumstance is also much more likely to occur on a laboratory scale than on a field scale.[3,22] Fourth, the flow lines leading to the core inlets must be completely filled with the diverting agent at the start of the displacement process. Otherwise (if the lines are filled with water instead of diverting agent), the diverting agent could penetrate well into the most-permeable core before it reaches the inlet face of the less-permeable core.[2] Fifth, if both cores become filled with a shear-thinning fluid, then the ratio of flow rates for the two cores can erroneously lead one to believe that the fluid is unusually selective in entering the most-permeable core.[20] In summary, results from parallel linear corefloods are often misleading, and they provide a poor method to evaluate the effectiveness of a diversion process.

To properly evaluate the effectiveness of a fluid diversion process in the laboratory, experiments should be performed to determine the permeability reduction (residual resistance factor) provided by the gel in cores with different permeabilities. For the reasons mentioned above, these corefloods should be performed separately rather than in parallel. Rocks should be used that are representative of those to be contacted by gel in the intended field application.

This section describes an experimental investigation of the effects of rock permeability and lithology on the performance of several gels. During our experiments, particular attention was paid to (1) the importance of pH to gelation, (2) gel performance as a function of fluid velocity, and (3) the use of tracers to assess the fraction of the pore space that was occupied by gel. Our work on the effects of oil and wettability on gel performance are described in Section 3 and Ref. 22.

Gelants and Gelant Placement Procedures

Gelants Studied. In this work, experiments were performed with four different gelants, including resorcinol-formaldehyde, colloidal silica[23] (DuPont's Ludox SM®), Cr^{3+}(chloride)-xanthan, and Cr^{3+}(acetate)-polyacrylamide[24-26] (Marathon's MARCIT®). Eight different formulations were investigated. The compositions of these formulations are listed in Table 1. The two resorcinol-formaldehyde gelants had the same composition, except that one was buffered at pH=9, while the other was buffered at pH=6.0-6.5. The two different pH values were chosen because we knew that gel performance was radically different at these pH values. For the other gelants, the pH was selected based on recommendations of the vendor or developer of the gelant (to provide the "strongest" gel for that composition). DuPont supplied the colloidal silica, and Pfizer provided the xanthan[11] (Flocon 4800®). Marathon provided the polyacrylamide, characterized by a molecular weight of about 2 million daltons and a degree of hydrolysis of 2 percent. All other chemicals were reagent grade.

Table 1. Gelant Compositions and Properties (at 41°C)

Gelant Composition	pH	Viscosity, cp @ 11 s^{-1}	Gelation time, hrs.	Gel-strength code[24]
3% resorcinol, 3% formaldehyde, 0.5% KCl, 0.42% $NaHCO_3$	6.0-6.5	0.67	6	*
3% resorcinol, 3% formaldehyde, 0.5% KCl, 0.42% $NaHCO_3$	9.0	0.67	4	I
4% colloidal silica, 0.7% NaCl	7.0	1.0	15	I
10% colloidal silica, 0.7% NaCl	8.2	2.0	5	J
0.4% xanthan, 154-ppm Cr^{3+} (as $CrCl_3$), 0.5% KCl	4.3	253	10	I
0.4% xanthan, 154-ppm Cr^{3+} (as $CrCl_3$), 0.5% KCl, 0.3% CH_3COOH	4.5-4.8	250	10	F-G
1.39% polyacrylamide, 212-ppm Cr^{3+} [as $Cr_3(OH)_2(CH_3COO)_7$], 1% NaCl	5.9	33	15	H
1.39% polyacrylamide, 636-ppm Cr^{3+} [as $Cr_3(OH)_2(CH_3COO)_7$], 1% NaCl	5.9	33	7	I

* Product could be described better as a precipitate than as a gel.

For the eight gelants, Table 1 lists the viscosities (at 11 s^{-1}, 41°C) immediately after preparation. The resorcinol-formaldehyde gelants (with viscosities near that of water) were the least viscous of the formulations. Newtonian behavior was observed for the resorcinol-formaldehyde, colloidal-silica, and Cr^{3+}(acetate)-polyacrylamide gelants. The Cr^{3+}-xanthan gelants were the most viscous. Their viscosity was about 250 cp at 11 s^{-1}. The viscosity (μ) exhibited a strong shear-thinning character that was described by Eq. 1 for shear rates (γ) between 0.1 s^{-1} and 11 s^{-1}.

$$\mu = 1520\ \gamma^{-0.75} \quad (1)$$

Approximate gelation times and gel-strength codes are also listed in Table 1. Gelation times were estimated by observing the fluidity of gelant in bottles. Gelation times for the eight gels ranged from four hours to fifteen hours. The system for assessing gel strength was taken from Ref. 24 and is listed in Table 2. In this system, the codes range alphabetically from A to J, with code A representing a fluid liquid, code J representing a rigid, ringing gel, and code F representing a highly deformable nonflowing gel.

Table 2. Gel-Strength Codes[24]

Code

A No detectable gel formed: The gel appears to have the same viscosity as the original polymer solution and no gel is visually detectable.

B Highly flowing gel: The gel appears to be only slightly more viscous than the initial polymer solution.

C Flowing gel: Most of the obviously detectable gel flows to the vial top upon inversion.

D Moderately flowing gel: Only a small portion (about 5 to 15%) of the gel does not readily flow to the vial top upon inversion—usually characterized as a tonguing gel (i.e., after hanging out of the jar, the gel can be made to flow back into the bottle by slowly turning the bottle upright).

E Barely flowing gel: The gel can barely flow to the vial top and/or a significant portion (>15%) of the gel does not flow upon inversion.

F Highly deformable nonflowing gel: The gel does not flow to the vial top upon inversion.

G Moderately deformable nonflowing gel: The gel flows about half way down the vial upon inversion.

H Slightly deformable nonflowing gel: The gel surface only slightly deforms upon inversion.

I Rigid gel: There is no gel-surface deformation upon inversion.

J Ringing rigid gel: A tuning-fork-like mechanical vibration can be felt after tapping the bottle.

Rocks Used. Three types of rock were used during our core experiments, including (1) a high-permeability Berea sandstone, (2) a low-permeability Berea sandstone, and (3) an Indiana limestone. Porosities for the three types of rock averaged 0.22, 0.19, and 0.19, respectively. Table 3 lists permeabilities of the cores. Each core was about 14-cm long with a cross-sectional area of 10 cm^2. The cores were cast in a metal alloy (Cerrotru®). Each core had one internal pressure tap that was located approximately 2 cm from the inlet rock face. The first core segment was treated as a filter, whereas the second core segment (12-cm length) was used to measure mobilities and residual resistance factors. The cores were not fired.

Table 3. Rock Permeabilities

Gelant to be injected	Permeability, md		
	High-permeability Berea sandstone	Low-permeability Berea sandstone	Indiana limestone
Resorcinol-formaldehyde, pH=6.0-6.5	704	61	7.4
Resorcinol-formaldehyde, pH=9	570	49	7.4
4% colloidal silica	546	67	13.4
10% colloidal silica	630	50	12.0
Unbuffered Cr^{3+}-xanthan	728	68	15.3
Cr^{3+}-xanthan buffered with acetate	840	93	--
Cr^{3+}(acetate)-polyacrylamide (212-ppm Cr^{3+})	746	74	10.7
Cr^{3+}(acetate)-polyacrylamide (636-ppm Cr^{3+})	662	65	11.0

Coreflood Sequence. The sequence followed during our core experiments is listed in Table 4. The cores were saturated with brine and porosities were determined at ambient conditions (Step 1 of Table 4). All subsequent steps were performed at 41 °C. When saturating a given core, the brine composition was the same as that used in preparing the gelant formulation.

Tracer studies were routinely performed to characterize pore volumes and dispersivities of the cores. These studies involved injecting a brine bank that contained potassium iodide as a tracer. The tracer concentration in the effluent was monitored spectrophotometrically at a wavelength of 230 nm. Usually, four replicates were performed for each tracer study. Also, the replicates included studies performed at different injection rates. For all of the tracer studies described in this work, an error-function solution[27] fit the tracer curves fairly well.

Table 4. Sequence Followed During Core Experiments

Step

1. Saturate core with brine and determine porosity.
2. Perform tracer study to confirm the pore volume (V_{po}) and to determine the core dispersivity (α_o).
3. Determine absolute brine permeability and mobility.
4. Inject gelant using a superficial velocity of 15.7 ft/d.
5. Shut in core for several days to allow gelation to occur.
6. Inject brine to determine residual resistance factor (F_{rrw}) as a function of superficial velocity (u).
7. Perform tracer study to determine the fractional pore volume remaining (V_p/V_{po}) and the relative dispersivity (α/α_o).

For a given core, many pore volumes of gelant (typically, 10 PV) were injected to ensure that the cores were saturated (i.e., most of the chemical retention sites in the rock were occupied). Thus, in field applications, the gel properties reported in this study are more relevant to the region behind (upstream of) the front of the gel bank than to the region at the front of the gel bank. While injecting the gelants, resistance factors were continuously monitored in both segments of the core. Effluent properties were also monitored, including pH, viscosity, composition, appearance, gelation time, and final gel strength. Detailed gel-placement data are listed in Tables 5 through 13 for the experiments that were performed during the past year. Detailed gel-placement data for experiments performed in previous years of the project can be found in Refs. 2 and 3.

Table 5. Placement of 4% Colloidal-Silica Gelant in 546-md Sandstone

Pore volumes injected	0	1	2	3	4	5	6	7	8	9	10
F_r in first core segment	1.6	3.1	4.0	4.9	5.8	7.0	7.5	8.5	10.7	12.3	13.3
F_r in second core segment	1.0	1.4	1.5	1.5	1.6	1.7	1.8	1.8	2.0	2.1	2.2
Effluent pH	9.53	8.74	7.25	7.16	7.12	7.16	7.15	7.15	7.14	7.14	7.15
Gel Code	A	A	E	I	I	I	I	I	I	I	I

Table 6. Placement of 4% Colloidal-Silica Gelant in 67-md Sandstone

Pore volumes injected	0	1	2	3	4	5	6	7	8	9	10
F_r in first core segment	1.0	1.2	1.5	1.7	1.9	2.1	2.3	2.5	2.8	3.0	3.2
F_r in second core segment	1.0	1.6	2.2	2.7	3.3	4.1	4.8	5.7	6.8	8.1	9.6
Effluent pH	9.42	8.64	7.77	7.71	7.68	7.65	7.64	7.64	7.63	7.63	7.62
Gel Code	A	A	C	I	I	I	I	I	I	I	I

Table 7. Placement of Buffered Cr^{3+}-Xanthan Gelant in 840-md Sandstone

Pore volumes injected	0	1	2	3	4	5	6	7	8	9	10
F_r in first core segment	1.0	12.2	14.2	20.2	30.0	45.0	70.5	94.8	130	150	149
F_r in second core segment	1.0	13.9	23.4	24.2	25.6	27.3	28.6	29.8	30.8	31.9	32.5
Effluent $[Cr^{3+}]/[Cr^{3+}]_o$	0.00	0.01	0.17	0.57	0.75	0.76	0.93	0.90	0.92	0.94	0.96
Effluent pH	5.39	5.48	4.83	4.73	4.66	4.61	4.58	4.55	4.54	4.53	4.52
Gel Code	A	A	A	A	B	C	C	G	G	G	G

Table 8. Placement of Buffered Cr^{3+}-Xanthan Gelant in 93-md Sandstone

Pore volumes injected	0	1	2	3	4	5	6	7	8	9	10
F_r in first core segment	1.0	18.2	18.9	21.2	24.0	28.0	32.9	38.6	44.8	52.1	59.3
F_r in second core segment	1.0	4.5	12.9	14.8	16.1	17.8	19.8	22.2	24.8	27.9	31.0
Effluent pH	5.12	5.79	5.37	5.26	5.20	5.14	5.10	5.07	5.04	5.02	5.01

Table 9. Placement of 212-ppm Cr^{3+} (as Acetate) in 925-md Sandstone

Pore volumes injected	0	1	2	3	4	5	6	7	8	9	10
F_r in first core segment	1.0	1.1	1.0	1.1	1.2	1.2	1.3	1.3	1.3	1.3	1.2
F_r in second core segment	1.0	1.1	1.2	1.2	1.2	1.2	1.2	1.2	1.2	1.2	1.2
Effluent $[Cr^{3+}]/[Cr^{3+}]_o$	0.00	0.02	0.41	0.88	0.91	0.93	0.93	0.93	0.91	0.94	0.93
Effluent pH	5.21	5.18	5.18	5.19	5.19	5.19	5.23	5.26	5.27	5.33	5.34

Table 10. Placement of Cr^{3+}(Acetate)-Polyacrylamide in 746-md Sandstone (212-ppm Cr^{3+} as acetate)

Pore volumes injected	0	1	2	3	4	5	6	7	8	9	10
F_r in first core segment	1.0	30.7	32.8	33.8	34.5	35.2	35.5	36.5	37.1	37.7	38.5
F_r in second core segment	1.0	31.6	39.5	41.3	42.4	43.2	43.8	44.6	45.5	46.0	46.8
Effluent $[Cr^{3+}]/[Cr^{3+}]_o$	0.00	0.12	0.68	0.95	0.95	0.95	0.95	0.98	0.98	1.00	0.93
Effluent pH	6.91	7.22	6.83	6.46	6.27	6.21	6.16	6.13	6.12	6.10	6.08
Gel Code	A	A	D	H	H	H	H	H	H	H	H

Table 11. Placement of Cr^{3+}(Acetate)-Polyacrylamide in 74-md Sandstone (212-ppm Cr^{3+} as acetate)

Pore volumes injected	0	1	2	3	4	5	6	7	8	9	10
F_r in first core segment	1.0	34.5	34.5	36.0	37.0	38.0	42.4	44.4	46.9	48.8	49.8
F_r in second core segment	1.0	43.0	49.0	51.8	53.3	54.7	60.6	62.3	64.5	66.2	68.1
Effluent $[Cr^{3+}]/[Cr^{3+}]_o$	0.00	0.05	0.59	0.84	0.88	0.88	0.89	0.93	0.93	0.95	0.92
Effluent pH	8.28	8.19	7.54	7.15	6.88	6.71	6.56	6.50	6.44	6.40	6.37
Gel Code	A	A	D	H	H	H	H	H	H	H	H

Table 12. Placement of Cr^{3+}(Acetate)-Polyacrylamide in 662-md Sandstone (636-ppm Cr^{3+} as acetate)

Pore volumes injected	0	1	2	3	4	5	6	7	8	9	10
F_r in first core segment	1.0	22.8	19.2	20.1	21.2	22.3	23.6	25.6	27.8	30.3	35.0
F_r in second core segment	1.0	15.9	33.6	36.6	38.9	41.9	43.9	47.6	52.7	57.6	66.3
Effluent pH	8.45	8.65	6.90	6.23	6.07	6.03	5.98	5.94	5.91	5.90	5.87

Table 13. Placement of Cr^{3+}(Acetate)-Polyacrylamide in 65-md Sandstone
(636-ppm Cr^{3+} as acetate)

Pore volumes injected	0	1	2	3	4	5	6	7	8
F_r in first core segment	1.0	38.8	39.6	40.0	44.4	46.0	48.8	49.6	81.2
F_r in second core segment	1.0	25.1	39.3	43.6	52.0	59.1	76.2	99.4	192
Effluent $[Cr^{3+}]/[Cr^{3+}]_o$	0.00	0.11	0.57	0.89	0.93	0.93	0.89	0.96	1.01
Effluent pH	8.59	8.74	7.52	6.99	6.66	6.52	6.44	6.40	6.40
Gel Code	A	A	H	I	I	I	I	I	I

Chromium Propagation Without Polymer. Several experiments were performed to assess how well chromium propagates through porous rock. Fig. 1 shows results from six corefloods where solutions containing 154-ppm Cr^{3+} (as either chromium acetate or chromium chloride) were injected (at 15.7 ft/d) to displace brine. (These solutions did not contain polymer.) The effluent from the corefloods was analyzed for chromium using atomic absorption spectrometry. Fig. 1 plots the chromium concentration in the effluent relative to the injected chromium concentration. After injecting 10 PV of chromium solution, in no case did the effluent chromium concentration reach the injected concentration. For a given type of rock, chromium propagation was significantly more rapid when the counterion was acetate rather than chloride. Also, for a given counterion (i.e., acetate or chloride), chromium propagation was more rapid in the Berea sandstone cores than in the Indiana limestone cores. In fact, no chromium was detected in the effluent after injecting 10 PV of chromium chloride solution through a limestone core (bottom of Fig. 1). Of course, the latter observation raises concern about the ability of chromium chloride to propagate through carbonate reservoirs.

The propagation of Cr^{3+} through porous rock can be related to the pH dependence of chromium chemistry. Although controversy exists about the exact forms of chromium that participate in gelation,[29-34] there is agreement that Cr^{3+} is most soluble at acidic pH values and that chromium association is promoted as pH is increased—ultimately leading to the formation of a colloid or a precipitate at neutral or alkaline pH values. If an unbuffered chromium solution (e.g., one containing $CrCl_3$) is injected at low pH, rock minerals can raise the pH and induce formation of colloidal chromium (i.e., insoluble chromium hydroxide). Deposition in or filtration by the porous medium may then inhibit propagation of the colloidal chromium. In contrast, a buffered chromium solution (e.g., one containing acetate) will resist pH changes, and the soluble chromium will propagate through porous rock more effectively than a colloid. Formation of chromium-carboxylate complexes may also promote chromium solubility at pH values of 6 or higher.[31,32]

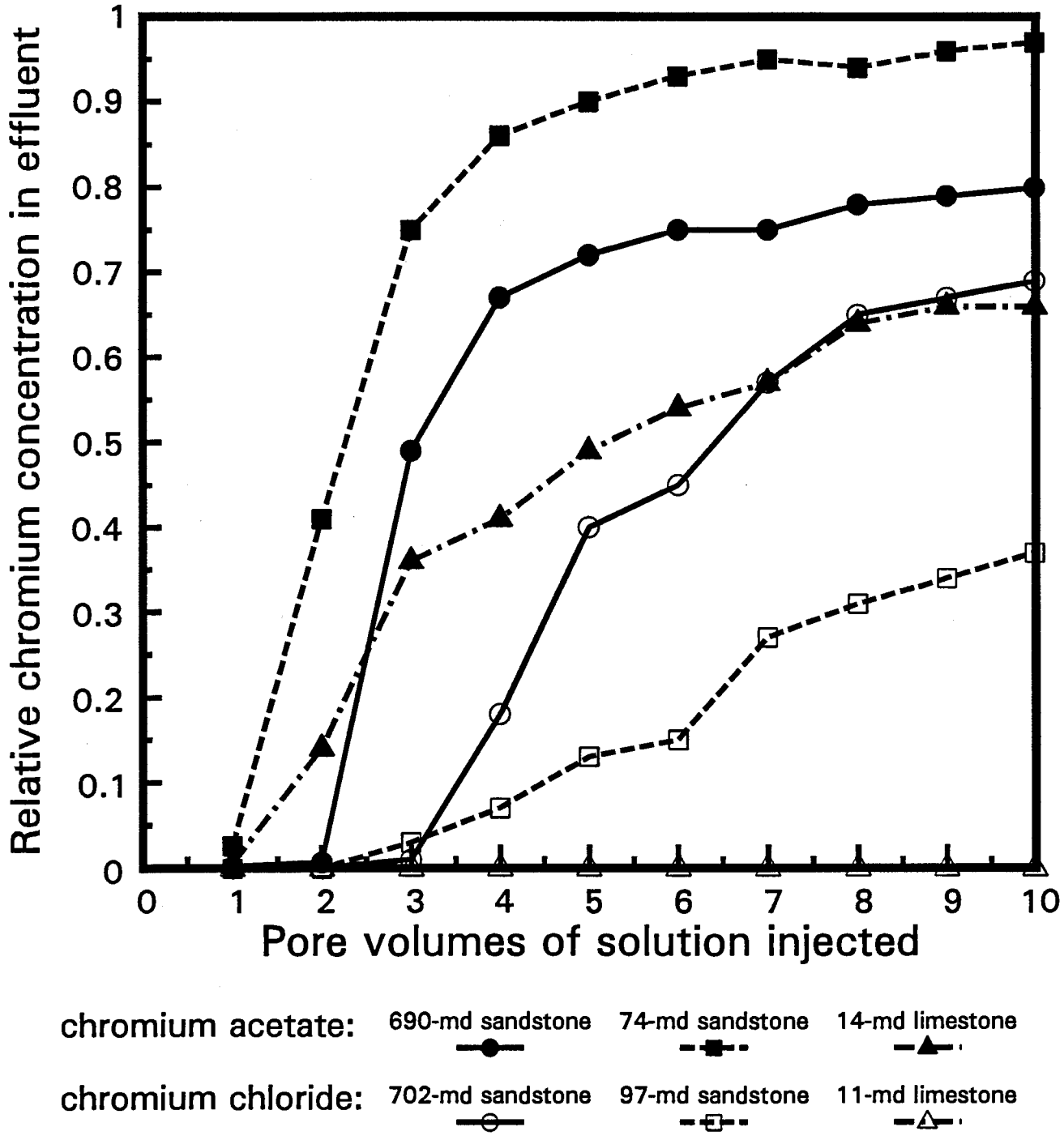

Fig. 1. Chromium propagation through cores. Injected solutions contain 154-ppm chromium.

The above ideas are supported by the effluent pH values that accompanied our chromium propagation data.[3] For the unbuffered chromium-chloride solutions, the effluent pH can be correlated with chromium propagation. The pH was 3.35 for the unbuffered chromium-chloride solution before injection. After injecting 10 PV, the pH values were 4.89, 5.05, and 7.03 for effluent from the high-permeability sandstone, the low-permeability sandstone, and the limestone, respectively. For the chromium-chloride solutions, Fig. 1 shows that the effluent chromium concentrations after 10 PV were greatest for the high-permeability sandstone and least for the limestone.

Results from our experiments using chromium acetate are consistent with reports that chromium solubility at neutral pH values is increased by the presence of carboxylate compounds.[31,32] For the chromium-acetate solution, the pH was 5.90 before injection. After injecting 10 PV, the pH values were 6.01, 5.65, and 5.92 for effluent from the high-permeability sandstone, the low-permeability sandstone, and the limestone, respectively. Thus, the acetate effectively buffered the solutions in the porous rock. Also, in spite of a pH value near 6, chromium propagation in all three types of rock was as good or better with the acetate than that for chromium-chloride solutions with lower pH values.

Chromium Propagation With Polymer. Propagation of chromium in the presence of 0.4% xanthan is illustrated in Fig. 2. In all four cases shown, the 154-ppm chromium was added as $CrCl_3$. In one case, 0.3% acetic acid was added as a buffer. As expected, chromium propagated most rapidly for the gelant that contained the acetate buffer. For the three gelants that did not contain acetate, chromium propagation was most rapid in the high-permeability sandstone and least rapid in the limestone. This ordering was the same as that observed for chromium-chloride propagation without xanthan. Again, the rate of chromium propagation for the unbuffered solutions can be correlated with effluent pH values. After injecting 10 PV of gelant, the effluent pH values were 4.38, 4.55, and 6.57 for effluent from the high-permeability sandstone, the low-permeability sandstone, and the limestone, respectively. The pH value was 4.3 before injection.

A close comparison of Figs. 1 and 2 suggests that the rate of chromium propagation for unbuffered chromium-chloride solutions is greater in the presence of 0.4% xanthan than in its absence. This observation was made for all three rock types. We note that Garver *et al.*[35] suggested the opposite possibility. However, the apparent difference in interpretation can readily be explained. In the experiments of Garver *et al.*, injection rates were relatively low, so gelation could occur during gelant injection. As Garver *et al.* noted, filtration of gel by the core probably caused very high chromium retention in the presence of polymer. In our experiments, injection rates were relatively high, so gelation and filtration of gel particles occurred to a lesser extent during gelant injection.

Fig. 3 illustrates effluent pH values during the course of injecting four solutions. For the three solutions without acetate, the first effluent from the cores had pH values between 8.3 and 9.4. This observation requires explanation. Before gelant injection, the cores were saturated with 0.5% KCl brine. Even though the KCl brine was injected at a pH value between 6 and 7, it emerged from the core at a pH value between 8.3 and 9.4. Previous workers[36] showed that this behavior occurs because dissolution of carbonates in the rock leads to a pH increase. If the brine had contained divalent cations, the increased pH may not have occurred because dissolution of carbonates could have been suppressed.

As discussed earlier, the effluent pH decreased to values between pH 4.38 and 5.05 during the course of injecting 10 PV of unbuffered chromium-chloride formulation into Berea sandstone. During injection of an unbuffered gelant into limestone, the pH only decreased to 6.57 after 10 PV.

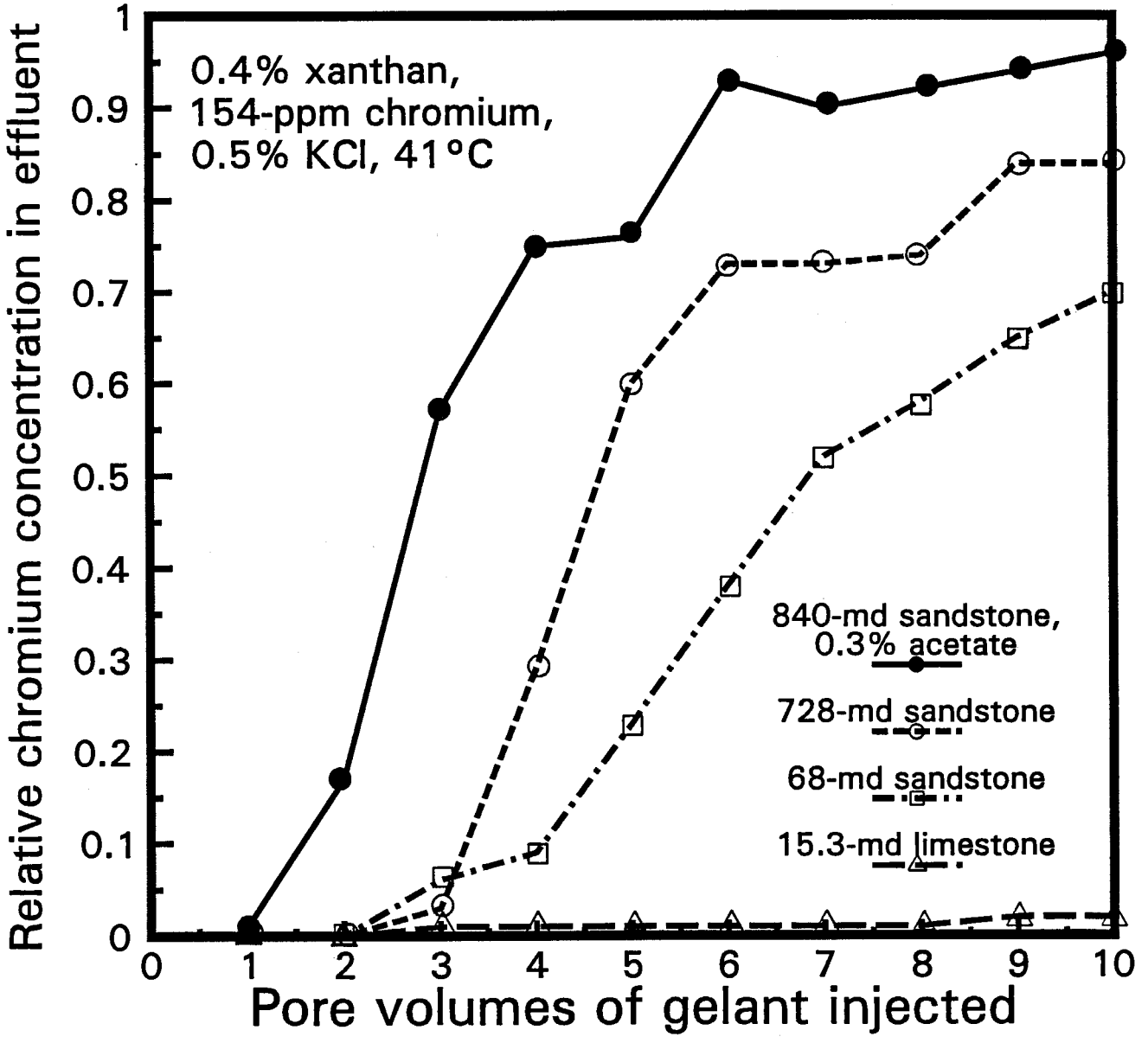

Fig. 2. Chromium propagation for solutions that contain 0.4% xanthan and 154-ppm chromium (as chromium chloride).

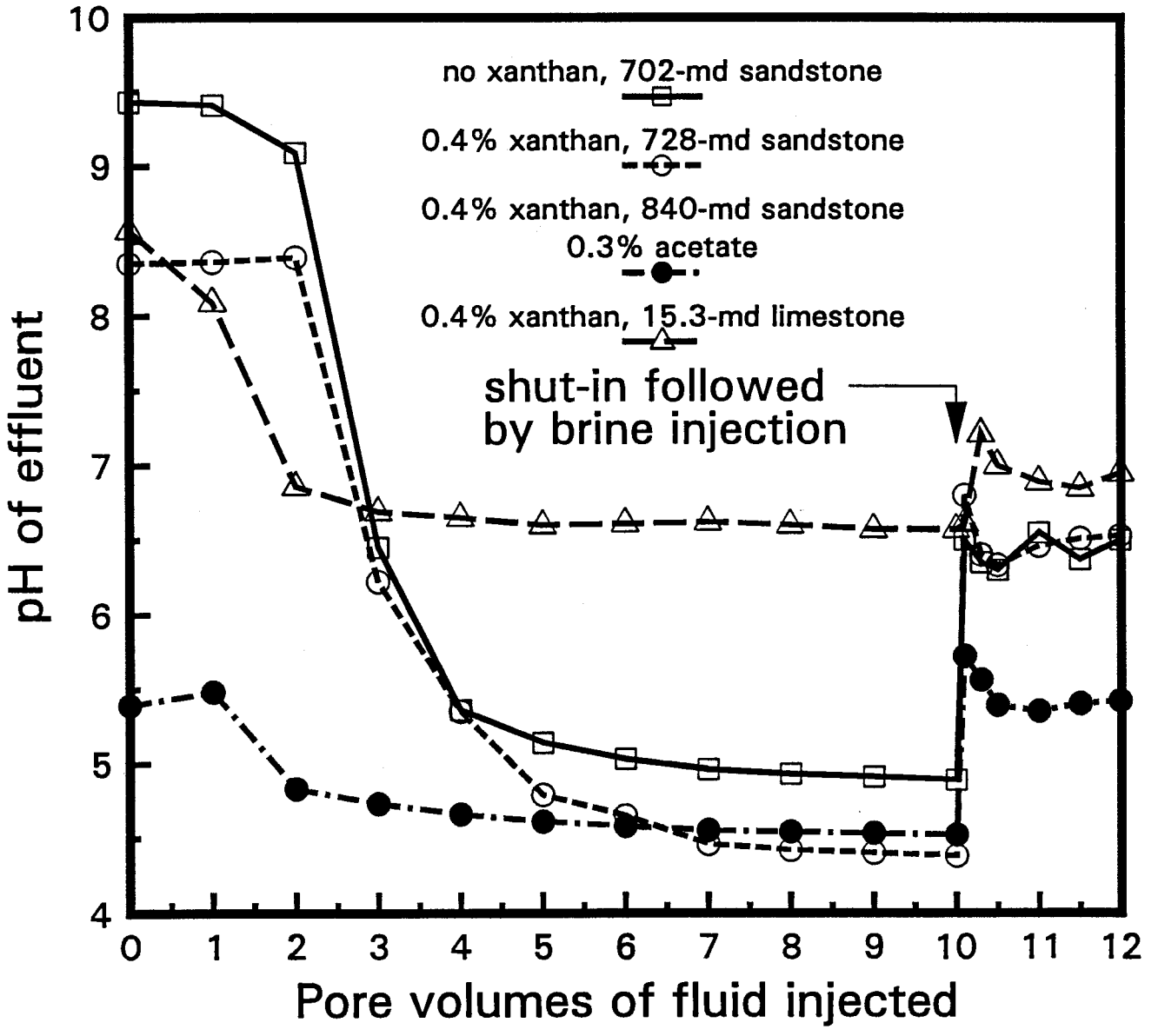

Fig. 3. Effluent pH during gelant injection. 154-ppm chromium, 0.5% KCl.

For the formulation with 0.3% acetate, the core was first saturated with brine buffered at pH=4.8. At the start of gelant injection, the pH of the effluent was 5.39. Presumably, the effluent pH was greater than 4.8 because reaction with rock minerals neutralized some of the acid. Even so, the buffering action of the acetate prevented the pH from rising to the values observed for the unbuffered brines. Also, the pH remained low during injection of 10 PV of gelant.

After injecting 10 PV of gelant, the core was shut in for several days. After this shut-in period, brine was reinjected. Fig. 3 shows that the pH of the first effluent after the shut-in period was significantly higher than that just before shut-in. Evidently, reactions with rock minerals increased the gelant pH during the shut-in period. As expected, the pH increase in Berea sandstone during the shut-in period was less for the buffered gelant than for the unbuffered gelant.

The preceding observations raise concerns about the practice of injecting unbuffered gelants. During laboratory corefloods and, especially, in field applications, a pH gradient will form in the rock when injecting an unbuffered gelant. This pH gradient will depend upon the gelant composition, the injection rate, and the rock mineralogy. For gelation reactions that are sensitive to pH, the pH gradient and the performance of the gel treatment may be difficult to predict. In contrast, for buffered gelants, gelation should be more predictable and controllable.

Fig. 4 illustrates chromium propagation during injection of a Cr^{3+}(acetate)-polyacrylamide gelant in high- and low-permeability Berea sandstone. It also illustrates chromium propagation for a chromium solution (without polymer) through high-permeability Berea sandstone. Previously, we noted that chromium propagation is relatively rapid in the presence of acetate. The data in Fig. 4 are consistent with our previous findings.

Limited Gelant Injection in Limestone Cores. During three sets of experiments in Indiana limestone, small volumes of gelant were injected because excessive pressure gradients developed and mandated that injection be stopped. Because these three cores may not have been completely saturated with gelant, the results observed while using these cores should be viewed with caution. Two of these core experiments involved gelants containing 1.39% polyacrylamide in 11-md Indiana limestone. The Cr^{3+} concentrations in the gelants were 212 ppm and 636 ppm. During placement in the cores, only 0.9 and 1.2 PV of gelant were injected, respectively. We suspect that the high molecular weight of the polyacrylamide was responsible for the premature core plugging. If this type of gelant is intended to penetrate a significant distance into a low-permeability rock matrix, it may be appropriate to use a polymer with a lower molecular weight (i.e., less than 2 million daltons).

During injection of the 4% colloidal-silica gelant into 13.4-md limestone, only 1.2 pore volumes of gelant could be injected before excessive pressure gradients forced injection to be curtailed. This was unexpected because no problems were experienced while injecting 10 pore volumes of a 10% colloidal-silica gelant into 12-md limestone (Table 8 of Ref. 3). Perhaps the differences in injectivity are related to the different pH values for the gelants. The pH required to induce gelation in the desired time frame was lower for the 4% colloidal-silica gelant (pH=7.0) than for the 10% colloidal-silica gelant (pH=8.2).

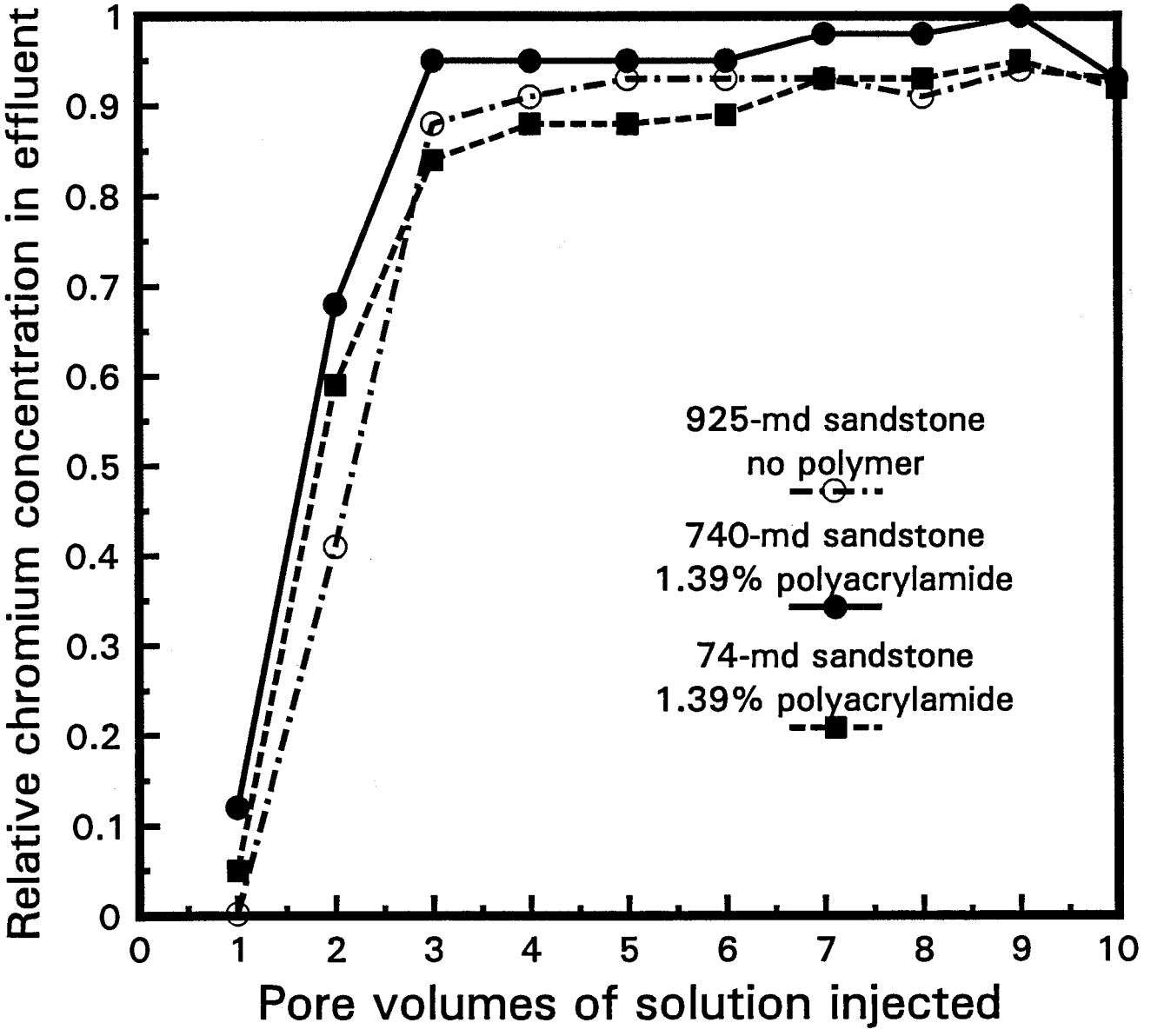

Fig. 4. Chromium propagation through Berea sandstone for solutions that contain 212-ppm chromium (as chromium acetate).

Residual Resistance Factors

After injecting a given gelant, the core was shut in for three to six days. In all cases, the gelation times were substantially less (by factors ranging from 12 to 40) than the shut-in times. Following the shut-in period, brine was injected to determine residual resistance factors (F_{rrw}). These F_{rrw} values were determined by dividing brine mobility before gel placement by brine mobility after gelation. Residual resistance factors were determined as a function of injection rate. Low injection rates were used first. A note was made of how rapidly F_{rrw} values stabilized and whether any gel was forced from the core along with the effluent. After stabilization, brine injection rates were increased, and the observations were repeated. Then, the injection rate was decreased to determine whether F_{rrw} values at lower rates had changed. This process was repeated with successively higher injection rates. The objectives of this procedure were to (1) determine whether gel mobilization or breakdown occurred at a particular flow rate or pressure gradient, and (2) determine the apparent rheology of the gel in porous media. Detailed listings of the residual resistance factors (as a function of fluid velocity) are documented in Appendix A for experiments that were performed in the third year of the project. Other data obtained in prior years can be found in Refs. 2 and 3. All of the residual resistance factors reported in this paper apply to the second segment ($\approx$ 12 cm) of the core.

Table 14 provides a summary and a comparison of residual resistance factors for the eight gels that were studied. This information is not meant to suggest that one gel is better or worse than another. The residual resistance factors provided by a given gel can be increased or decreased by adjusting the composition of the gelant. The primary purpose of Table 14 is to illustrate the effects of permeability and lithology on gel performance.

Table 14. Comparison of Residual Resistance Factors for Several Gels (41°C)

Gel	Residual resistance factor		
	High-permeability Berea sandstone	Low-permeability Berea sandstone	Indiana limestone
Resorcinol-formaldehyde, pH=6.0-6.5	1.8	2.1	1.5
Resorcinol-formaldehyde, pH=9	2,170	3,800	1,600
4% colloidal silica	6,100	1,400	102
10% colloidal silica	23,200	3,810	819
Unbuffered Cr^{3+}-xanthan	43.8 $u^{-0.31}$	57.7 $u^{-0.44}$	--
Cr^{3+}-xanthan buffered with acetate	3.6 $u^{-0.095}$	8.1 $u^{-0.14}$	--
Cr^{3+}(acetate)-polyacrylamide (212-ppm Cr^{3+})	34,700 $u^{-0.46}$	200 $u^{-0.53}$	49.7 $u^{-0.46}$
Cr^{3+}(acetate)-polyacrylamide (636-ppm Cr^{3+})	187,000	44,600	5,810

u is superficial velocity in ft/d

Cr^{3+}-Xanthan Gels. Residual resistance factors for Cr^{3+}-xanthan gels can decrease significantly with increased injection rate. This behavior can have a reversible component and an irreversible component. Fig. 5 shows F_{rrw} values for an unbuffered Cr^{3+}-xanthan gel in 68-md Berea sandstone. When brine was first injected at 0.2 ft/d, F_{rrw}=243. When the velocity was decreased to 0.1 ft/d, 0.05 ft/d, and 0.025 ft/d, F_{rrw} values increased to 365, 571, and 870, respectively. As indicated by the first entry in Table 15 and by the open circles in Fig. 5, this data can be described very well using Eq. 2.

$$F_{rrw} = 89.8\ u^{-0.62} \tag{2}$$

When brine was subsequently injected at 1.57 ft/d, F_{rrw}=63. Then, when the velocity was decreased, the F_{rrw} data could be described using Eq. 3.

$$F_{rrw} = 71.0\ u^{-0.59} \tag{3}$$

The above procedure was repeated using successively higher injection velocities. As shown in Fig. 5 and in Table 15, each set of data could be described quite well using a power-law relation. With each successive exposure to a new high in velocity (or pressure gradient), the power-law exponent increased (became less negative), and the velocity coefficient decreased. This behavior suggests that (1) the gel physically breaks down with exposure to higher velocities and pressure gradients, and (2) the gel exhibits a reversible "shear-thinning" character during brine injection. Of course, brine is a Newtonian fluid, so this apparent shear-thinning behavior must be attributed to the gel in the core rather than to the brine.

Table 15. F_{rrw} Relations Shown in Fig. 5 (Unbuffered Gel)
0.4% Xanthan, 154-ppm Cr^{3+}, 0.5% KCl in 68-md Berea Sandstone

Maximum superficial velocity, ft/d	Maximum pressure gradient, psi/ft	Residual resistance factor relation	Correlation coefficient
0.20	74	$F_{rrw} = 89.8\ u^{-0.62}$	0.999
1.57	150	$F_{rrw} = 71.0\ u^{-0.59}$	0.984
3.14	215	$F_{rrw} = 70.6\ u^{-0.48}$	0.994
6.28	305	$F_{rrw} = 66.6\ u^{-0.46}$	0.994
15.7	453	$F_{rrw} = 57.7\ u^{-0.44}$	0.997

The apparent shear-thinning character was noted for both buffered and unbuffered Cr^{3+}-xanthan gels in both low- and high-permeability Berea sandstone. This is illustrated in Fig. 6. Power-law equations describing the relations between residual resistance factors and superficial brine velocities are also shown. For both buffered and unbuffered gels, the velocity coefficient and the absolute value of the power-law exponent are both greater in low-permeability sandstone than in high-permeability sandstone. For a given gel at a fixed superficial velocity, the residual resistance factor in low-permeability Berea sandstone is greater than that in high-permeability Berea sandstone. Using the procedures described in Refs. 2 and 37, calculations can be made to show that the apparent shear-thinning character will not aid in profile modification in field applications.

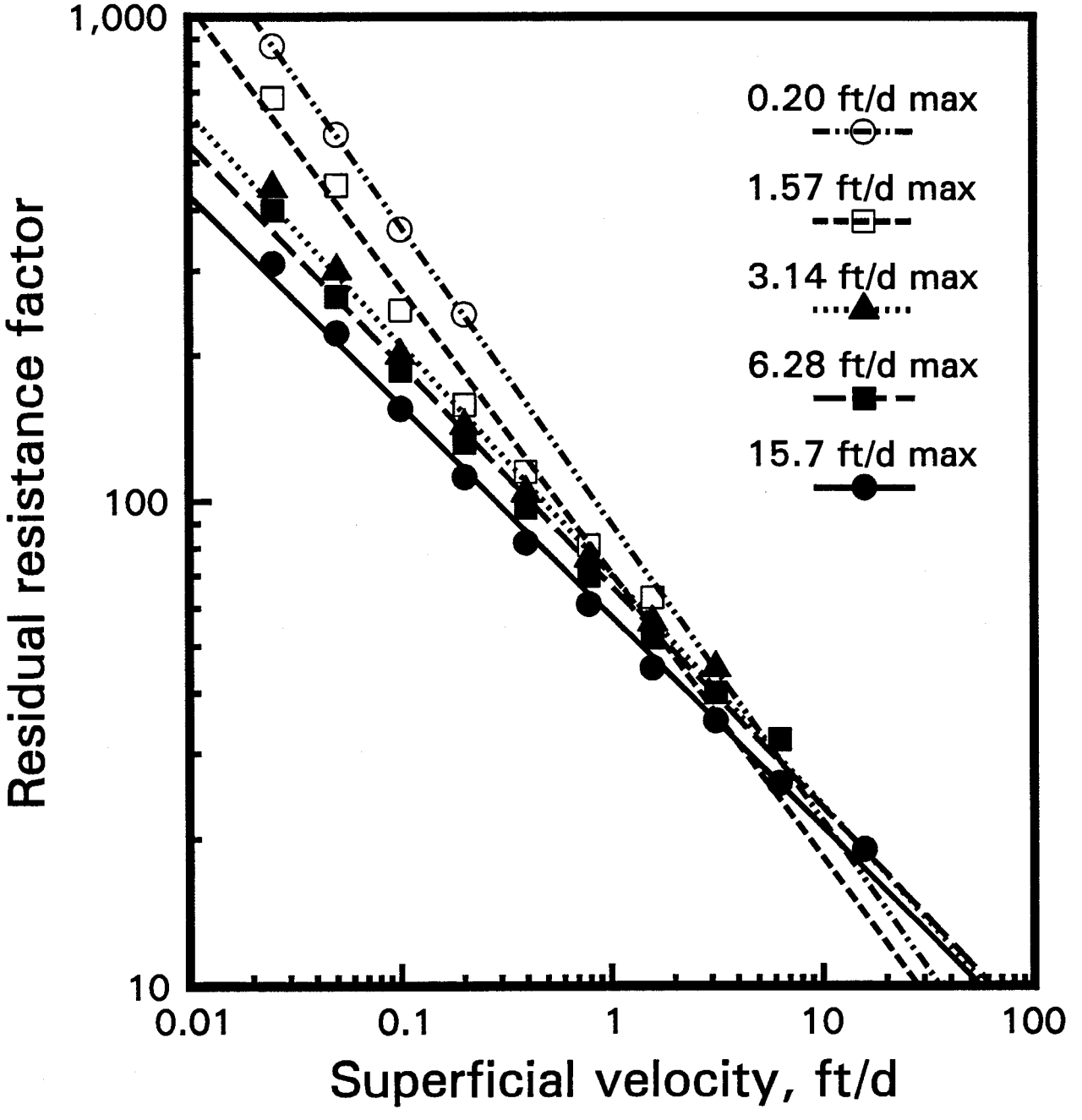

Fig. 5. Residual resistance factors for an unbuffered chromium-xanthan gel in 68-md Berea sandstone. 0.4% xanthan, 154-ppm chromium, 0.5% KCl.

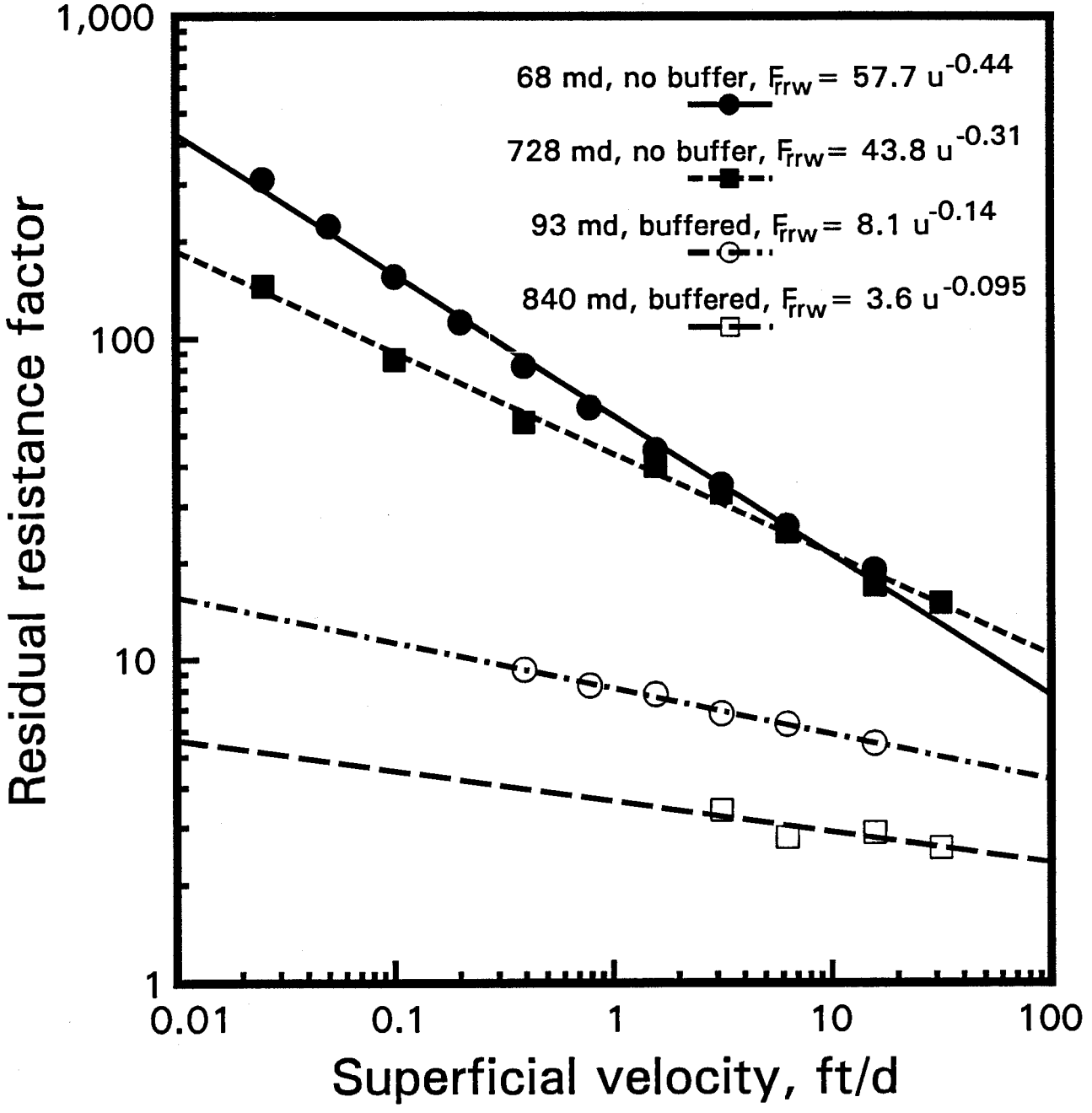

Fig. 6. Velocity dependence of residual resistance factors in Berea sandstone. Gel: 0.4% xanthan, 154-ppm chromium, 0.5% KCl.

The residual resistance factors for the buffered gel were significantly lower than those for the unbuffered gel. This observation is interesting. Originally, we expected the acetate buffer to allow stronger gels to form in the porous media because the average pH during gelation was lower for the buffered gelant than that for the unbuffered gelant. Therefore, we expected to find residual resistance factors that were much higher for the buffered gel than those for the unbuffered gel. However, since dissolved acetate or carboxylate groups on the polymer molecule compete for Cr^{3+}, the acetate apparently caused Cr^{3+}-xanthan gels to be weaker or less rigid than analogous gels formed when acetate was not present. During gelation studies in bottles, we noted that the unbuffered Cr^{3+}-xanthan formulations formed more rigid gels than the buffered formulations.

Resorcinol-Formaldehyde Gels. For the resorcinol-formaldehyde gels, a much more detailed description of our studies can be found in Refs. 2 and 28. Although residual resistance factors for these gels can show a slight shear-thinning character, their behavior is essentially Newtonian. As with most gels, residual resistance factors for resorcinol-formaldehyde formulations are sensitive to gelation pH. Table 14 shows that F_{rrw} values are very high for gels formed at pH 9 and are very low for gels formed between pH 6.0 and 6.5. In Berea sandstone, F_{rrw} values increased with decreased permeability. However, F_{rrw} values can be higher in Berea sandstone than in less-permeable limestone cores. Like the Cr^{3+}-xanthan gels, resorcinol-formaldehyde gels can experience physical breakdown upon exposure to successively higher fluid velocities.[2,28]

Colloidal-Silica Gels. For the 10% colloidal-silica gel, residual resistance factors averaged 23,200 in 630-md Berea sandstone, 3,810 in 50-md Berea sandstone, and 819 in 12-md Indiana limestone (Table 14). Thus, residual resistance factors decrease significantly with decreased permeability. Considered another way, the final permeabilites after gelation average 27 μD in 630-md Berea sandstone, 13 μD in 50-md Berea sandstone, and 15 μD in 12-md Indiana limestone. Thus, the colloidal-silica gel reduced the permeability of consolidated porous media to between 10 and 30 μD, regardless of the initial permeability of the rock. This conclusion is consistent with the findings of Jurinak *et al.*[23] (Detailed results from our experiments with 10% colloidal silica can be found in Table A-1 of Appendix A in Ref. 3.)

In one sense, the above permeability dependence of the F_{rrw} values could be very desirable. All gel-contacted portions of a heterogeneous reservoir could be altered to have nearly the same permeability. However, with 10% colloidal silica, the permeability is so low that flow is effectively stopped. In order to eliminate the need for zone isolation during gel placement, the residual permeability after gelation should be much higher than 30 μD. It may be possible to find a gel of this type with higher residual permeabilities.

Jurinak *et al.* found that a 4% colloidal-silica gel uniformly reduced the permeability of different permeable media to about 1 md (see Fig. 20 of Ref. 23). We performed several core experiments with 4% colloidal silica to try to verify Jurinak's findings. Residual resistance factors averaged 6,100 in 546-md Berea sandstone, 1,400 in 67-md Berea sandstone, and 102 in 13.4-md Indiana limestone (from Tables 14 and A-1). Considered another way, the final permeabilites after gelation average 90 μD in 546-md Berea sandstone, 47 μD in 67-md Berea sandstone, and 130 μD in 13.4-md Indiana limestone. Further work will be needed to determine why these residual permeabilities were significantly less than those reported by Jurinak *et al.*

Our studies of the 10% colloidal-silica gel did not reveal conclusive evidence of gel breakdown, even after exposure to pressure gradients as high as 1300 psi/ft. In earlier work, Jurinak *et al.* found that pressure gradients above 2500 psi/ft were required to cause gel breakdown. For two of the core experiments involving 4% colloidal silica (in 13.4-md limestone and in 67-md sandstone), the gel withstood pressure gradients in excess of 1000 psi/ft without experiencing significant physical breakdown (see Tables A-1a and A-1c).

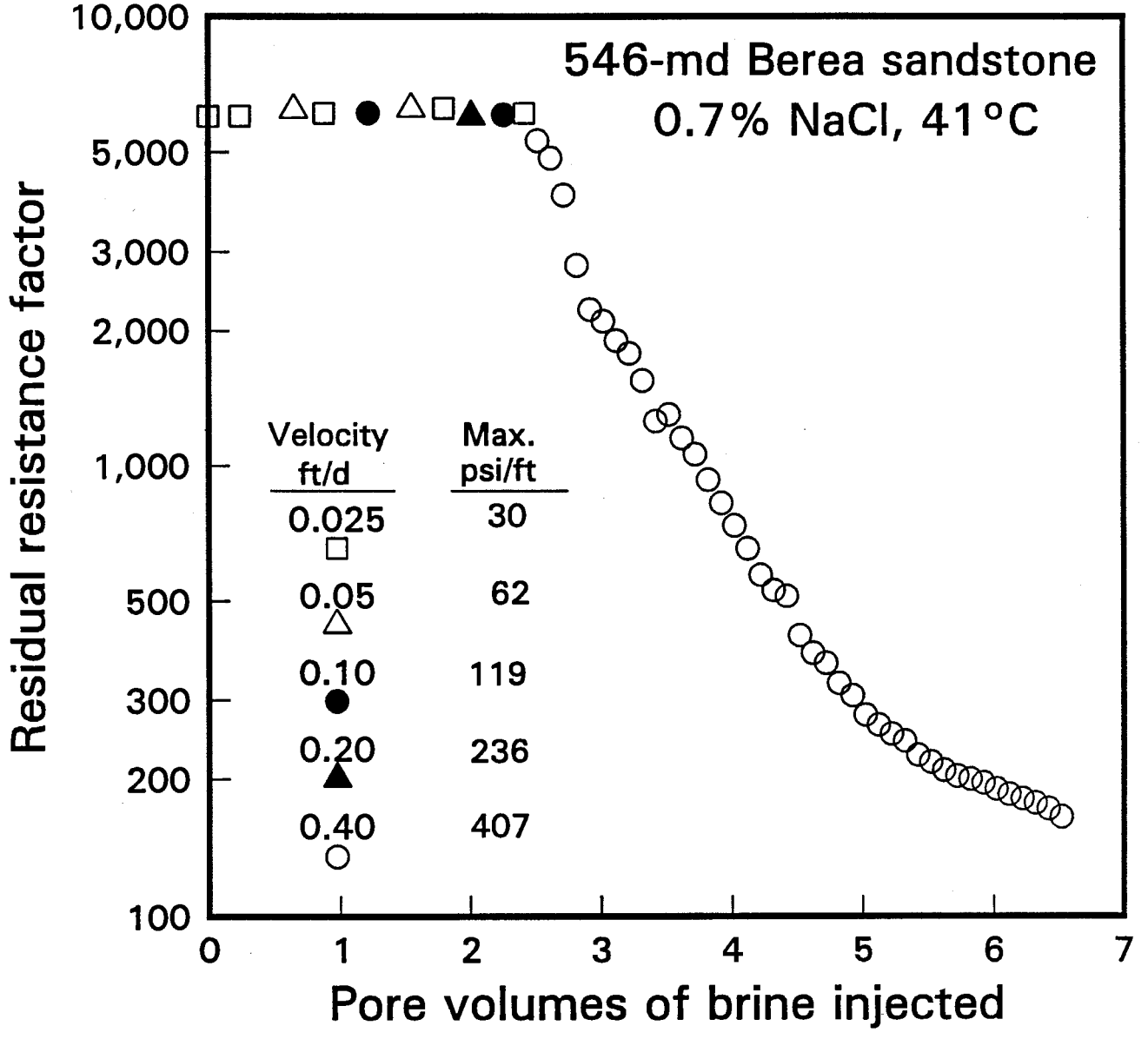

Fig. 7. Breakdown of a 4%-colloidal-silica gel during brine injection after gelation.

However, gel breakdown was apparent during core experiments with 4% colloidal silica in 546-md sandstone. This is illustrated in Fig. 7. When brine was first injected using superficial velocities between 0.025 ft/d and 0.203 ft/d, stable Newtonian behavior was observed, and residual resistance factors averaged 6100. After injecting about 2.5 pore volumes of brine at various rates, the injection rate was increased to 0.4 ft/d. During the course of injecting four additional pore volumes at this rate, the residual resistance factor steadily dropped from 6000 to less than 200. (The maximum pressure gradient observed before gel breakdown became apparent was 407 psi/ft.) The core was subsequently exposed to successively higher injection rates. With each new high in fluid velocity, residual resistance factors decreased—indicating additional gel breakdown. After exposure to the highest injection rate (15.7 ft/d), the final residual resistance factor was about 20 (see Table A-1b in Appendix A).

Cr^{3+}(Acetate)-Polyacrylamide Gels. For the Cr^{3+}(acetate)-polyacrylamide gels, one set of experiments was performed using 212-ppm Cr^{3+}. A second set of experiments was performed using 636-ppm Cr^{3+}. As expected, a stiffer gel was formed using the higher chromium concentration (gel code I, compared with H for the lower concentration). Using the higher chromium concentration, residual resistance factors averaged 187,000 in 662-md Berea sandstone, 44,600 in 65-md Berea sandstone, and 5,810 in 11-md Indiana limestone (Table 14). Considered another way, the final permeabilites after gelation average 3.5 μD in 662-md Berea sandstone, 1.5 μD in 65-md Berea sandstone, and 1.9 μD in 11-md Indiana limestone. Thus, the gel reduced the permeability of consolidated porous media to between 1 and 4 μD, regardless of the initial permeability of the rock. This behavior parallels that for the colloidal-silica gel. Because the residual resistance factors were so high, experiments could only be performed at a single, low injection rate. Thus, we were not able to determine how F_{rrw} varied with injection rate for this gel.

For the experiments performed using Cr^{3+}(acetate)-polyacrylamide gels with 212-ppm Cr^{3+}, F_{rrw} values were lower than those for gels with 636-ppm Cr^{3+} (see Table 14). Therefore, we were able to determine F_{rrw} values as a function of injection rate. As in the case for the Cr^{3+}-xanthan gels, residual resistance factors decreased with increased injection rate. Fig. 8 illustrates how F_{rrw} varies with superficial velocity in 74-md Berea sandstone. Both a reversible and an irreversible component to the velocity dependence are observed in Fig. 8. For velocities below 1 ft/d, the relations between F_{rrw} and u could be described fairly well using power law equations. However, above 1 ft/d, the data deviates from power-law behavior.

For the gel with 212-ppm Cr^{3+}, it is somewhat surprising that the F_{rrw} values in 74-md sandstone were significantly less than those in 746-md sandstone. In both cores, the relationship between F_{rrw} and u values can be described using power-law equations where the velocity exponent is near -0.5 (see Table 14). However, the velocity coefficient is more than 100 times greater for gel in the 746-md rock than in the 74-md rock. During brine injection after gelation, the first PV of effluent from the 74-md core had a viscosity of about 20 cp and a chromium concentration that was 7% of the injected value. This data suggests that a significant amount of uncrosslinked or lightly crosslinked polymer was displaced from the core after the shut-in period. Since washout of the gel was not observed in the 746-md core and was rarely observed in our experiments with other gels, further work will be needed to explain why gel washout occurred in the case with 74-md sandstone. More detailed results from our experiments with Cr^{3+}(acetate)-polyacrylamide gels can be found in Tables A-3 and A-4 in Appendix A.

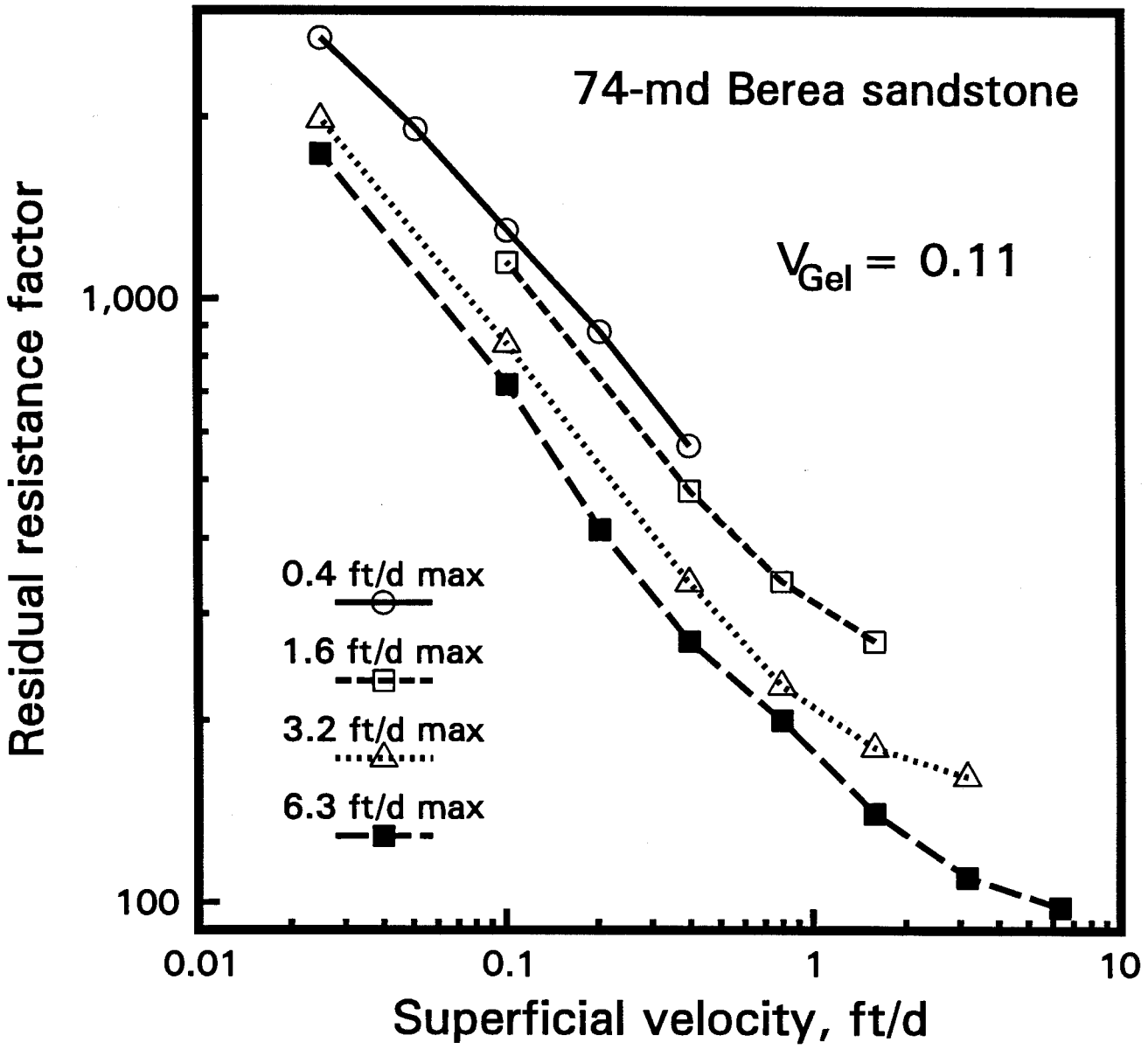

Fig. 8. Residual resistance factor vs. fluid velocity for gel containing 1.39% polyacrylamide and 212-ppm chromium (as acetate).

Results From Tracer Studies

After measuring F_{rrw} values, tracer studies were performed to determine (1) the fraction of the pore volume that remained available to flow, and (2) the new dispersivity of the core. The results from our tracer studies are listed in Table 16. In Table 16, V_p/V_{po} refers to the fraction of the original pore volume that was sampled by the iodide tracer during a given tracer study. The difference, $1-V_p/V_{po}$, provides an indication of the fraction of the original pore volume that was occupied by gel. The original pore volume of a given core (V_{po}) was typically about 30 cm^3.

For the 10% colloidal-silica gel and the resorcinol-formaldehyde gel formed at pH=9, Table 16 indicates that the gels occupied most (i.e., from 73% to 99%) of the original pore space. These results seem qualitatively consistent with the high F_{rrw} values that were observed for these gels (see Table 14). Resistance to flow is expected to be high when most of the pore space is occupied by gel. The behavior of the resorcinol-formaldehyde gel formed at pH=6.0-6.5 can also be rationalized using this logic. In particular, the gel provided low F_{rrw} values (Table 14) and occupied no more than 1% of the pore space (Table 16).

In contrast, the unbuffered Cr^{3+}-xanthan gel provided fairly high F_{rrw} values but apparently occupied no more than 13% of the pore space. Perhaps, small gel particles lodge in pore throats—thereby, dramatically reducing brine permeability without occupying much volume. Experiments performed using 154-ppm Cr^{3+} without xanthan indicate that this behavior was not due to the chromium alone. These chromium solutions had no significant effect on the apparent pore volume, the dispersivity, or the permeability of the cores.

For most cases when Cr^{3+}(acetate)-polyacrylamide gels were used, the flow rates were so low during brine injection after gelation that tracer studies could not be performed. In view of the very high residual resistance factors (Table 14), we suspect that these gels occupied most of the pore space. However, in two cases (using gelant with 212-ppm Cr^{3+}), F_{rrw} values were low enough so that tracer studies were performed. In these cases, the gel apparently occupied from 11% to 13% of the pore space (see Table 16). For the case using 74-md sandstone, the tracer result (11% PV occupied by gel) is qualitatively consistent with the washout of polymer noted in the previous section. For the case using 10.7-md limestone, the tracer result (13% PV occupied by gel) could be attributed to either polymer washout or insufficient gelant injection during the process of gelant placement (as discussed in the previous section). In the 74-md sandstone and the 10.7-md limestone, the gel provides high residual resistance factors while only occuping a small fraction of the pore space. As for the case with the Cr^{3+}-xanthan gels, we speculate that small gel particles lodge in pore throats—thereby, dramatically reducing brine permeability without occupying much volume.

Table 17 lists dispersivity results obtained during the tracer studies. The quantity, α/α_o, refers to the final dispersivity during tracer injection after gelation divided by the initial dispersivity value before gel placement. Initial dispersivity values (α_o) for the Berea cores were approximately 0.1 cm. Dispersivity values for cores before exposure to gel were roughly the same in high-permeability Berea sandstone as in low-permeability Berea sandstone ($\approx$0.1 cm). However, dispersivity values for Indiana limestone were typically five to ten times greater than those for Berea sandstone.

Table 17 demonstrates that the gels usually increase dispersivity in the cores. Qualitatively, this data means that the gels broaden the range of flow paths through the porous medium. Gels could create some short pathways simply as a consequence of filling the pore space. On the other hand, longer flow paths could result if the gel acts as a medium that is permeable to the brine.

Table 16. Fraction of Pore Volume Remaining After Gel Placement (V_p/V_{po})

Gel	V_p/V_{po}		
	High-permeability Berea sandstone	Low-permeability Berea sandstone	Indiana limestone
Resorcinol-formaldehyde, pH=6.0-6.5	0.99	1.00	0.99
Resorcinol-formaldehyde, pH=9	0.09	0.13	0.01
4% colloidal silica	0.18	0.42	0.78
10% colloidal silica	0.18	0.27	--
Unbuffered Cr^{3+}-xanthan	0.92	0.90	0.87
Cr^{3+}-xanthan buffered with acetate	0.87	0.90	--
154-ppm Cr^{3+} (no xanthan)	1.00	1.00	0.98
Cr^{3+}(acetate)-polyacrylamide (212-ppm Cr^{3+})	--	0.89	0.87

Table 17. Relative Dispersivities After Gel Placement (α/α_o)

Gel	α/α_o		
	High-permeability Berea sandstone	Low-permeability Berea sandstone	Indiana limestone
Resorcinol-formaldehyde, pH=6.0-6.5	1.5	1.0	1.5
Resorcinol-formaldehyde, pH=9	106	11.5	2.9
4% colloidal silica	3.0	4.0	1.8
10% colloidal silica	8.5	5.3	--
Unbuffered Cr^{3+}-xanthan	9.9	8.3	1.6
Cr^{3+}-xanthan buffered with acetate	1.2	2.7	--
154-ppm Cr^{3+} (no xanthan)	1.0	1.0	1.0
Cr^{3+}(acetate)-polyacrylamide (212-ppm Cr^{3+})	--	0.5	1.7

Conclusions

1. During injection of gelants that contained Cr^{3+}, chromium propagation was significantly more rapid when the counterion was acetate rather than chloride. For a given counterion, chromium propagation was more rapid in Berea sandstone cores than in Indiana limestone cores. It is doubtful that unbuffered chromium-chloride gelants can propagate through carbonate reservoirs.

2. During core experiments, the "strongest" gels were found to reduce the permeability of all cores to approximately the same value (in the low microdarcy range). Tracer studies indicated that these gels occupied most of the available pore space.

3. For "weaker" gels (i.e., those leaving a significant permeability), residual resistance factors decreased with increased rock permeability in Berea sandstone. Tracer studies indicated that these gels occupied a small fraction of the pore space in a core. Experiments revealed that gelation in the porous rock was often far less complete than that in a bottle. For unbuffered gelants in porous rocks, the pH at which gelation occurs may be determined more by rock mineralogy than by the pH of the injected gelant. Thus, the buffering action of reservoir rocks should be considered when evaluating gel performance in the laboratory.

4. Residual resistance factors for Cr^{3+}-xanthan and Cr^{3+}(acetate)-polyacrylamide gels can exhibit a reversible shear-thinning character during brine injection. In contrast, residual resistance factors for the resorcinol-formaldehyde gels were generally Newtonian.

3. REDUCTION OF OIL AND WATER PERMEABILITIES USING GELS

Applications of near-wellbore gel treatments in production wells are intended to reduce excess water production without sacrificing oil production. In a previous study,[5] we developed a theoretical model using fractional flow and material balance concepts to quantify the degree of gelant penetration into oil-productive zones as well as into water-source zones. (The term "gelant" here refers to the liquid formulation prior to gelation.) The study showed that gelants can penetrate to a significant degree into all open zones—not just those zones with high water saturations. The study also indicated that oil productivity can be impaired even if the gel reduces water permeability without affecting oil permeability. The principal advantage of the disproportionate reduction of the water and oil relative permeabilities is in reducing the need for zone isolation during gel placement. Realizing this advantage generally requires high fractional oil flow from the zone(s) of interest. During the study, the effects of capillary pressure were neglected in order to obtain a closed-form solution to the water conservation equation.

In a separate study,[3] we examined the effects of capillary pressure on gel placement. This study showed that, in experiments with oil-wet cores, capillary effects could inhibit an aqueous gelant from entering a core. However, in field applications, the pressure drop between injection and production wells is usually so large that capillary effects will not prevent gelant penetration into oil-productive zones. Under field-scale conditions, the effects of capillary pressure on gelant fractional flow are negligible. Hence, capillary pressure effects do not change the conclusions reached in Ref. 5.

Several researchers[38-45] reported that some polymers and gels can reduce permeability to water more than to oil. Fig. 9 provides a summary of the results from different researchers. In this figure, the permeability reduction for water at residual oil saturation is plotted against the permeability reduction for oil at residual water saturation. A given permeability-reduction value was determined by dividing the endpoint permeability before exposure to polymer or gel by the endpoint permeability after exposure to polymer or gel. Using this definition, two factors contributed to the permeability reductions—(1) changes in permeability at a given fluid saturation and (2) changes in endpoint fluid saturations. The available evidence indicates that the polymer or gel usually shifted the entire water relative permeability curve to lower values without significantly changing the residual oil saturation. In contrast, the position of the oil relative permeability curve was often unaffected by the polymer or gel, except that the irreducible water saturation was increased. Thus, the increase in the irreducible water saturation was largely responsible for permeability reductions for oil.

In this study, we examined how different types of gels reduce oil and water permeabilities in high-permeability Berea sandstone. The impact of wettability on reduction of oil and water permeabilities was investigated. We also examined whether hysteresis of endpoint oil and water permeabilities occurs during the "pump-in, pump-out" sequence used during gel treatments in production wells.

Gelants Studied

Four types of gels were investigated in this study, including: (1) resorcinol-formaldehyde, (2) Cr^{3+}(chloride)-xanthan, (3) Cr^{3+}(acetate)-polyacrylamide (Marathon's MARCIT®), and (4) colloidal silica (DuPont's Ludox SM®). For the Cr^{3+}(acetate)-polyacrylamide gel, three formulations of different final strength were used. Table 18 lists the compositions of these gelants. Pfizer provided the xanthan (Flocon 4800®); DuPont supplied the colloidal silica; and Marathon provided the polyacrylamide. The polyacrylamide (HPAM) had a molecular weight of about 2 million daltons and a degree of hydrolysis of 2 percent. The other chemicals used in this study were reagent grade.

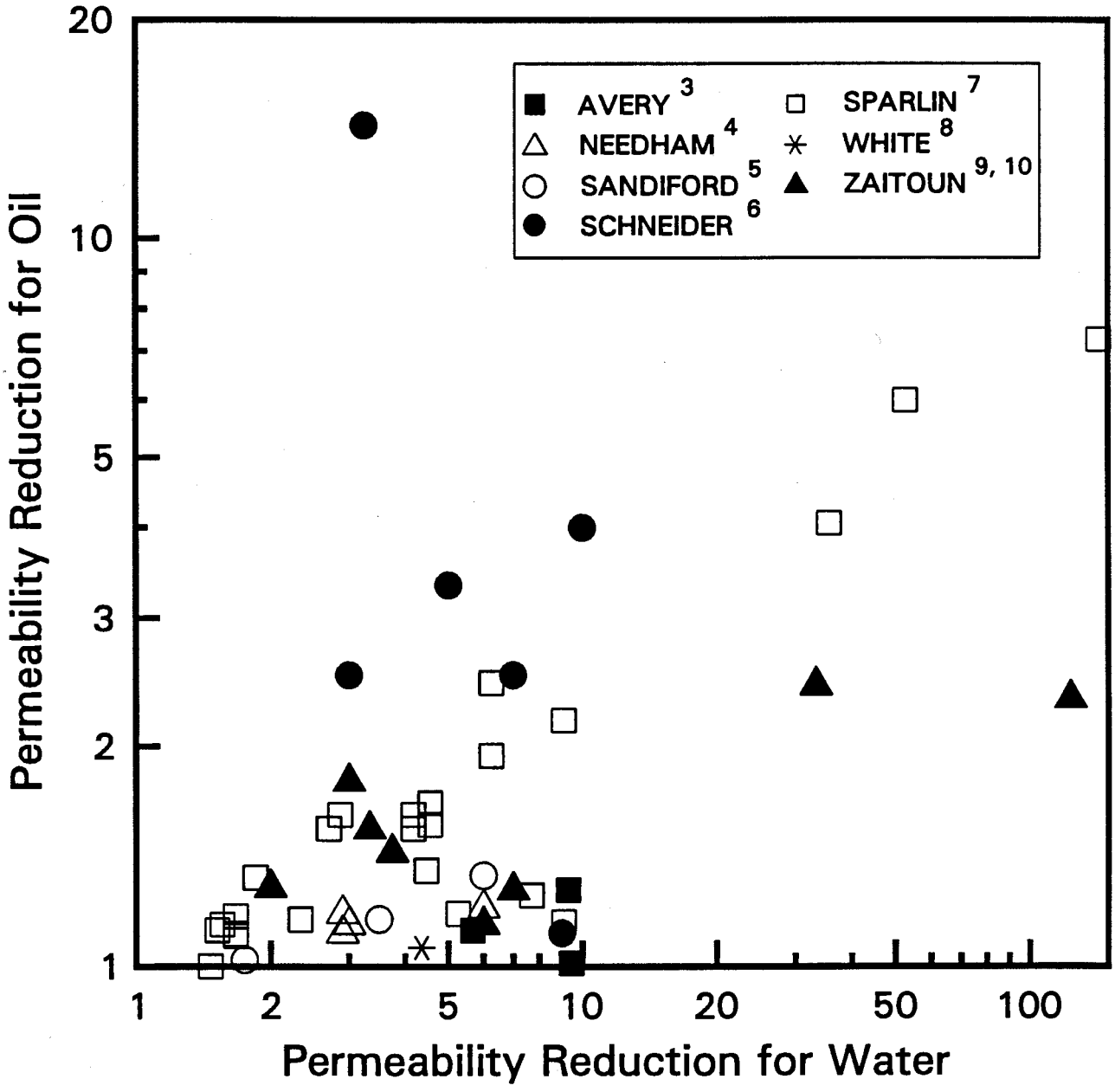

Fig. 9. Disproportionate permeability reduction by polymers and gels.

Table 18. Gelant Compositions for Oil/Water Corefloods

Gelant Composition	pH
3% resorcinol, 3% formaldehyde, 0.5% KCl, 0.05M $NaHCO_3$	6.5
0.4% xanthan, 154-ppm Cr^{3+} (as $CrCl_3$), 0.5% KCl	4.0
1.39% polyacrylamide (HPAM), 636-ppm Cr^{3+} (as acetate), 1% NaCl	6.0
1.39% polyacrylamide (HPAM), 212-ppm Cr^{3+} (as acetate), 1% NaCl	6.0
0.7% polyacrylamide (HPAM), 318-ppm Cr^{3+} (as acetate), 1% NaCl	6.0
10% colloidal silica, 0.7% NaCl	8.2

Experimental Procedures

Corefloods were performed to study how different types of gels reduce permeability to water and to oil. High-permeability Berea sandstone cores were used as the porous medium. All cores were about 15 cm long and 3.6 cm in diameter, and all cores had one internal pressure tap located 2.5 cm from the inlet rock face. The cores were not fired. Either a refined oil (Soltrol-130®) or a West Texas crude oil (Moutray) was used as the oil phase. All experiments were conducted at 41°C (105°F).

Table 19 is a summary of the sequence followed during our core experiments. In each of the corefloods, the core was first saturated with brine, and the porosity and permeability to brine were determined. (The brine used in each coreflood had the same composition as that used for gelant preparation.) The core then was put through a cycle of oilflooding followed by waterflooding to establish an irreducible oil saturation (using flow direction #1). A constant pressure drop was maintained across the core during the process. (The pressure drop was maintained at 30 psi when the gelant to be injected was resorcinol-formaldehyde. When the gelant to be injected was the more viscous Cr^{3+}(chloride)-xanthan gelant, the Cr^{3+}(acetate)-polyacrylamide gelants or the colloidal silica gelant, the pressure drop was 100 psi. These pressure drops were chosen to avoid mobilizing residual oil during gelant injection.) The endpoint oil and water permeabilities were determined at the irreducible water saturation after the oilflood and at the irreducible oil saturation after the waterflood, respectively. For corefloods SSH-15, SSH-17, SSH-22, SSH-23, the flow direction was reversed (flow direction #2), and the above procedure was repeated to determine the effect of hysteresis. Also, in order to verify the results, each step was repeated.

Water-tracer studies were performed after the core was first saturated with brine and after each waterflood. These studies involved injecting a brine bank that contained 40-ppm potassium iodide as a tracer. The tracer concentration in the effluent was monitored spectrophotometrically at a wavelength of 230 nm. For our latest experiments, oil-tracer studies were performed after each oilflood. These studies involved injecting an oil bank that contained 20-ppm trans-stilbene as a tracer. The tracer concentration in the effluent was monitored spectrophotometrically at a wavelength of 300 nm. Usually, four replicates were performed for each tracer study. Also, the replicates included studies performed at different injection rates. Retention of trans-stilbene in Berea sandstone was found to be negligible (less than 0.01 μg/g of rock).

Table 19. Sequence Followed During Oil/Water Core Experiments

Step

1. Saturate core with brine and determine porosity.
2. Determine absolute brine permeability and mobility.
3. Perform water-tracer study to confirm the pore volume (V_{po}) and to determine core dispersivity (α_o).
4. Inject oil (flow direction #1) to displace brine at a constant pressure drop of 100 psi* across the core and to determine oil mobility at residual water saturation.
5. Perform oil-tracer study (flow direction #1) to determine the fraction of the original pore volume remaining (V_p/V_{po}) and the relative dispersivity (α/α_o).
6. Inject brine (flow direction #1) to displace oil at a constant pressure drop of 100 psi* across the core and to determine brine mobility at residual oil saturation.
7. Perform water-tracer study (flow direction #1) to determine V_p/V_{po} and α/α_o.
8. Repeat Steps 4 through 7 (flow direction #1) to verify that the results are reproducible.
9. Reverse the flow direction (flow direction #2), and repeat Steps 4 through 7 to determine the effect of hysteresis.
10. Repeat Step 9 (flow direction #2) to verify that the results are reproducible.
11. Inject gelant using the highest possible injection rate without exceeding the pressure constraint (flow direction #1).
12. Shut in core to allow gelation.
13. Inject brine (flow direction #2) to determine the residual resistance factors to water (F_{rrw}).
14. Perform water-tracer study to determine V_p/V_{po} and α/α_o (flow direction #2).

15a. Inject oil (flow direction #2) to determine the residual resistance factor to oil (F_{rro}).

15b. Perform oil-tracer study to determine V_p/V_{po} and α/α_o (flow direction #2).

15c. Inject brine (flow direction #2) to determine F_{rrw}.

15d. Perform water-tracer study to determine V_p/V_{po} and α/α_o (flow direction #2).

16. Repeat Steps 15a through 15d (second oil-water injection cycle after shut-in).
17. Repeat Steps 15a through 15d (third oil-water injection cycle after shut-in).

* 30 psi if gelant was resorcinol-formaldehyde.

In order to simulate the "pump-in, pump-out" sequence used during gel treatments in production wells, the gelant was injected into the core from one direction, and residual resistance factors (F_{rr}) were measured in the opposite direction. Resistance factor (F_r) and effluent pH were monitored continuously during gelant injection. Effluent samples were collected and monitored to determine whether the gelation characteristics of the effluent differed from those of gelant that had not been injected. After injecting the gelant, the core was shut in for five days (at 41 °C). After shut-in, brine was injected from the opposite direction to determine the residual resistance factors to water (F_{rrw}) after gel treatment. To determine the apparent rheology of the gel in porous media, and whether gel mobilization occurred at a given flow rate, residual resistance factors were determined as a function of injection rate. Measurements of residual resistance factors were first made at a very low injection rate. After stabilization, the measurements were repeated at a higher injection rate. Then, the rate of brine injection was lowered to the previous injection rate to determine whether the F_{rrw} value at that injection rate had changed. This cycle was repeated several times using successively higher injection rates until the pressure drop across the core approached the pressure constraint used in the process of establishing residual saturations.

Tracer studies were then performed to determine the final pore volume that was occupied by the gel, and the effect of the gel treatment on the dispersivity of the core. After the tracer studies, oil was injected into the core, and the procedure described above was repeated to determine the residual resistance factor to oil (F_{rro}). Again, to verify the results, the residual-resistance-factor measurements for both water and oil were repeated at the highest possible injection rates without exceeding the pressure constraint used in the process of establishing residual saturations. Tracer studies were also repeated.

Effect of Flow-Direction Reversal on Endpoint Permeabilities Before Gel Placement

The relative permeability of a given phase is often both path- and history-dependent.[46,47] Gel treatments in production wells involve a "pump-in, pump-out" sequence where a gelant is injected into a production well from one direction, and later, oil is produced from the opposite direction. Hysteresis of relative permeability curves can result in significant damage to oil productivity.[5] Thus, the impact of this hysteresis should be considered prior to a gel treatment. Our coreflood experiments were designed to examine the effect of flow-direction reversal on endpoint oil and water relative permeabilities at irreducible water and oil saturations, respectively.

High-permeability Berea sandstone cores were used in this study. Rock and fluid properties for each core are listed in Table 20. Additional core and fluid properties for the corefloods can be found in Tables B-1a through B-1i in Appendix B.

To achieve an intermediate wettability[48-50], some cores were aged with Moutray crude oil at 80°C for eight days after the first oilflood (Step 4 in Table 19). Then, the old crude oil was displaced by three pore volumes (PV) of fresh crude oil, and the oil mobility was determined. Tests revealed that the Amott indexes for oil and water were both near zero—indicating intermediate wettability. When the refined oil was used in place of the crude oil, cores were strongly water-wet.

Table 20. Rock and Fluid Properties (41°C)

Core ID	Porosity	Oil Phase	Wettability	Brine	k_w, md
SSH-15	0.247	Moutray	Intermediate	0.5% KCl	803
SSH-17	0.240	Soltrol-130	Strongly water-wet	0.5% KCl	795
SSH-22	0.247	Soltrol-130	Strongly water-wet	0.5% KCl	809
SSH-23	0.259	Moutray	Intermediate	0.5% KCl	815
SSH-26	0.258	Soltrol-130	Strongly water-wet	1% NaCl	742
SSH-27	0.256	Soltrol-130	Strongly water-wet	1% NaCl	765
SSH-31	0.243	Soltrol-130	Strongly water-wet	1% NaCl	718
SSH-32	0.236	Soltrol-130	Strongly water-wet	0.7% NaCl	767
SSH-33	0.24	Soltrol-130	Strongly water-wet	0.7% NaCl	788

In each of the corefloods, Steps 1 through 10 (outlined in Table 19) were performed to characterize the core and to establish baselines before gelant injection. Table 21 provides a summary of the hysteresis studies before gelant injection. The results were reproducible during replicate cycles. Tables B-2a through B-2e in Appendix B show detailed results of the hysteresis studies. For the strongly water-wet cores (i.e., the cores with the refined oil), no significant hysteresis of endpoint permeabilities (either for water or oil) was observed as a result of the flow-direction reversal. However, for the cores with intermediate wettability (i.e., the cores with the crude oil), flow-direction reversal caused a 45 to 73% increase in endpoint permeability to water. A much smaller hysteresis was observed for endpoint oil permeability.

The main value of these studies is that they quantify the importance of hysteresis in our fluid/rock systems prior to the introduction of gel. Especially for those parameters that were unaffected by flow-reversal and multiple imbibition and drainage cycles, gel effects can now be distinguished from hysteresis effects during our subsequent gel studies.

Table 21. Effect of Flow-Direction Reversal on Endpoint Permeabilities (41°C)

Core ID	Wettability	k_o^o, md	k_o^{o*}, md	k_w^o, md	k_w^{o*}, md
SSH-17	Strongly water-wet	718	719	182	169
SSH-22	Strongly water-wet	706	792	186	206
SSH-26	Strongly water-wet	593	594	177	170
SSH-15	Intermediate	1680	1413	151	261
SSH-23	Intermediate	891	909	277	402

* Flow-direction reversed.

Gelant Placement in the Cores

For the resorcinol-formaldehyde gelant, retention studies in Berea sandstone cores revealed no significant loss of gelant components, either by adsorption or by partitioning into the oil phase. Therefore, only three PV of the gelant were injected. This gelant was water-like during the injection process (Step 11). In contrast, ten PV of Cr^{3+}(chloride)-xanthan gelant were injected to ensure that the cores were saturated with the gelant. For the Cr^{3+}(acetate)-HPAM gelant with 1.39% HPAM and 636-ppm Cr^{3+}, approximately four PV of gelant were injected because a high pressure gradient developed. For the less concentrated Cr^{3+}(acetate)-HPAM gelants, eight to ten PV were injected. Ten PV of gelant were also injected during the experiments with colloidal silica.

We examined how the presence of oil affects gelation. During tests in bottles, both the refined oil and Moutray crude had no effect on the gelation times or the appearance of the gels. Also, during all of the core experiments, injected and non-injected gelant formulations exhibited similar gelation times and final gel strengths. The shut-in times (five days) were 8 to 33 times longer than the gelation times. The gelant placement data are summarized in Table 22.

Effluent samples were collected throughout the process of injecting the Cr^{3+}(chloride)-xanthan and Cr^{3+}(acetate)-HPAM gelants. These samples were analyzed for chromium concentration using atomic absorption spectrometry. The results for Cr^{3+}(chloride)-xanthan gelant are presented in Fig. 10. A case with no residual oil present[3] is included for comparison with the two cases where residual oil was present. In all three cases, the porous medium was a high-permeability Berea sandstone core. For the case without residual oil, the first chromium in the effluent was detected after injecting three PV of gelant. After injecting ten PV, the chromium concentration in the effluent reached about 80% of its injected value. Fig. 10 indicates that chromium propagates more readily in porous media with residual oil present. For the cases with residual oil present, the first chromium in the effluent was detected after injecting one pore volume of gelant. The chromium concentration in the effluent then increased steadily and leveled off at over 90% of the injected concentration. A comparison of Figs. 10 and 11 shows that the more rapid breakthrough of chromium when oil is present occurs partly because residual oil decreases the pore volume occupied by water. (In Fig. 11, the PV values were adjusted to exclude residual oil.) However, Fig. 11 also shows that this explanation does not entirely account for the different Cr^{3+} propagation rates with vs. without residual oil.

Table 22. Gelant Placement Data (41°C)

Core ID	Oil Phase	Gel Type	No. of PVs Injected	Gelation Time, days	Shut-In Time, days
SSH-17	Soltrol-130	resorcinol-formaldehyde	3	0.25	5
SSH-15	Moutray	resorcinol-formaldehyde	3	0.25	5
SSH-22	Soltrol-130	Cr^{3+}(chloride)-xanthan	10	0.42	5
SSH-23	Moutray	Cr^{3+}(chloride)-xanthan	10	0.42	5
SSH-26	Soltrol-130	1.39% HPAM, 636-ppm Cr^{3+}	4	0.15	5
SSH-27	Soltrol-130	0.7% HPAM, 318-ppm Cr^{3+}	10	0.45	5
SSH-31	Soltrol-130	1.39% HPAM, 212-ppm Cr^{3+}	8	0.63	5
SSH-32	Soltrol-130	colloidal silica	10	0.21	5
SSH-33	Soltrol-130	colloidal silica	10	0.21	5

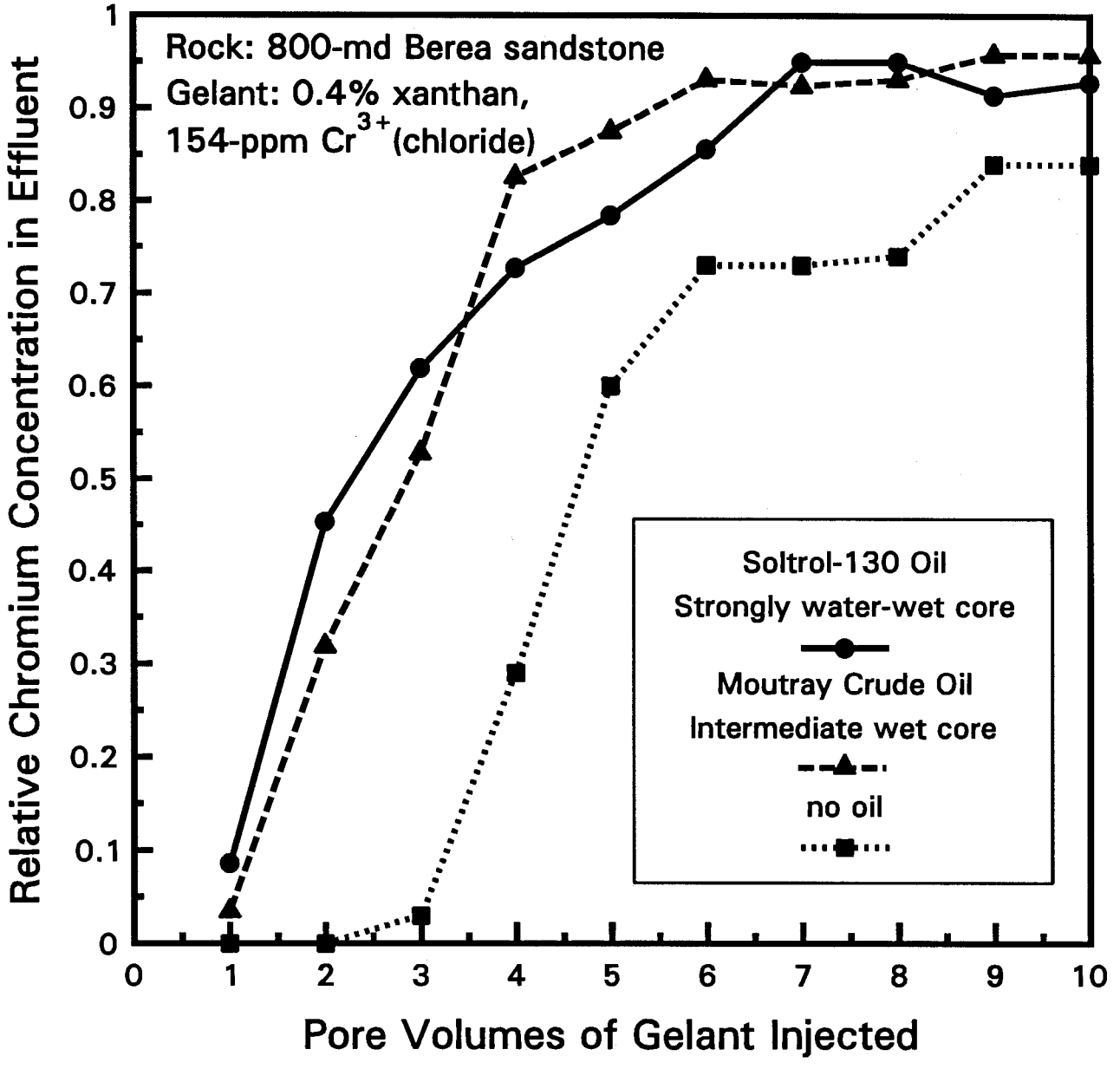

Fig. 10. Effects of residual oil on chromium propagation.

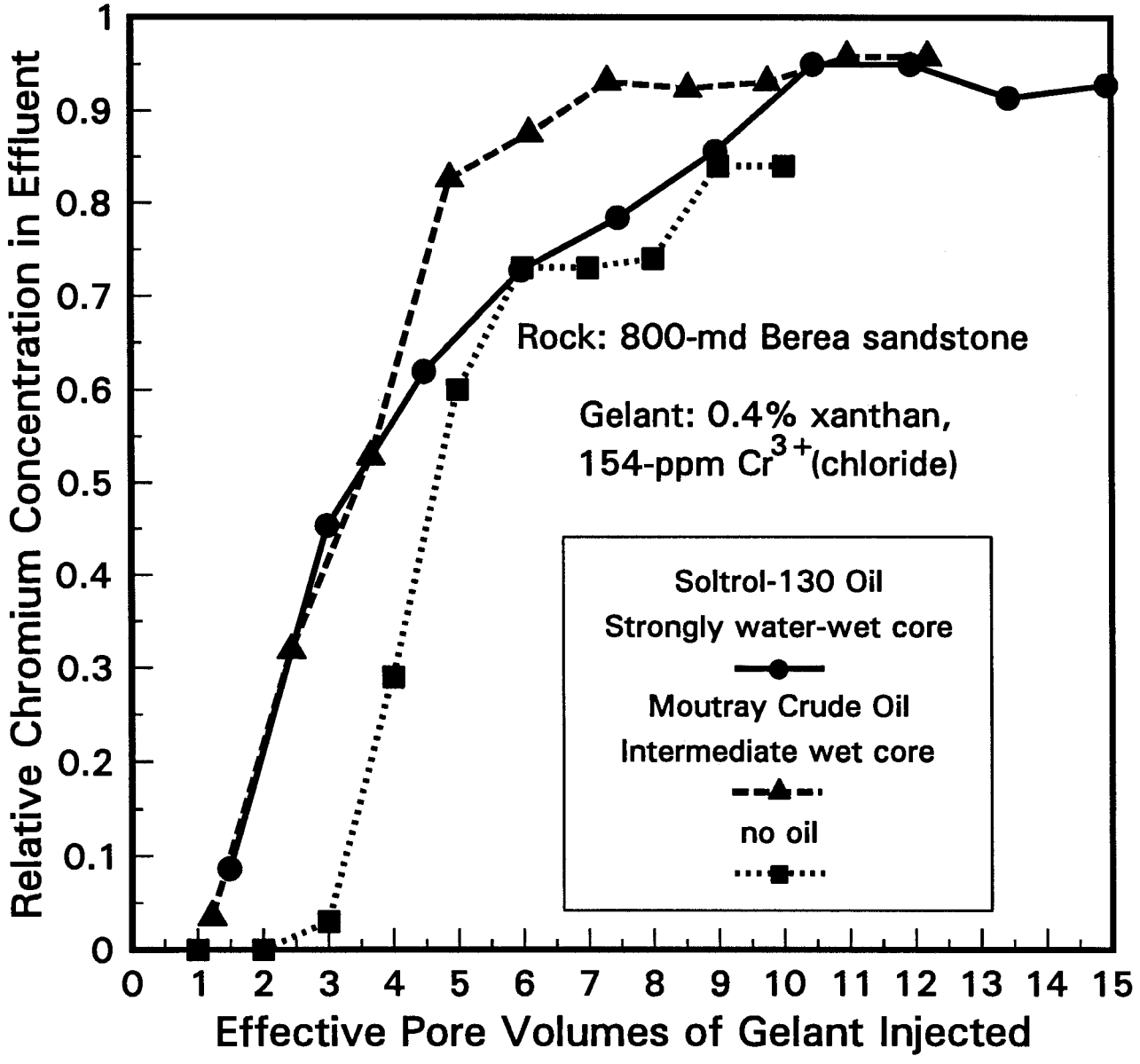

Fig. 11. Effects of residual oil on chromium propagation.

Chromium propagation results for Cr^{3+}(acetate)-HPAM gelants are presented in Fig. 12. All cases had residual oil present. For all the Cr^{3+}(acetate)-HPAM formulations, the first chromium in the effluent was detected after injecting one PV of the gelant. The chromium concentration in the effluent then increased sharply and leveled off at values between 80% and 95% of the injected value.

Effluent pH was also routinely monitored during gelant injections and during subsequent F_{rrw} measurements. The results from our pH measurements are summarized in Fig. 13 (for Cr^{3+}(chloride)-xanthan), Fig. 14 (for the Cr^{3+}(acetate)-HPAM gelants), and Fig. 15 (for the colloidal-silica gelant). In our future work, we will continue to characterize the propagation of chromium and pH fronts through cores. Based on previous work,[32] we expect more rapid chromium propagation in a low pH environment because chromium solubility increases with decreased pH.

After the shut-in period for the Cr^{3+}(chloride)-xanthan gels, brine (0.5% KCl) was injected to determine the residual resistance factors to water. Fig. 13 shows that the pH of the first effluent after the shut-in period was between 6 and 7 for all three cores. These values are significantly higher pH values than those observed just before shut-in. The pH increase can be attributed to reactions with rock minerals during the shut-in period (e.g., dissolution of carbonates and ion exchange). As noted in our earlier studies,[3] the Cr^{3+}(chloride)-xanthan gelant has very little buffering capacity, so the pH at which the gelation reaction actually occurs depends more on the mineralogy of the porous medium than on the pH of the injected gelant.

Permeability Reduction for Oil and Water After Gel Treatment

Following the five-day shut-in period, Steps 13 through 17 (from Table 19) were performed to determine the residual resistance factors for brine (F_{rrw}) and for oil (F_{rro}). (See Nomenclature for definitions of these terms.) In order to simulate the "pump-in, pump-out" sequence used during gel treatments in production wells, the gelant was injected into the core from one direction (flow direction #1), and residual resistance factors were measured in the opposite direction (flow direction #2). The hysteresis effects, if present, were eliminated by using the end-point mobilities measured in the same direction (flow direction #2) before and after gel treatments to calculate residual resistance factors. Results are summarized in Table 23 and in Tables B-3a through B-3i in Appendix B.

Resorcinol-Formaldehyde. For the resorcinol-formaldehyde gel in both the water-wet and intermediate-wet systems, residual resistance factors were more or less Newtonian (velocity independent) during continuous injection of either water or oil (see Tables B-3a and B-3b). (We also noted Newtonian behavior during water injection in a previous study where no oil was present.[28]) However, F_{rrw} values during the second waterflood (Step 15c) were less than the previous F_{rrw} values (Step 13). This suggests that the gel experienced physical breakdown during the oil-water injection cycle. Further gel breakdown was not observed during a subsequent oil-water injection cycle (Steps 16a through 16d).

Cr^{3+}(Chloride)-Xanthan. The F_{rrw} and F_{rro} values for the Cr^{3+}(chloride)-xanthan gels were generally lower than those for the other gels. The F_{rrw} values were also much lower than those measured in our previous studies without a residual oil saturation.[21,37] Gel breakdown was not observed during the oil-water injection cycles. The flow-rate dependence of F_{rrw} values was very weak for the data with residual oil present (see Tables B-3c and B-3d). In contrast, a strong apparent shear-thinning behavior was observed during other studies, where residual oil was not present.[21,37] Further work will be needed to understand the reasons for these differences.

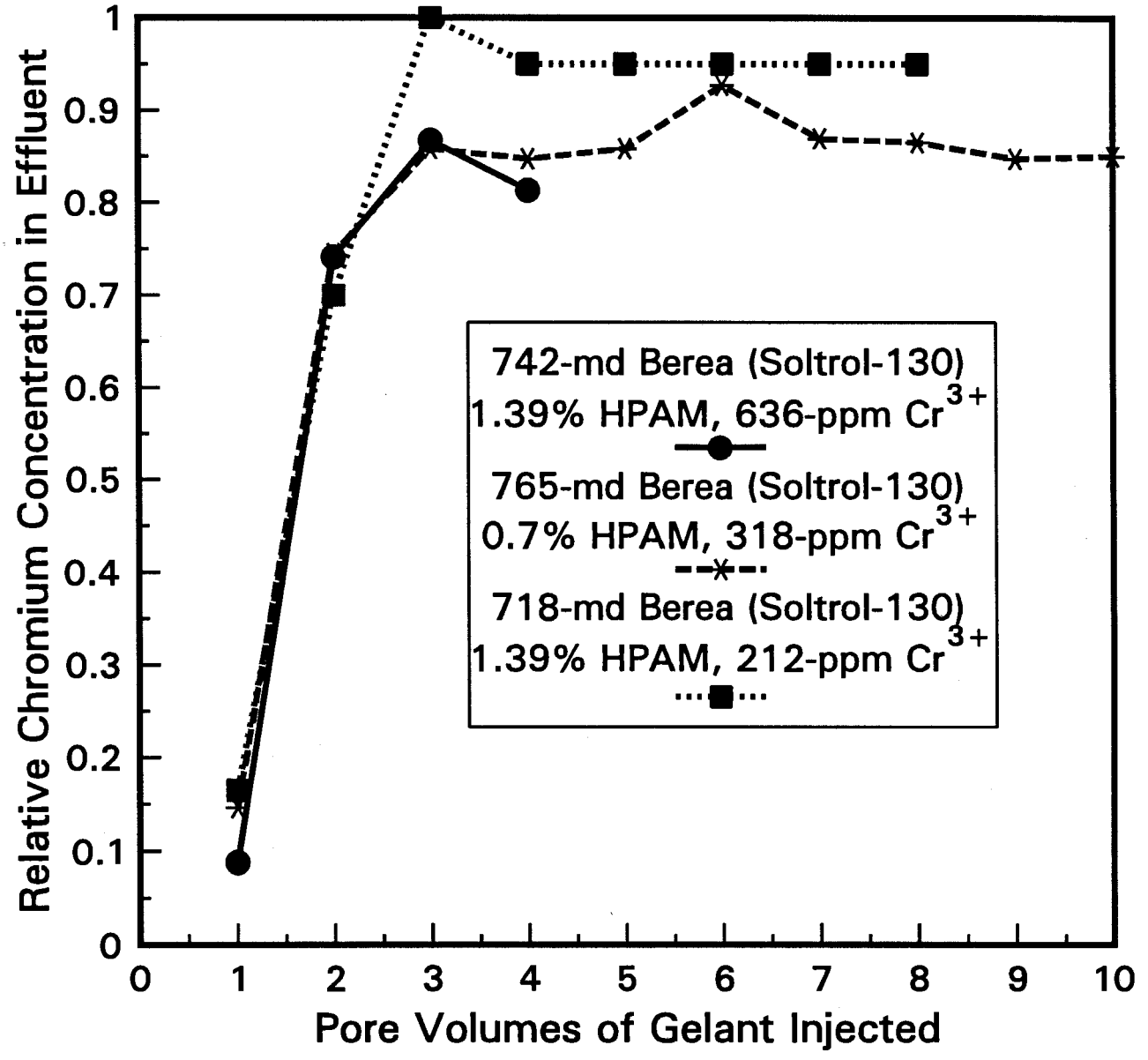

Fig. 12. Chromium propagation through porous media.

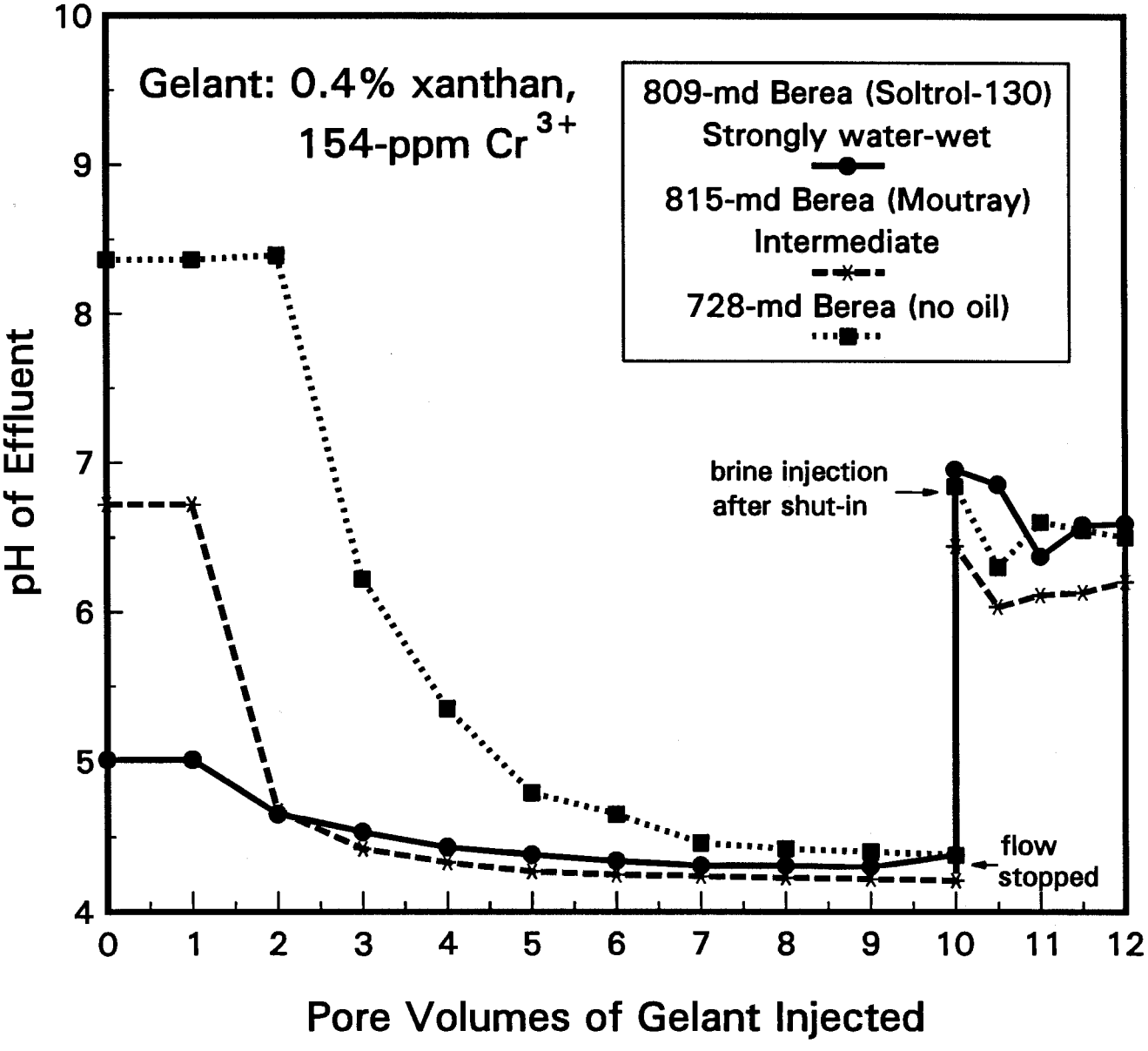

Fig. 13. Effluent pH during gelant injection.

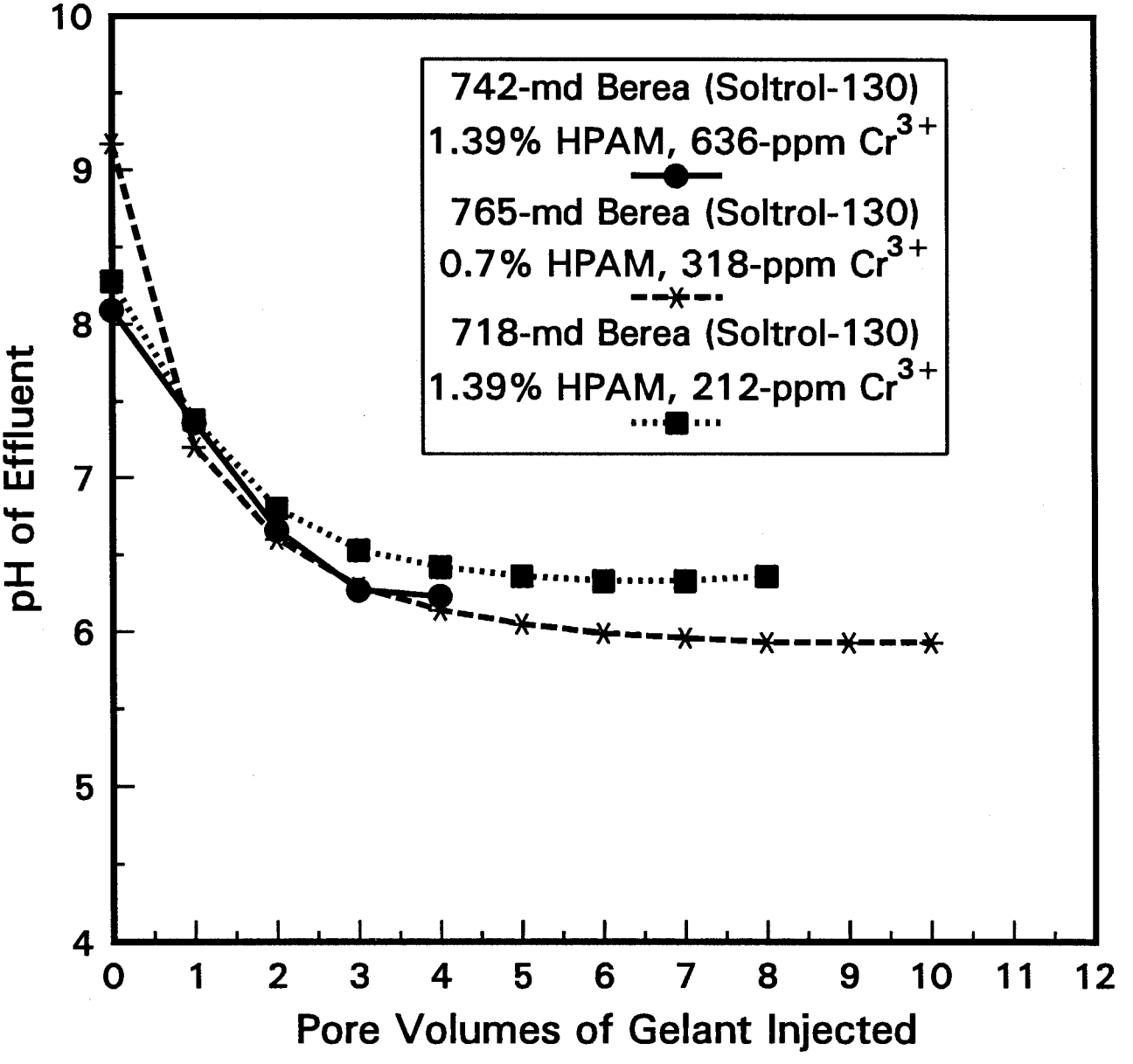

Fig. 14. Effluent pH during gelant injection.

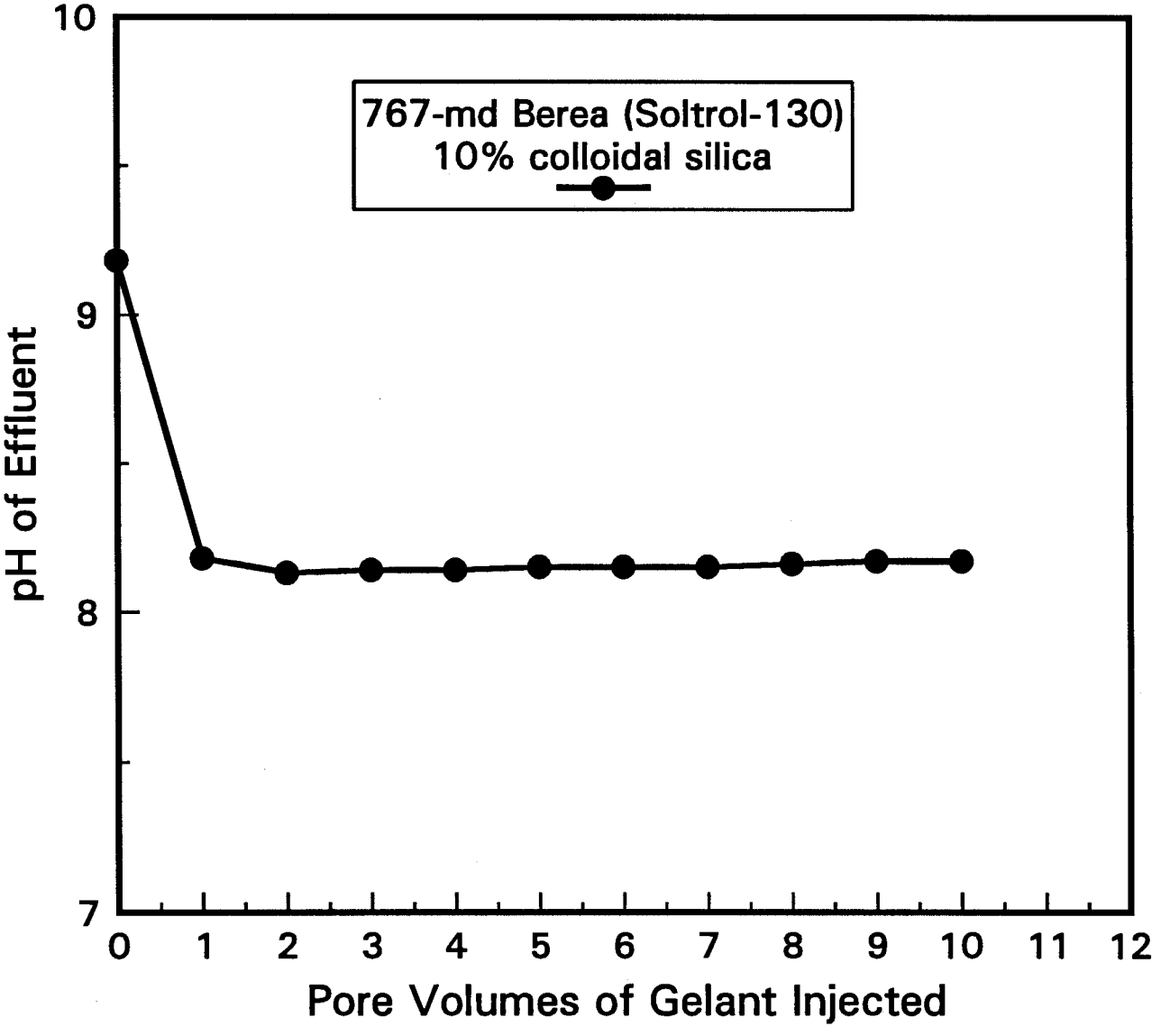

Fig. 15. Effluent pH during gelant injection.

Table 23. Summary of Residual Resistance Factors for Brine (F_{rrw}) and Oil (F_{rro})

Core ID	Wettability	Gel Type	F_{rrw} (Step 13)	F_{rro} (Step 15a)	F_{rrw} (Step 15c)	F_{rro} (Step 16a)	F_{rrw} (Step 16c)	F_{rro} (Step 17a)	F_{rrw} (Step 17c)
SSH-17	Strongly water-wet	resorcinol-formaldehyde	49	11	40	12	41	--	--
SSH-15	Intermediate	resorcinol-formaldehyde	510	26	180	29	241	--	--
SSH-22	Strongly water-wet	Cr^{3+}(chloride)-xanthan	8	5	12	4	8	--	--
SSH-23	Intermediate	Cr^{3+}(chloride)-xanthan	22	14	31	16	42	--	--
SSH-26	Strongly water-wet	1.39% HPAM, 636-ppm Cr^{3+}	40,000	1,020	12,314	148	2,175	100	$409\ u^{-0.43}$
SSH-27	Strongly water-wet	0.7% HPAM, 318-ppm Cr^{3+}	$829\ u^{-0.45}$	20	$117\ u^{-0.29}$	15	$33\ u^{-0.33}$	6	$8.5\ u^{-0.18}$
SSH-31	Strongly water-wet	1.39% HPAM, 212-ppm Cr^{3+}	52,954	50	$972\ u^{-0.50}$	25	$357\ u^{-0.49}$	14	$105\ u^{-0.55}$
SSH-32	Strongly water-wet	colloidal silica	26	23	14	9	12	6	8
SSH-33	Strongly water-wet	colloidal silica	8	16	13	12	10	--	--

u is superficial velocity (in ft/d)

For both the resorcinol-formaldehyde gel and the Cr^{3+}(chloride)-xanthan gel, the F_{rrw} and F_{rro} values were lower for the strongly water-wet cores than for the intermediate-wet cores (see Table 23). Thus, these gels reduced oil and water permeabilities to a greater extent in the intermediate-wet cores than in the strongly water-wet systems. For the Cr^{3+}(chloride)-xanthan gel, the impact of wettability on the ratio, F_{rrw}/F_{rro}, was not significant. However, for the resorcinol-formaldehyde gel, the disproportionate permeability reduction was more pronounced for the system of intermediate wettability than for the strongly water-wet system. A high F_{rrw}/F_{rro} ratio is beneficial in reducing the need for zone isolation during gel placement in production wells.[5] Of course, F_{rro} values greater than one will reduce oil productivity to some extent.

Cr^{3+}(Acetate)-HPAM. For the Cr^{3+}(acetate)-HPAM gel with 1.39% HPAM and 212-ppm Cr^{3+}, results shown in Fig. 16 indicate that the flow of brine in the porous medium exhibited a strong apparent "shear-thinning" behavior where the F_{rrw} decreased with increasing superficial velocity. The residual resistance factors for water, in this case, can be described by a power-law equation, $F_{rrw}=105\ u^{-0.55}$. Fig. 16 also shows that the flow behavior for oil was more or less Newtonian. Three Cr^{3+}(acetate)-HPAM formulations were examined in this study. In all cases, the flow of brine in the porous medium exhibited a strong apparent "shear-thinning" behavior, while the flow of oil remained Newtonian (see Tables B-3e through B-3g). As indicated in Table 23, the relationship between F_{rrw} and superficial velocity, u, can be described using a power-law equation. In some cases, because the residual resistance factors for water were so high, experiments could only be performed at a single, low injection rate. Thus, we were not able to determine, in these cases, how F_{rrw} varied with injection rate. For all the Cr^{3+}(acetate)-HPAM formulations, both F_{rrw} and F_{rro} values were reduced during the subsequent oil-water injection cycles (Table 23).

The largest ratios of F_{rrw} to F_{rro} were observed for the Cr^{3+}(acetate)-HPAM gels. For example, the Cr^{3+}(acetate)-HPAM gel with 1.39% HPAM and 212-ppm Cr^{3+} provided an extremely high F_{rrw} value (53,000) during brine injection immediately after shut-in. During the following oil-water injection cycle, the residual resistance factor for oil (Soltrol-130) was 50, and the residual resistance factors for water can be described by a power-law equation, $F_{rrw}=972\ u^{-0.50}$. After two additional oil-water injection cycles, the F_{rro} value stabilized at 14. At the end, the F_{rrw} values could be described by a power-law equation, $F_{rrw}=105\ u^{-0.55}$. For the same Cr^{3+}(acetate)-HPAM formulation, similar behavior was reported in previous water-CO_2 experiments.[3]

Colloidal Silica. For the colloidal-silica gel, continuous gel breakdown was observed in core SSH-32 during the first brine injection after shut-in. The first F_{rrw} value measured immediately after shut-in at a superficial velocity of 0.023 ft/d was about 3,200 (see Table B-3h). The F_{rrw} values then decreased with increased flow-velocity and eventually stabilized at about 26. Table 23 shows that further gel breakdown occurred during the subsequent oil-water injection cycles. During these experiments, the pressure gradient never exceeded 200 psi/ft. In contrast, in earlier work, Jurinak *et al.*[23] found that pressure gradients above 2500 psi/ft were required to caused gel breakdown. Additional work is needed to explain this finding. The flow behavior for either the refined oil or brine in the porous medium was Newtonian.

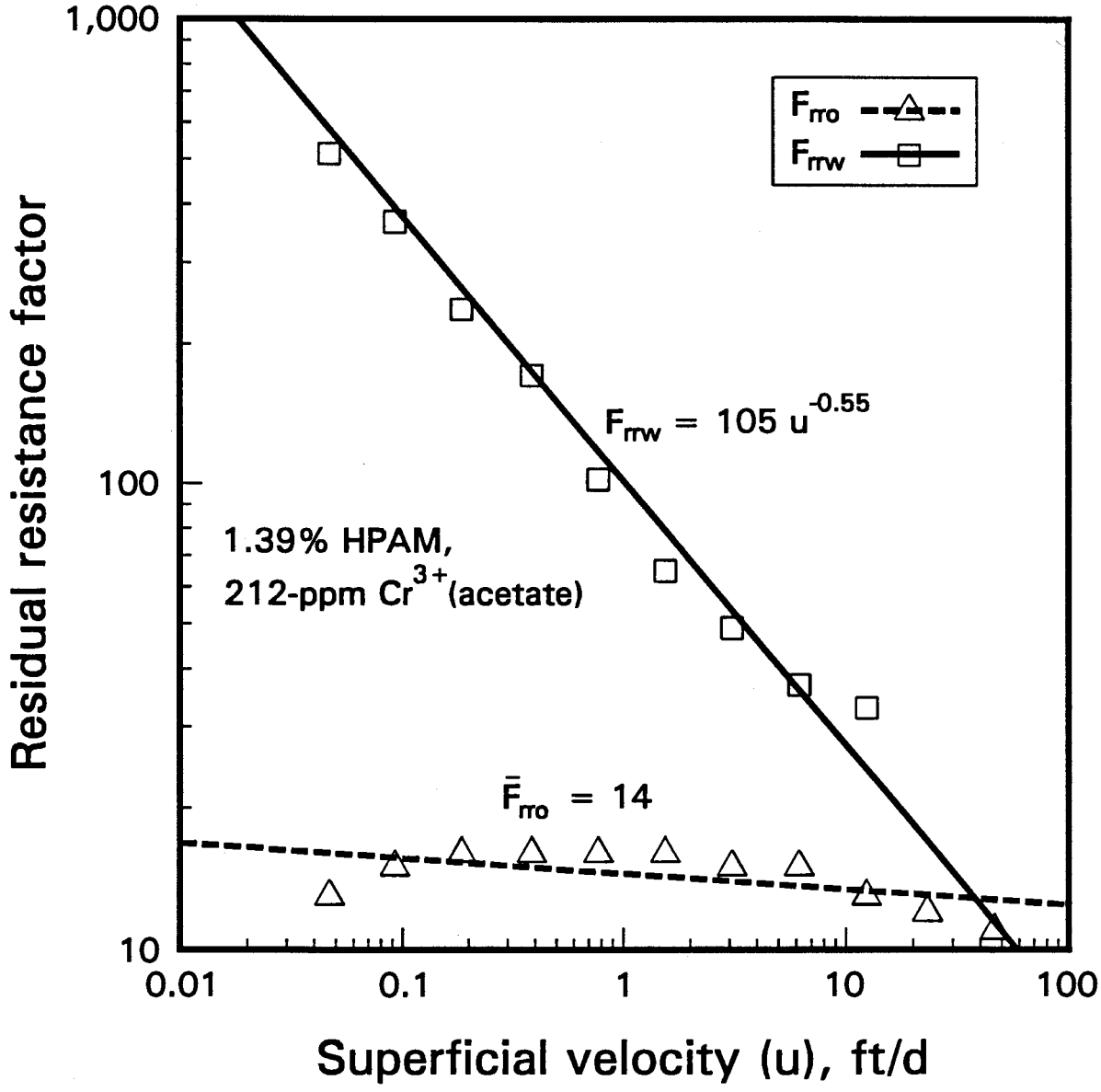

Fig. 16. Apparent rheology during oil and water injection.

Similar behavior was observed for the same colloidal-silica formulation in a separate coreflood experiment (Core SSH-33) where the process of establishing residual oil saturation was modified to study the effect of residual oil saturation on gel performance (see Tables 23 and B-3i). In this case, during the process of establishing residual oil saturation, instead of injecting all the brine at a constant pressure gradient of 200 psi/ft, the first four pore volumes of the brine were injected at a constant rate of 5 ml/hr. Then the remaining brine was injected at a constant pressure gradient of 200 psi/ft.

Table 23 shows that, except for the colloidal-silica gel, all other gels tested in this study reduced water permeability more than oil permeability ($F_{rrw} > F_{rro}$). For the colloidal-silica gel, F_{rrw} and F_{rro} values were about the same during a given oil-water cycle.

Results from Tracer Studies

Tracer studies were performed to determine pore volumes and dispersivities of the cores. Traditional error-function solutions[27] did not fit the tracer curves well during water injection when residual oil was present. In particular, the tracer curve was very asymmetric. Therefore, volume balances were required to determine the fraction of the pore volume that remained open to flow. Fig. 17 presents a schematic diagram of the effluent tracer concentration as a function of the number of pore volumes of tracer injected. This figure illustrates how the effective remaining pore volume, V_p, can be determined from a tracer curve. In Fig. 17, V_p is the number of pore volumes that makes Area A equal to Area B. If the tracer curve was symmetric, then V_p would be associated with a normalized tracer concentration of 0.5.

We did not develop the oil-tracer procedure until after completing the studies of the resorcinol-formaldehyde and Cr^{3+}(chloride)-xanthan gels. Therefore, results from oil-tracer studies are only available for the Cr^{3+}(acetate)-HPAM and the colloidal-silica gels. Results from our tracer studies are summarized in Tables 24 through 37 and in Tables B-4a through B-4n in Appendix B. The ratio, V_p/V_{po}, represents the fraction of the original pore volume sampled by the tracer during a given tracer study. The difference, $1-V_p/V_{po}$, represents the fraction of the original pore volume occupied by the other (immobile) phase and/or gel. The quantity α/α_o refers to the dispersivity during a given tracer study divided by the initial dispersivity of the core (at $S_w=1.0$). The α/α_o (10/90) values were obtained using a mixing zone that extends from 10% to 90% of the injected tracer concentration.[27] The α/α_o (20/50) values were obtained using a mixing zone that extends from 20% to 50% of the injected tracer concentration.[27]

The first parts of Tables 24 through 37 show that prior to gel placement, the S_{wr} and S_{or} values obtained from the oil- and water-tracer studies usually agreed well with those from volumetric measurements. The discrepancies found in the Moutray systems (Tables 24 and 27) were caused by emulsification experienced during the displacement process. The $1-V_p/V_{po}$ values from our first oil-tracer studies were more disparate from the S_{wr} values from volumetric measurements (Tables 31 and 33). The results of pore volume determinations from both oil- and water-tracer studies were reproducible during replicate cycles.

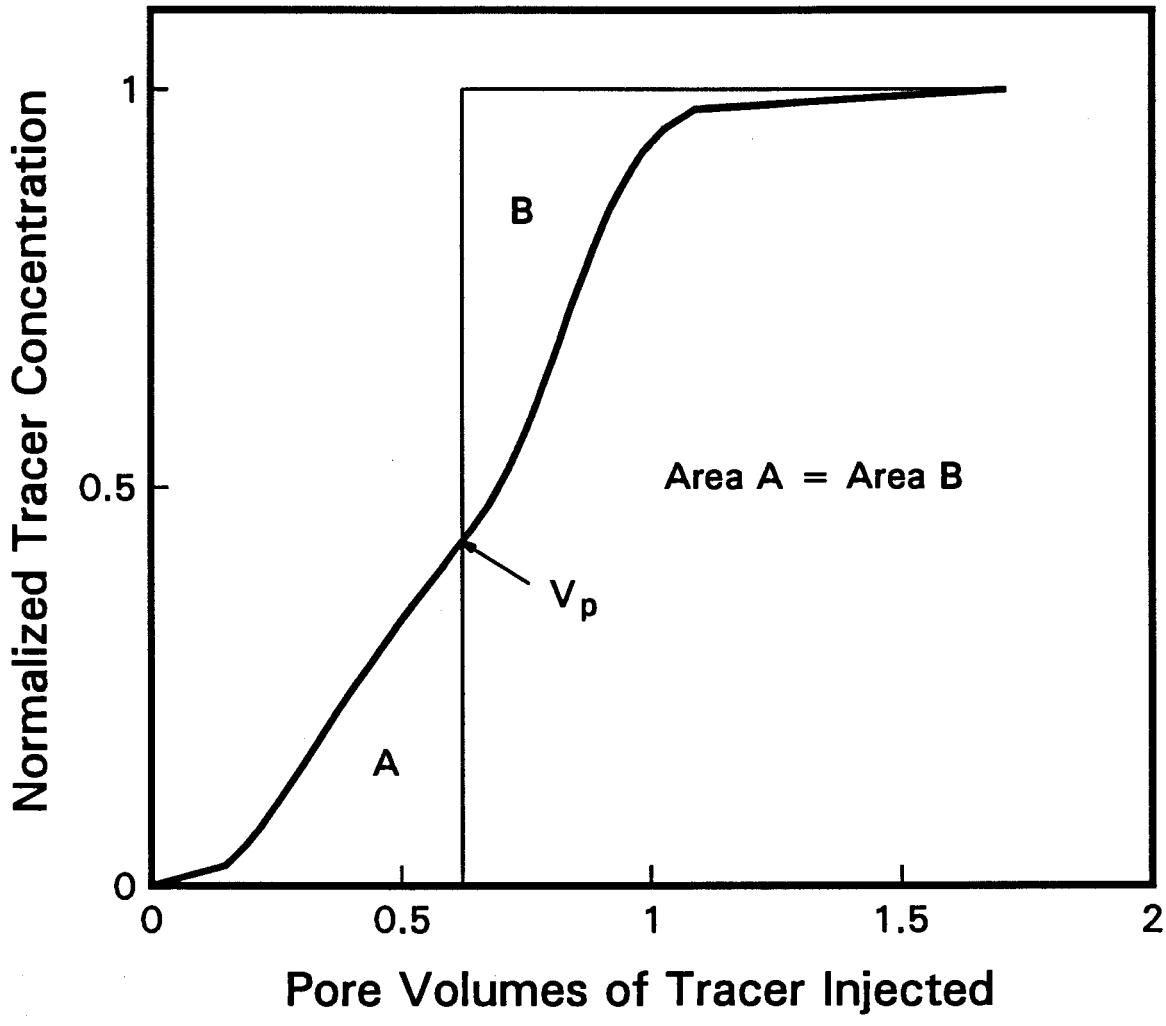

Fig. 17. Schematic diagram of a tracer curve.

Table 24. Pore Volume Determinations from Water-Tracer Studies, Core SSH-15 (Oil Phase: Moutray Crude, Gelant: Resorcinol-Formaldehyde)

Tracer Study	V_p/V_{po}	$1-V_p/V_{po}$	S_{or}
After 1st waterflood (Step 7)*	0.77	0.23	0.26
After 2nd waterflood (Step 8)	0.79	0.21	0.24
After 3rd waterflood (Step 9)	0.83	0.17	0.17
After 4th waterflood (Step 10)	0.83	0.17	0.13

*All steps in this table and subsequent tables are described in Table 19.

Table 25. Pore Volume Determinations from Water-Tracer Studies, Core SSH-17 (Oil Phase: Soltrol-130, Gelant: Resorcinol-Formaldehyde)

Tracer Study	V_p/V_{po}	$1-V_p/V_{po}$	S_{or}
After 1st waterflood (Step 7)	0.72	0.28	0.28
After 2nd waterflood (Step 8)	0.72	0.28	0.29
After 3rd waterflood (Step 9)	0.69	0.31	0.32
After 4th waterflood (Step 10)	0.69	0.31	0.34
1st waterflood after gel treatment (Step 14)	0.63	0.37	0.34
2nd waterflood after gel treatment (Step 15d)	0.38	0.62	--

Table 26. Pore Volume Determinations from Water-Tracer Studies, Core SSH-22 (Oil Phase: Soltrol-130, Gelant: Cr^{3+}-Xanthan)

Tracer Study	V_p/V_{po}	$1-V_p/V_{po}$	S_{or}
After 1st waterflood (Step 7)	0.68	0.32	0.31
After 2nd waterflood (Step 8)	0.67	0.33	0.34
After 3rd waterflood (Step 9)	0.65	0.35	0.33
After 4th waterflood (Step 10)	0.67	0.33	0.33
1st waterflood after gel treatment (Step 14)	0.39	0.61	0.33
2nd waterflood after gel treatment (Step 15d)	0.20	0.80	--
3rd waterflood after gel treatment (Step 16d)	0.19	0.81	--

Table 27. Pore Volume Determinations from Water-Tracer Studies, Core SSH-23 (Oil Phase: Moutray Crude, Gelant: Cr^{3+}-Xanthan)

Tracer Study	V_p/V_{po}	$1-V_p/V_{po}$	S_{or}
After 1st waterflood (Step 7)	0.71	0.29	0.23
After 2nd waterflood (Step 8)	0.77	0.23	0.21
After 3rd waterflood (Step 9)	0.79	0.21	0.20
After 4th waterflood (Step 10)	0.80	0.20	0.18
1st waterflood after gel treatment (Step 14)	0.51	0.49	0.18
2nd waterflood after gel treatment (Step 15d)	0.54	0.46	--

Table 28. Pore Volume Determinations from Water-Tracer Studies,
Core SSH-31 (Oil Phase: Soltrol-130, Gelant: Cr^{3+}(acetate)-HPAM; 1.39% HPAM, 212-ppm Cr^{3+})

Tracer Study	V_p/V_{po}	$1-V_p/V_{po}$	S_{or}
After 1st waterflood (Step 7)	0.72	0.28	0.29
1st waterflood after gel treatment (Step 14)	--	--	0.29
2nd waterflood after gel treatment (Step 15d)	--	--	0.34
3rd waterflood after gel treatment (Step 16d)	0.15	0.85	0.33
4th waterflood after gel treatment (Step 17d)	0.16	0.84	0.33

Table 29. Pore Volume Determinations from Oil-Tracer Studies,
Core SSH-31 (Oil Phase: Soltrol-130, Gelant: Cr^{3+}(acetate)-HPAM; 1.39% HPAM, 212-ppm Cr^{3+})

Tracer Study	V_p/V_{po}	$1-V_p/V_{po}$	S_{wr}
After 1st oilflood (Step 5)	0.72	0.28	0.29
1st oilflood after gel treatment (Step 15b)	0.12	0.88	0.59*
2nd oilflood after gel treatment (Step 16b)	0.14	0.86	0.57*
3rd oilflood after gel treatment (Step 17b)	0.20	0.80	0.55*

* $S_{wr}+S_{gel}$

Table 30. Pore Volume Determinations from Water-Tracer Studies,
Core SSH-26 (Oil Phase: Soltrol-130, Gelant: Cr^{3+}(acetate)-HPAM; 1.39% HPAM, 636-ppm Cr^{3+})

Tracer Study	V_p/V_{po}	$1-V_p/V_{po}$	S_{or}
After 1st waterflood (Step 7)	0.72	0.28	0.27
After 2nd waterflood (Step 8)	0.73	0.27	0.28
After 3rd waterflood (Step 9)	0.74	0.26	0.27
After 4th waterflood (Step 10)	0.73	0.27	0.29
1st waterflood after gel treatment (Step 14)	--	--	0.29
2nd waterflood after gel treatment (Step 15d)	--	--	0.29
3rd waterflood after gel treatment (Step 16d)	--	--	0.36
4th waterflood after gel treatment (Step 17d)	0.09	0.91	0.37

Table 31. Pore Volume Determinations from Oil-Tracer Studies,
Core SSH-26 (Oil Phase: Soltrol-130, Gelant: Cr^{3+}(acetate)-HPAM; 1.39% HPAM, 636-ppm Cr^{3+})

Tracer Study	V_p/V_{po}	$1-V_p/V_{po}$	S_{wr}
After 1st oilflood (Step 5)	0.75	0.25	0.33
After 2nd oilflood (Step 8)	0.76	0.24	0.32
After 3rd oilflood (Step 9)	0.76	0.24	0.32
After 4th oilflood (Step 10)	0.76	0.24	0.31
1st oilflood after gel treatment (Step 15b)	0.04	0.96	0.69*
2nd oilflood after gel treatment (Step 16b)	0.09	0.91	0.60*
3rd oilflood after gel treatment (Step 17b)	0.07	0.93	0.60*

* $S_{wr}+S_{gel}$

Table 32. Pore Volume Determinations from Water-Tracer Studies,
Core SSH-27 (Oil Phase: Soltrol-130, Gelant: Cr^{3+}(acetate)-HPAM; 0.7% HPAM, 318-ppm Cr^{3+})

Tracer Study	V_p/V_{po}	$1-V_p/V_{po}$	S_{or}
After 1st waterflood (Step 7)	0.70	0.30	0.30
1st waterflood after gel treatment (Step 14)	--	--	0.30
2nd waterflood after gel treatment (Step 15d)	0.27	0.73	0.31
3rd waterflood after gel treatment (Step 16d)	0.48	0.52	0.30
4th waterflood after gel treatment (Step 17d)	0.59	0.41	0.31

Table 33. Pore Volume Determinations from Oil-Tracer Studies,
Core SSH-27 (Oil Phase: Soltrol-130, Gelant: Cr^{3+}(acetate)-HPAM; 0.7% HPAM, 318-ppm Cr^{3+})

Tracer Study	V_p/V_{po}	$1-V_p/V_{po}$	S_{wr}
After 1st oilflood (Step 5)	0.75	0.25	0.30
1st oilflood after gel treatment (Step 15b)	0.26	0.74	0.53*
2nd oilflood after gel treatment (Step 16b)	0.32	0.68	0.54*
3rd oilflood after gel treatment (Step 17b)	0.53	0.47	0.47*

* $S_{wr}+S_{gel}$

Table 34. Pore Volume Determinations from Water-Tracer Studies, Core SSH-32 (Oil Phase: Soltrol-130, Gelant: Colloidal Silica)

Tracer Study	V_p/V_{po}	$1-V_p/V_{po}$	S_{or}
After 1st waterflood (Step 7)	0.72	0.28	0.28
1st waterflood after gel treatment (Step 14)	0.02	0.98	0.28
2nd waterflood after gel treatment (Step 15d)	0.07	0.93	0.29
3rd waterflood after gel treatment (Step 16d)	0.14	0.86	0.28
4th waterflood after gel treatment (Step 17d)	0.14	0.86	0.30

Table 35. Pore Volume Determinations from Oil-Tracer Studies, Core SSH-32 (Oil Phase: Soltrol-130, Gelant: Colloidal Silica)

Tracer Study	V_p/V_{po}	$1-V_p/V_{po}$	S_{wr}
After 1st oilflood (Step 5)	0.75	0.25	0.26
1st oilflood after gel treatment (Step 15b)	0.04	0.96	0.61*
2nd oilflood after gel treatment (Step 16b)	0.13	0.87	0.61*
3rd oilflood after gel treatment (Step 17b)	0.17	0.83	0.58*

* $S_{wr}+S_{gel}$

Table 36. Pore Volume Determinations from Water-Tracer Studies, Core SSH-33 (Oil Phase: Soltrol-130, Gelant: Colloidal Silica)

Tracer Study	V_p/V_{po}	$1-V_p/V_{po}$	S_{or}
After 1st waterflood (Step 7)	0.64	0.36	0.34
1st waterflood after gel treatment (Step 14)	0.03	0.97	0.31
2nd waterflood after gel treatment (Step 15d)	0.04	0.96	0.32
3rd waterflood after gel treatment (Step 16d)	0.06	0.94	0.33

Table 37. Pore Volume Determinations from Oil-Tracer Studies, Core SSH-33 (Oil Phase: Soltrol-130, Gelant: Colloidal Silica)

Tracer Study	V_p/V_{po}	$1-V_p/V_{po}$	S_{wr}
After 1st oilflood (Step 5)	0.74	0.26	0.29
1st oilflood after gel treatment (Step 15b)	0.07	0.93	0.63*
2nd oilflood after gel treatment (Step 16b)	0.08	0.92	0.62*

* $S_{wr}+S_{gel}$

Resorcinol-Formaldehyde. For the resorcinol-formaldehyde gel in a strongly water-wet core (Table 25), the water-tracer studies indicate that gel plus oil occupied 37% of the original pore volume immediately after the gel treatment. A comparison of this number with the residual oil saturation (S_{or}=0.34) indicates that the gel occupied only about 3% of the original pore volume. Because this gel provided significant permeability reductions (F_{rrw}= 40 to 49), the small quantity of gel may occupy strategic locations in pore throats. Because of the emulsion problem, no water-tracer study was possible after the gel treatment for the Moutray system (Table 24).

Cr^{3+}(Chloride)-Xanthan. For the Cr^{3+}(chloride)-xanthan gel in a strongly water-wet core (Table 26), a comparison of the water-tracer results and the S_{or} value indicates that the gel occupied 28% of the original pore volume (61% minus 33%). However, results from the subsequent water-tracer study show an increase from 61% to 80% for the pore volume occupied by the gel plus oil. Since no more gelant was injected during the process, this increase can only be attributed to the increase in residual oil saturation. Thus, the gel appears to trap additional oil during the latter oil-water injection cycles. This phenomenon was also observed with the resorcinol-formaldehyde gel (Table 25). The phenomenon was not observed for the case with Cr^{3+}(chloride)-xanthan gel in a core with intermediate wettability (Table 27). Additional work is needed to explain this phenomenon.

Cr^{3+}(Acetate)-HPAM. For the Cr^{3+}(acetate)-HPAM gel with 1.39% HPAM and 212-ppm Cr^{3+}, extremely high residual resistance factors for water precluded water-tracer studies during the first oil-water injection cycles. However, water- and oil-tracer studies were performed throughout the remainder of the study. The pore volume determinations from water-tracer studies and oil-tracer studies are summarized in Tables 28 and 29, respectively. Material balance calculations (Table 28) show an increase in residual oil saturation during the first oil-water injection cycle after gelation (from 29% to 34%). The water-tracer studies and the material balance calculations (last row of Table 28) indicate that gel occupied 51% of the original pore volume after three oil-water injection cycles (84% minus 33%).

The last row in Table 29 shows that the oil tracer sampled only 20% of the original pore volume. However, material balance calculations indicate that gel plus trapped water occupied about 55% of the original pore volume. This means that about 25% of the original pore volume was occupied by immobile oil. This value is near the residual oil saturation before treatment (Table 28). Thus, the gel appears to have encapsulated the original residual oil saturation and rendered it immobile during subsequent oil floods. Similar results were observed for the Cr^{3+}(acetate)-HPAM gel with 1.39% HPAM and 636-ppm Cr^{3+} (Tables 30 and 31).

Comparing the last V_p/V_{po} entries in Tables 28 and 29 suggests that between 16% and 20% of the pore space was open to flow for both oil and water. This result is interesting since F_{rrw} was much larger than F_{rro} at this point in the experiment (i.e., $F_{rrw} = 105\ u^{-0.55}$ and $F_{rro} = 14$, from Table 23).

For the Cr^{3+}(acetate)-HPAM gel with 0.7% HPAM and 318-ppm Cr^{3+}, the results from water-tracer studies and material balance calculations (Table 32) indicate that gel occupied 42% of the original pore volume after the first oil-water injection cycle. However, as a result of gel breakdown, the fraction of the original pore volume occupied by gel was reduced to 10% after two additional oil-water injection cycles. No increase in residual oil saturation was observed during the oil-water injection cycles. The oil-tracer studies and material balance calculations (Table 33) indicate that 21% of the original pore volume was occupied by immobile oil after the first oil injection after gel treatment. However, the last row in Table 33 shows that the amount of oil trapped by gel was reduced to zero after three oil-water

injection cycles. This suggests that the gel gradually lost its ability to encapsulate the original residual oil saturation as the gel breakdown continued throughout the oil-water injection cycles.

Colloidal Silica. For the colloidal-silica gel, the water-tracer studies and material balance calculations (Table 34) indicate that gel occupied about 56% of the original pore volume in core SSH-32 after three oil-water injection cycles (86% minus 30%). Although the gel occupied a significant portion of the original pore space (56%), the permeability reductions were relatively low (F_{rrw}=8, F_{rro}=6, from Table 23). No increase in residual oil saturation was observed during the second oil-water injection cycle. Table 35 shows that the oil tracer sampled only 17% of the original pore volume and the gel plus trapped water occupied 58% of the original pore volume. This means that 25% of the original pore volume was occupied by immobile oil. Thus, the gel seems to have encapsulated oil and rendered it immobile during the oil floods.

Comparing the second V_p/V_{po} entries in Tables 34 and 35 suggests that between 2% to 4% of the pore space was open to flow for both oil and water during the first water and oil injection after gel treatment. In view of these values, the residual resistance factors were surprisingly low for both oil and water (F_{rrw}=26; F_{rro}=23, from Table 23).

For the same colloidal silica formulation in core SSH-33 where the injection strategy was modified during the process of establishing residual oil saturation, a comparison of the first S_{or} entries in Tables 34 and 36 indicates that the residual oil saturation before gelant injection was 6% higher as a result of the change in injection strategy. After gel treatment, additional oil was produced during the first F_{rrw} measurements (see Table 36). The increase in water saturation resulting from the additional oil produced during the first waterflood after gel treatment resulted in a lower F_{rrw} value (Table 23). This suggests that the residual resistance factors are sensitive to the changes in residual saturations.

Water- and oil-tracer curves for tracer studies before and after a gel treatment are shown in Figs. 18 and 19. The quantity, α, shown in Figs. 18 and 19 refers to the dispersivity during a given tracer study. The α values were obtained using a mixing zone that extends from 10% to 90% of the injected tracer concentration.[27] In this case, the Cr^{3+}(acetate)-HPAM gel contained 1.39% HPAM and 212-ppm Cr^{3+}. Fig. 18 shows that the presence of residual oil and/or gel increased dispersivity. In contrast, the oil-tracer studies prior to gelant injection (Fig. 19) indicate that the presence of residual water had a much smaller effect on dispersivity. Relative dispersivities based on both the 10/90 and 20/50 mixing zones[27] are reported in Tables B-4a through B-4n in Appendix B. No significant changes in pore volume and dispersivity were observed as a result of the flow-direction reversal. For all of the cases studied, the presence of a residual oil saturation increased dispersivity. Also, the presence of gel increased dispersivity.

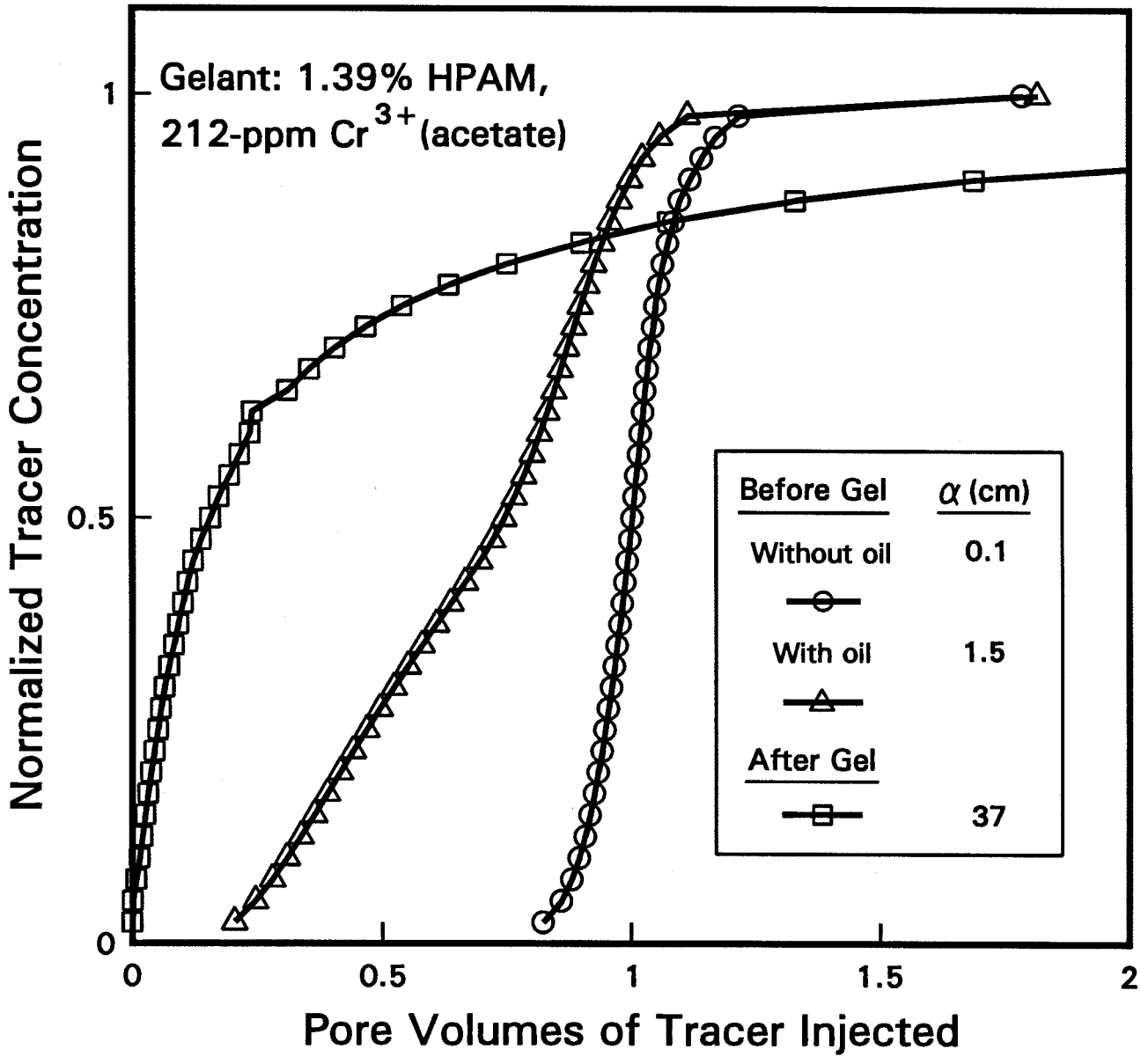

Fig. 18. Effects of residual oil and gel on dispersivities from water tracer studies.

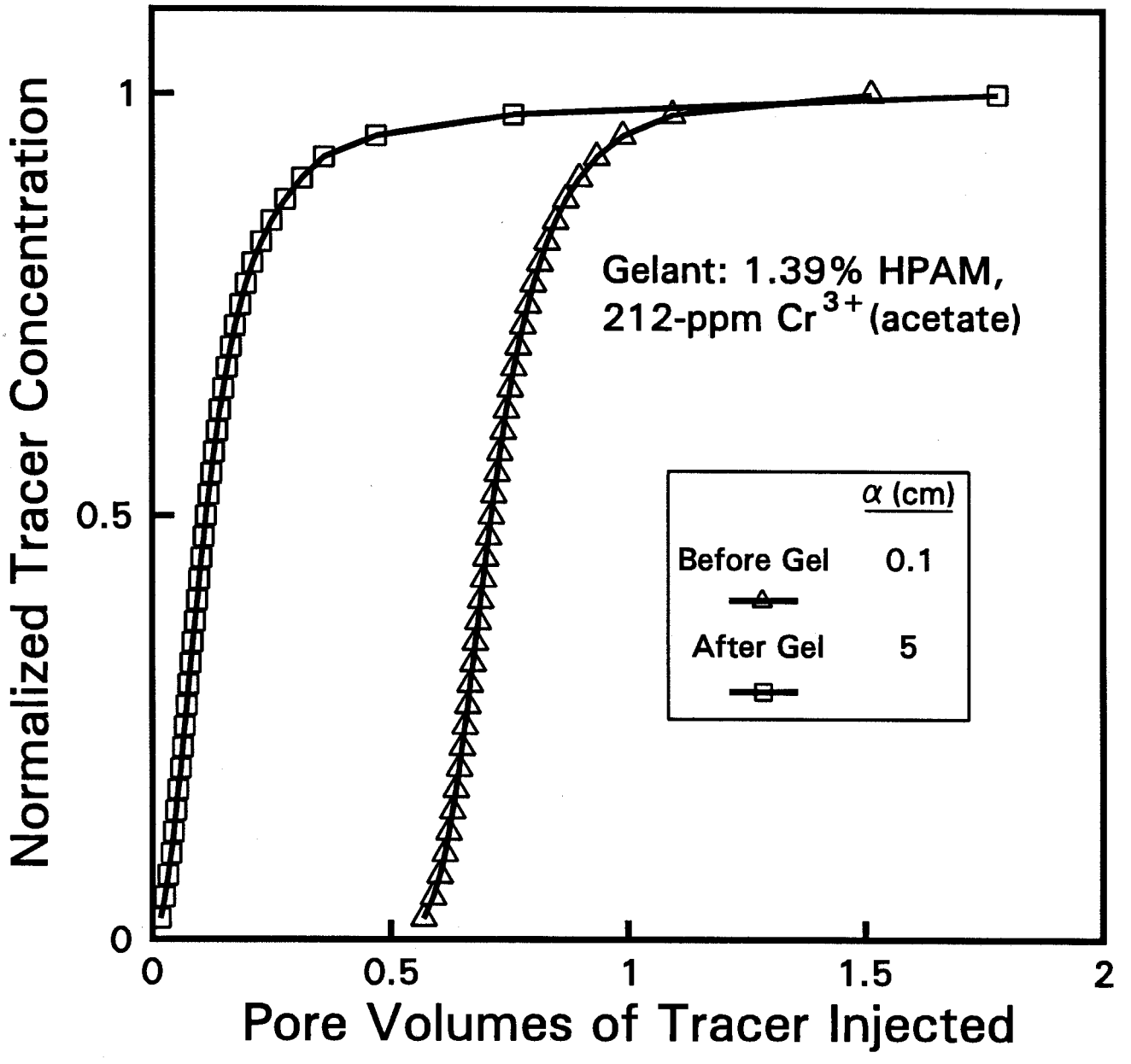

Fig. 19. Effects of residual water and gel on dispersivities from oil tracer studies.

Conclusions

We do not yet have a clear understanding of why some polymers and gels can reduce water permeability more than oil permeability. However, we have introduced some new tools and clues in this quest. First, before gel placement in cores, multiple imbibition and drainage cycles were performed in both flow directions. Results from these studies established that hysteresis of oil and water relative permeabilities were not responsible for the behavior observed during our subsequent gel studies. Second, several gels clearly reduced water permeability significantly more than oil permeability. Whereas previous literature reported this phenomenon for polymers and "weak" polymer-based gels, we also observed the disproportionate permeability reduction with a monomer-based gel (resorcinol-formaldehyde) as well as with both "weak" Cr^{3+}(chloride)-xanthan and "strong" Cr^{3+}(acetate)-HPAM gels. In contrast, a colloidal-silica gel reduced water and oil permeabilities by about the same factor.

Residual resistance factors for several gels were found to erode during multiple cycles of oil and water injection. In spite of this erosion, the disproportionate permeability reduction persisted through the cycles for most of the gels.

The impact of wettability on gel performance was found to vary with the gel. For a resorcinol-formaldehyde gel, the disproportionate permeability reduction was more pronounced in Berea sandstone with an intermediate wettability than in strongly water-wet Berea sandstone. In contrast, the performance of a Cr^{3+}(chloride)-xanthan gel was less sensitive to wettability.

For the Cr^{3+}(acetate)-polyacrylamide gels that were studied, an apparent shear-thinning behavior was observed during brine injection in Berea cores. For other gels, the rheology was more or less Newtonian during brine injection. For all gels investigated, the apparent rheology during oil injection was more or less Newtonian.

Studies using both oil and water tracers provided insight into the fraction of the pore volume occupied by gel. The strongest gels appeared to encapsulate the original residual oil saturation—thus rendering the residual oil inaccessible during subsequent oil flooding. For a Cr^{3+}(acetate)-polyacrylamide gel, the fraction of original pore volume that remained open to oil flow after gel placement was about the same as that for water flow (16% to 20%). However, the residual resistance factor for oil was substantially less than that for water. Also, an apparent shear-thinning behavior was observed during water injection, but Newtonian behavior was observed during oil injection.

In contrast, for a colloidal-silica gel, oil and water residual resistance factors were about the same (i.e., no disproportionate permeability reduction), and Newtonian behavior was observed during both oil and water injection. Tracer studies revealed that, during the first water and oil injection after gel treatment, the fraction of the original pore volume that remained open to the flow of water or oil (2% to 4%) was significantly less than those values for the Cr^{3+}(acetate)-polyacrylamide gel. Surprisingly, the oil and water residual resistance factors were also less for the colloidal-silica gel than for the Cr^{3+}(acetate)-polyacrylamide gel. Additional research will be needed to understand the origins of these unusual effects.

4. REDUCTION OF GAS AND WATER PERMEABILITIES USING GELS

In an earlier investigation, we studied how four different gels reduced permeability to water and compressed carbon dioxide in Berea sandstone (see pages 34-44 of Ref. 3). That investigation raised several issues we address in this section. The earlier study examined a "weak" resorcinol-formaldehyde gel formed at pH 6.5. In the present study, we will report the properties of a "strong" resorcinol-formaldehyde gel formed at pH values from 8.3 to 9.0. These properties will be compared with those of the four gels studied previously.

Several additional questions will be addressed, including:

1. Do endpoint mobilities for CO_2 and brine depend on whether flow is horizontal or vertical?
2. Do continued CO_2 injection or multiple water-alternating-gas cycles erode core properties?
3. Would our experimental results be different if wet CO_2 was used in place of dry CO_2?
4. Is the permeability reduction (residual resistance factor) provided by gel sensitive to the volume of CO_2 or brine injected?
5. Would the experimental results be different if N_2 was used in place of CO_2?
6. Would the results be different if the experiments were performed at 1500 psi rather than at 900 psi?

Gelants Studied

The gels that are studied and compared in this investigation include (1) a resorcinol-formaldehyde gel that was buffered and formed at pH values from 8.3 to 9.0, (2) a resorcinol-formaldehyde gel formed at pH=6.5, (3) a Cr^{3+}-xanthan gel, (4) a Cr^{3+}(acetate)-polyacrylamide gel, and (5) a colloidal-silica gel. The compositions of the five formulations are listed in Table 38. Pfizer provided the xanthan (Flocon 4800®); Marathon provided the polyacrylamide or HPAM (used in the gel, MARCIT®); and DuPont supplied the colloidal silica (Ludox SM®).

Core Preparation

In all core experiments, high-permeability Berea sandstone cores were used. Typically, each core was 14-cm long with a cross-sectional area of 10 cm^2. The cores were cast in a metal alloy (Cerrotru®). Each core had one internal pressure tap that was located approximately 2 cm from the inlet rock face. The first core segment was treated as a filter, while the second core segment (12-cm length) was used to measure mobilities and residual resistance factors. The cores were not fired.

Table 38. Gelant Compositions for High-Pressure Gas Experiments

Gelant Composition	pH
3% resorcinol, 3% formaldehyde, 0.5% KCl, 0.05 M $NaHCO_3$	6.5
3% resorcinol, 3% formaldehyde, 0.5% KCl, 0.05 M $NaHCO_3$	8.3-9.0
0.4% xanthan, 154-ppm Cr^{3+} (as $CrCl_3$), 0.5% KCl	3.8
1.39% HPAM, 212-ppm Cr^{3+} (as acetate), 1% NaCl	5.3-5.9
10% colloidal silica, 0.7% NaCl	8.2

The sequence followed during our core experiments is listed in Table 39. First, at ambient conditions, the cores were saturated with brine and porosities were determined (Step 1 of Table 39). All subsequent steps were performed at 41°C. Most experiments were performed at 900 psi (61 atm), but two floods were performed at 1500 psi (102 atm). The gels investigated at 1500 psi included resorcinol-formaldehyde (formed at pH=9) and Cr^{3+}(acetate)-HPAM. When saturating a given core, the brine composition was the same as that used in preparing the gelant formulation. Unless stated otherwise, the core was mounted so that the flow was horizontal.

Table 39. Sequence Followed During Core Experiments with Compressed Gases*

Step

1. Saturate core with brine and determine porosity.
2. Determine absolute brine permeability and mobility.
3. Perform tracer study to confirm the pore volume (V_{po}) and to determine the core dispersivity (α_o).
4. Inject gas to displace brine and determine gas mobility at residual water saturation.
5. Inject brine to displace gas and determine brine mobility at residual gas saturation.
6. Perform tracer study to determine the fraction of the original pore volume remaining (V_p/V_{po}) and the relative change in dispersivity (α/α_o).
7. Inject gelant using 15.7 ft/d superficial velocity.
8. Shut in core to allow gelation.
9. Inject brine to determine the residual resistance factor for brine (F_{rrw}).
10. Perform tracer study to determine V_p/V_{po} and α/α_o.
11. Inject gas to determine the residual resistance factor for gas (F_{rrgas}).
12. Inject brine to determine F_{rrw}.
13. Perform tracer study to determine V_p/V_{po} and α/α_o.
14. Inject gas to determine F_{rrgas}.
15. Inject brine to determine F_{rrw}.
16. Perform tracer study to determine V_p/V_{po} and α/α_o.
17. Inject gas to determine F_{rrgas}.
18. Inject brine to determine F_{rrw}.
19. Perform tracer study to determine V_p/V_{po} and α/α_o.

* Except for Step 1, all steps were performed at 41°C.

Steps 1 through 6 were performed to characterize permeabilities, porosities, and brine and gas mobilities. Results of these characterizations are listed in Table 40. This table shows that the rock and fluid properties were similar for the eight core experiments. Brine permeability averaged 650 md, and porosity averaged 0.21. During injection with a 900-psi back pressure, the mobility of brine was the same as that at atmospheric pressure.

Tracer studies were routinely performed to characterize pore volumes and dispersivities of the cores. These studies involved injecting a brine bank containing potassium iodide as a tracer. The tracer concentration in the effluent was monitored spectrophotometrically at a wavelength of 230 nm. Usually, four replicates were performed for each tracer study. Also, the replicates included studies performed at different injection rates. An error-function solution[27] fit the tracer curves fairly well for all of the tracer studies described in this work.

Our coreflood apparatus includes an in-line high-pressure spectrophotometer that allows tracer studies to be performed without depressurizing the core. Thus, after the initial saturation of a given core with brine, experiments were conducted entirely at high pressure. Maintenance of a high pressure minimizes complications introduced by gas expansion when cores are depressurized.

Gelant Placement in the Cores

Gelant was injected into a given core (Step 7 in Table 39) using a superficial velocity of 15.7 ft/d. For all of the experiments, gel placement data are summarized in Table 41. In each case, several pore volumes of gelant were injected to ensure that the cores were saturated with gelant (i.e., most of the chemical retention sites in the rock were occupied). Thus, in field applications, the gel properties reported in this study are more relevant to the region behind (upstream of) the front of the gel bank than to the region at the front of the gel bank.

Effluent samples were collected during gelant injection. The samples were allowed to gel, and final gel strength was compared with a gelant that had not been injected into the core. In all cases, the last gelant effluent from the core before shut-in had final gel strengths similar to the non-injected formulations (see Table 41). The system for assessing gel strength was taken from Ref. 24. The codes used in this system are listed in Table 2. The code, J, represents the strongest gel (a rigid, "ringing" gel). The code, I, indicates a rigid gel, and the code, G, indicates a moderately deformable, nonflowing gel.

Table 41 also lists viscosities (at 11 s^{-1}, 41°C) for the gelants shortly after preparation. The resorcinol-formaldehyde gelants, with viscosities near that of water, were the least viscous of the formulations. Viscosities for the colloidal-silica gelant and the Cr^{3+}(acetate)-HPAM gelant were 2.0 cp and 33 cp, respectively. These gelants were found to be Newtonian. The Cr^{3+}-xanthan gelant was the most viscous; its viscosity was 253 cp at 11 s^{-1}. The viscosity exhibited a strong shear-thinning character. Gelation times were estimated by observing the fluidity of gelant in bottles. Gelation times for the gels ranged from 2.4 hours to 18 hours (see Table 41). For gelant that had been forced through a core, gelation times were approximately the same as those for a gelant that was not injected. After injecting a given gelant, the core was shut in for three to five days (Table 41). In all cases, the gelation times were substantially less (by factors ranging from 5 to 40) than the shut-in times. More detailed gelant placement data can be found in Tables 42 through 44 for three of the experiments. For the other experiments, more detailed gelant placement data can be found in Tables 30 through 33 in Ref 3.

Table 40. Rock and Fluid Properties, 41°C

Gelant to be placed in the core	Cr^{3+}-Xanthan	Resorcinol-Formaldehyde				Cr^{3+}(Acetate)-HPAM		Colloidal Silica
pH	3.8	6.5	8.3	9.0	9.0	5.3	5.9	8.2
Core	1	2	3	4	5	6	7	8
Gas used	CO_2	CO_2	CO_2	N_2	CO_2	CO_2	CO_2	CO_2
System pressure, psi	900	900	900	900	1500	900	1500	900
Absolute permeability to brine, md	630	704	811	630	603	605	470	750
Porosity	0.191	0.206	0.229	0.204	0.233	0.232	0.206	0.203
Brine mobility prior to gas, md/cp	940	1050	1210	940	900	930	700	1155
Gas mobility at residual water, md/cp	1760	2200	1867	1430	1700	1830	1200	1680
Brine mobility at residual gas, md/cp	875	960	1071	480	675	884	560	870

Table 41. Gelant Placement Data for Gas Floods

Gelant	Cr^{3+}-Xanthan	Resorcinol-Formaldehyde				Cr^{3+}(Acetate)-HPAM		Colloidal Silica
pH	3.8	6.5	8.3	9.0	9.0	5.3	5.9	8.2
Core	1	2	3	4	5	6	7	8
Gas used	CO_2	CO_2	CO_2	N_2	CO_2	CO_2	CO_2	CO_2
System pressure, psi	900	900	900	900	1500	900	1500	900
Pore volumes of gelant injected	10	3	8	10	10	10	10	10
Gelant viscosity at 41°C, cp at 11 s^{-1}	253	0.67	0.67	0.67	0.67	33	33	2.0
Final gel strength, gelant not injected	G	*	I	I	I	I	H	J
Final gel strength, gelant effluent from core	G	*	I	I	I	I	H	J
Gelation time at 41°C in a bottle, days	0.42	0.25	0.10	0.17	0.17	0.75	0.75	0.21
Shut-in time, days	5	3	4	4	3	4	4	5

* Product could be described better as a precipitate than as a gel.

Table 42. Placement of Resorcinol-Formaldehyde Gelant in Core 4

Pore volumes injected	0	1	2	3	4	5	6	7	8	9	10
F_r in first core segment	1.0	1.0	1.0	1.1	1.2	1.3	1.5	1.6	1.7	1.9	2.0
F_r in second core segment	1.0	1.1	1.1	1.2	1.2	1.2	1.2	1.2	1.3	1.3	1.4
Effluent pH	8.63	8.63	8.38	8.45	8.38	8.40	8.49	8.57	8.66	8.74	8.77
Gel Code	A	B	H	I	I	I	I	I	I	I	I

Table 43. Placement of Resorcinol-Formaldehyde Gelant in Core 5

Pore volumes injected	0	1	2	3	4	5	6	7	8	9	10
F_r in first core segment	4.8	6.0	6.8	7.3	7.5	8.1	8.6	9.3	10.2	11.4	11.8
F_r in second core segment	1.1	1.4	1.5	1.6	1.7	1.8	1.9	1.9	1.9	1.9	1.9
Gel Code	A	G	I	I	I	I	I	I	I	I	I

Table 44. Placement of Cr^{3+}(Acetate)-Polyacrylamide Gelant in Core 7

Pore volumes injected	0	1	2	3	4	5	6	7	8	9	10
F_r in first core segment	1.0	27	29	30	31	32	34	35	36	37	38
F_r in second core segment	1.0	17	32	36	37	39	40	43	44	46	47
Effluent $[Cr^{3+}]/[Cr^{3+}]_o$	0	0.05	0.46	0.88	0.92	0.95	1.00	0.99	0.96	0.99	1.00
Effluent pH	7.40	7.40	7.00	6.33	6.27	6.23	6.21	6.17	6.18	6.14	6.08
Gel Code	A	A	B	G	H	H	H	H	H	H	H

Residual Resistance Factors

Following the shut-in period, brine was injected (Step 9 in Table 39) to determine the residual resistance factor for brine (F_{rrw}). These F_{rrw} values were determined by dividing brine mobility (at residual gas saturation) before gel placement by brine mobility after gel placement. Usually, these residual resistance factors were determined as a function of injection rate.

After measuring F_{rrw} values, tracer studies (Step 10 in Table 39) were performed to determine the new dispersivity of the core and the fraction of the pore volume that remained available to flow. Next, gas was injected to determine the residual resistance factors for gas (F_{rrgas}, F_{rrCO2}, F_{rrN2}). These F_{rrgas} values were determined by dividing gas mobility (at residual water saturation) before gel placement by gas mobility after gel placement. These values were also measured as a function of injection rate.

After finding F_{rrgas} values, brine was injected to redetermine F_{rrw} values. Also, another tracer study was performed. For most of the gel systems, the water-alternating-gas cycle of gas injection, brine injection, and tracer studies were repeated two more times. Residual resistance factors from these experiments are summarized in Table 45. For four of the experiments, a detailed listing of results is included in Appendix C. For the other four experiments, a detailed listing of results is included in Appendix C of Ref. 3. In all cases, these residual resistance factors apply to the second core segment. In each table in Appendix C of this report and in Appendix C of Ref. 3, the data are presented in the chronological order in which they were collected.

For all core experiments, the highest residual resistance factors were obtained during the first brine injection after gelation. In agreement with our previous work,[28,37] relatively low residual resistance factors were found for the Cr^{3+}-xanthan gel and the resorcinol-formaldehyde gel formed at pH=6.5. Extremely high residual resistance factors were obtained for the resorcinol-formaldehyde gel formed at pH values from 8.3 to 9.0, the Cr^{3+}(acetate)-HPAM gels, and the colloidal-silica gel. These very high F_{rrw} values were anticipated based on previous work.[23,24,28]

Table 45 shows that for all of the gels investigated, the residual resistance factors decreased sharply when compressed gas was injected. During gas injection, F_{rrgas} values sometimes decreased with increased injection rate (e.g., see Tables C-1b, C-1d, and C-1f in Appendix C). However, when velocities were subsequently reduced, the F_{rrgas} values appeared more or less Newtonian. This behavior suggests that the decrease in F_{rrgas} with increasing velocity may be a result of gel breakdown.

In a previous report,[3] the following conclusions were reached after testing four gels:

1. All four gels can reduce water permeability in Berea sandstone to a greater extent than CO_2 permeability.

2. All four gels experienced some breakdown during a water-alternating-gas cycle.

3. For the polymer-based gels, an apparent shear-thinning behavior was observed during brine injection.

4. During CO_2 injection, the apparent rheology in porous media was more or less Newtonian for all four gels.

Table 45. Summary of Residual Resistance Factors for Brine (F_{rrw}) and Compressed Gas (F_{rrgas})

Gelant	Cr^{3+}-Xanthan	Resorcinol-Formaldehyde				Cr^{3+}(Acetate)-HPAM		Colloidal Silica
pH	3.8	6.5	8.3	9.0	9.0	5.3	5.9	8.2
Core	1	2	3	4	5	6	7	8
Gas used	CO_2	CO_2	CO_2	N_2	CO_2	CO_2	CO_2	CO_2
System pressure, psi	900	900	900	900	1500	900	1500	900
F_{rrw} during 1st WAG (Step 9)	417 $u^{-0.38}$	7	21,600	10,400	19,600	272,000	4970 $u^{-0.72}$	32,000
F_{rrgas} during 1st WAG (Step 11)	12	2	101	126	17	500	148	400
F_{rrw} during 2nd WAG (Step 12)	23	5	570	520	23	1720 $u^{-0.72}$	472 $u^{-0.48}$	3,800
F_{rrgas} during 2nd WAG (Step 14)			60	64	14	50	64	380
F_{rrw} during 3rd WAG (Step 15)			400	484	18	549 $u^{-0.58}$	177 $u^{-0.43}$	2,600
F_{rrgas} during 3rd WAG (Step 17)			57	61	11	13	34	290
F_{rrw} during 4th WAG (Step 18)			361	370	20	131 $u^{-0.47}$	94 $u^{-0.43}$	1,800

Note: u is superficial velocity of brine in units of ft/d.

These conclusions remain unchanged upon consideration of the results from our new studies. However, the new studies provide some interesting additional insights. In particular, note the similarity in behavior for the results from Cores 3 and 4 in Table 45. Both of these experiments involved resorcinol-formaldehyde gels and a system pressure of 900 psi. In one case, compressed CO_2 was injected, while compressed N_2 was used in the other case. The similarity in results suggests that the observed behavior is not sensitive to the type of gas used. To expand on this point, (1) for both compressed CO_2 and compressed N_2, the gel can reduce brine permeability significantly more than gas permeability, and (2) multiple water-alternating-gas (WAG) cycles degrade the residual resistance factors to about the same extent for CO_2 as for N_2. These results are especially interesting considering the corrosive nature of CO_2 and the inert nature of N_2.

Most of our experiments were performed at 900 psi. This pressure was selected because the upper pressure limit for our in-line spectrophotometer was stated by the manufacturer to be 1000 psi. However, concern was expressed that the behavior of CO_2 at 900 psi (where CO_2 density is 0.156 g/cm^3) might be much different than that for CO_2 at 1500 psi (where CO_2 density is 0.641 g/cm^3). Therefore, we performed two experiments at 1500 psi—one using a resorcinol-formaldehyde gel (at pH=9) and one using a Cr^{3+}(acetate)-HPAM gel.

For the resorcinol-formaldehyde gel, a comparison of the results from Cores 3 and 5 in Table 45 suggests that gel breakdown during the first WAG cycle is more severe at 1500 psi than at 900 psi. However, gel breakdown at 1500 psi is less evident during subsequent WAG cycles. At both pressures, residual resistance factors for water are consistently greater than those for gas.

For the Cr^{3+}(acetate)-HPAM gel, a comparison of the results from Cores 6 and 7 in Table 45 reveals many similarities in behavior at the two pressures. At both pressures, (1) Newtonian behavior is observed during CO_2 injection; (2) an apparent shear-thinning behavior is observed during brine injection; (3) resistance factors are consistently greater for brine than for CO_2; and (4) residual resistance factors decrease during multiple WAG cycles. However, gel breakdown during multiple WAG cycles appears to be less severe at 1500 psi than at 900 psi. Overall, the behavior at 1500 psi does not appear to be radically different from that at 900 psi.

High-Pressure Visualization Experiments

High-pressure visualization experiments were performed to determine whether macroscopic changes in the gels could be observed during exposure to water, oil (Soltrol 130®), and CO_2 at 1500 psi. Two gels were studied during these experiments—a resorcinol-formaldehyde gel (formed at pH=9) and a Cr^{3+}(acetate)-HPAM gel (formed at pH=5.8). Compositions of these gels are indicated in Table 38. For the Cr^{3+}(acetate)-HPAM case, 60 ml of gelant was placed in a high-pressure visualization cell (~100 ml total volume) and allowed to gel for several days at 41°C. After gelation, the cell was pressurized with water to 1500 psi. The gel shrank very slightly during this pressurization. After observing the gel for 24 hours, the water was replaced by oil without depressurization. The gel was then observed for another day at 1500 psi and 41°C. This procedure was repeated using the following sequence of fluids to contact the gel: brine, oil, brine, oil, CO_2, brine, CO_2, oil. The gel showed no significant changes during these procedures. When the cell was depressurized, gas boiled out from the gel, causing the gel to fracture. Similar results were observed during exposure of the resorcinol-formaldehyde gel to brine-CO_2 cycles. Thus, no significant macroscopic changes were observed for the gels when exposed to brine, CO_2, or oil at 1500 psi.

Results from Tracer Studies

The results from our tracer studies are listed in Tables 46 and 47. In Table 46, V_p/V_{po} refers to the fraction of the original pore volume that was sampled by the iodide tracer during a given tracer study. The difference, $1-V_p/V_{po}$, provides an indication of the fraction of the original pore volume that was occupied by gel and/or gas. The original pore volume of a given core (V_{po}) was typically about 30 cm^3.

Tracer studies provide interesting insights about the fraction of the total pore volume that was occupied by gel and/or gas. Step 6 in our procedure was a tracer study performed after reaching a residual gas saturation but before gelant injection. Results from this step indicate that the residual gas saturation (either CO_2 or N_2) was quite low—ranging from 0 to 0.08 (see the top data line of Table 46).

Step 10 in our procedure provided tracer results during brine injection after gelation. For the resorcinol-formaldehyde gels in Cores 2 and 3, the V_p/V_{po} values were 0.35 and 0.58, respectively (Table 46). This suggests that the gels (plus the residual CO_2) occupied 65% and 42% of the original pore space, respectively. Surprisingly, the weak resorcinol-formaldehyde gel formed at pH=6.5 apparently occupied a larger fraction of the pore volume than the strong resorcinol-formaldehyde gel formed at pH=8.3. We can only speculate about why this occurred. Perhaps more of the gel was located in pore throats for the gel formed at pH=8.3 than for the gel formed at pH=6.5. During the tracer study after the first WAG cycle (Step 13), V_p/V_{po} increased for the gels. Possibly, this increase indicates that some gel may have washed out of the core during the WAG cycle between Steps 10 and 13.

A comparison of the results in Table 46 for Cores 3 and 4 indicates that the gel generally occupied less pore volume during the CO_2 experiment than during the corresponding N_2 experiment. Since very similar residual resistance factors were observed during these experiments, we can only speculate that the location of the gel in the pores is different for the different cases.

For the Cr^{3+}(acetate)-HPAM gel at 900 psi (in Core 6), the extremely high residual resistance factor (272,000) precluded a tracer study during Step 10. Tracer studies were successfully performed after the first, second, and third WAG cycles. The values for V_p/V_{po} were 0.40, 0.68, and 0.78, respectively. This increase with successive WAG cycles may be related to gel breakdown. These tracer results were qualitatively similar for the Cr^{3+}(acetate)-HPAM gel at 1500 psi (see results for Core 7 in Table 46).

For the colloidal-silica gel, the tracer study after gel placement (Step 10) indicated that the tracer sampled virtually all of the original pore volume (i.e., $V_p/V_{po}=1$). This observation is consistent with earlier reports.[23] In view of the very high F_{rrw} value (32,000), the tracer during Step 10 appears to have propagated through the gel matrix in the core (rather than flowing around gel particles in the porous medium). This behavior is very different from that observed with the other gels, where the gels appear to be impermeable to the aqueous tracer during the course of the tracer experiments. During subsequent tracer studies with the colloidal-silica gel (Steps 13, 16, and 19), the V_p/V_{po} values were less than 1. Perhaps, this decrease results from the gel breakdown that occurs during the WAG cycles. Gel breakdown could form flow paths around (rather than through) the gel.

Table 46. Pore Volume Determinations (V_p/V_{po}) from Tracer Studies

Gelant	Cr^{3+}-Xanthan	Resorcinol-Formaldehyde				Cr^{3+}(Acetate)-HPAM		Colloidal Silica
pH	3.8	6.5	8.3	9.0	9.0	5.3	5.9	8.2
Core	1	2	3	4	5	6	7	8
Gas used	CO_2	CO_2	CO_2	N_2	CO_2	CO_2	CO_2	CO_2
System pressure, psi	900	900	900	900	1500	900	1500	900
V_p/V_{po} at residual gas, before gel (Step 6)	0.99	0.94	0.92	1.00	1.02	0.99	1.04	1.00
V_p/V_{po} after gel (Step 10)	0.21	0.35	0.58	--	0.79	--	0.48	1.00
V_p/V_{po} after gel, after 1st WAG (Step 13)	0.24	0.42	0.77	0.48	0.76	0.40	0.65	0.64
V_p/V_{po} after gel, after 2nd WAG (Step 16)			0.77	0.44	0.76	0.68	0.66	0.70
V_p/V_{po} after gel, after 3rd WAG (Step 19)			0.79	0.47	0.75	0.78	0.73	0.74

Table 47. Relative Dispersivities (α/α_o) from Tracer Studies

Gelant	Cr^{3+}-Xanthan	Resorcinol-Formaldehyde				Cr^{3+}(Acetate)-HPAM		Colloidal Silica
pH	3.8	6.5	8.3	9.0	9.0	5.3	5.9	8.2
Core	1	2	3	4	5	6	7	8
Gas used	CO_2	CO_2	CO_2	N_2	CO_2	CO_2	CO_2	CO_2
System pressure, psi	900	900	900	900	1500	900	1500	900
α_p/α_{po} at residual gas, before gel (Step 6)	1.0	0.9	1.2	1.1	1.0	1.0	1.1	0.9
α_p/α_{po} after gel (Step 10)	31	12	124	--	8	--	18	4
α_p/α_{po} after gel, after 1st WAG (Step 13)	25	11	8	312	3	49	12	20
α_p/α_{po} after gel, after 2nd WAG (Step 16)			12	181	3	38	12	20
α_p/α_{po} after gel, after 3rd WAG (Step 19)			10	133	3	21	12	15

Table 47 lists dispersivity results obtained during the tracer studies. The quantity α/α_o refers to the final dispersivity during tracer injection after gelation divided by the initial dispersivity value. Initial dispersivity values (α_o) for the Berea cores were approximately 0.1 cm. Before gelant injecton, the gas saturation (either CO_2 or N_2) did not significantly change the dispersivity of the core. [See the top data line of Table 47. The variation among these numbers is less than the standard deviation associated with a dispersivity measurement (typically $\pm 30\%$).] Dispersivity values after gelation were invariably much greater than those before gel placement. Qualitatively, this increase in dispersivity means that the gels broaden the range of flow paths through the porous medium. Gels could create some short pathways simply as a consequence of filling the pore space. On the other hand, longer flow paths could result if the gel acts as a medium that is permeable to the brine. We note that the highest dispersivity values were obtained for the experiments where N_2 was used.

Effects of Gas and Water Injection Before Gelant Injection

This subsection will address the following three questions concerning the effects of gas and water injection before gelant placement:

1. Do endpoint mobilities for gas (CO_2 or N_2) and brine depend on whether flooding occurs horizontally or vertically?

2. Do continued CO_2 injection or multiple water-alternating-gas cycles erode the properties of the core (e.g., by increasing porosity or permeability)?

3. Would the results from our experiments be significantly different if wet CO_2 (CO_2 saturated with water prior to injection) was used in place of dry CO_2?

To answer these questions, we performed a number of experiments with CO_2 and a Berea sandstone core that had a permeability of 804 md and a porosity of 0.206. These experiments were performed at 41 °C and 900 psi. Alternating slugs of brine and gas were injected. The slug sizes varied from 10 to 100 pore volumes. Table 48 lists the results of the CO_2 experiments in the chronological order in which they were obtained. Each time brine was injected, a tracer study was performed to determine the percent of the original pore volume (% of PV) that was open to flow and the relative dispersivity, α/α_o. (The original core dispersivity, α_o, was 0.0473 cm.) These values are listed in Table 48.

The first experiments were performed with the core oriented horizontally. The endpoint mobilities for CO_2 (dry) and brine were 2118 md/cp and 1250 md/cp, respectively (see Entries 2 and 3 in Table 48). In similar experiments performed earlier (see Table 40), mobilities in this type of rock ranged from 1680 md/cp to 2200 md/cp for CO_2 and from 870 to 1071 md/cp for brine.

For the experiments where the cores were mounted vertically, the fluid was injected into the top of the core and produced from the bottom. The endpoint CO_2 mobilities (after 10 pore volumes of injection) were 2213 md/cp and 1871 md/cp for wet and dry CO_2, respectively (Entries 5 and 8 in Table 48). These values are not significantly different from the horizontal value (Entry 2—2118 md/cp).

For vertical flow, the endpoint mobility for brine was 927 md/cp (Entry 4 in Table 48). This value is 26% less than that for horizontal flow (Entry 3), and this difference is statistically significant. However, it is not obvious that vertical flow should be preferred to horizontal flow in our experiments.

Table 48. Summary of Results During Injection of CO_2 and Brine Before Gel Placement

Entry	Injectant	Flow Direction	Pore Volumes Injected	Fluid Mobility, md/cp	% of PV Open to Flow	α/α_o
1	Brine (no CO_2 saturation)	horizontal	15	1200	100	1.0
2	Dry CO_2 (@ residual water)	horizontal	10	2118		
3	Brine (@ residual CO_2)	horizontal	10	1250	98	1.0
4	Brine (@ residual CO_2)	vertical	10	927	99	1.2
5	Wet CO_2 (@ residual water)	vertical	10	2213		
6	Wet CO_2 (@ residual water)	vertical	100	2947		
7	Brine (@ residual CO_2)	vertical	13	915	99	1.0
8	Dry CO_2 (@ residual water)	vertical	10	1871		
9	Dry CO_2 (@ residual water)	vertical	100	4163		
10	Brine (@ residual CO_2)	vertical	27	841	98	1.3

Total pore volumes injected: 75 PV for brine; 210 PV for CO_2.

Experiments were also performed to assess whether the throughput of CO_2 affected the endpoint mobilities. In these experiments, mobilities were monitored during the course of injecting 100 pore volumes of compressed CO_2. The results are presented in Table 49. For both wet and dry CO_2, the mobilities averaged around 2200 md/cp during injection of the first 40 pore volumes. Between 40 and 60 pore volumes, the mobilities experienced a significant increase for both wet and dry CO_2. This increase in mobility may have resulted because CO_2 eventually stripped the residual water from the core. Of course, if this explanation is accepted, then our wet CO_2 must not have been totally saturated with water. After injecting 100 pore volumes, we note that the mobility for dry CO_2 was significantly higher than that for wet CO_2 (4163 md/cp versus 2947 md/cp). This difference may be due to the different moisture contents for the CO_2 gases.

Perhaps, the most important result of this set of experiments is that CO_2 throughput had little effect on mobilities during the first 40 pore volumes of injection for either wet or dry CO_2. Also, the endpoint mobility values and the tracer results do not suggest that the sequence of CO_2 and brine injection described in Table 48 had a permanent (or irreversible) effect on the permeability or porosity of the core.

Table 49. Mobilities of Wet and Dry CO_2 vs. Pore Volumes Injected

Pore Volumes Injected	10	20	30	40	50	60	70	80	90	100
Mobility of Wet CO_2, md/cp	2213	2219	2138	2260	2793	2683	2038	2900	3000	2947
Mobility of Dry CO_2, md/cp	1871	2229	2066	2212	2150	3206	3705	4308	4195	4163

A set of experiments was also performed to compare the endpoint mobilities for N_2 and water with those for CO_2 and water. These experiments were performed at 41°C and 900 psi using Core 4. The results are summarized in Table 50. Dry N_2 was used during these experiments. The first experiments were performed with the core oriented horizontally. The endpoint mobilities for N_2 and brine were 1430 md/cp and 480 md/cp, respectively (see Entries 2 and 3 in Table 50). Both of these values were noticably less than those for the CO_2 experiments (2118 md/cp and 1250 md/cp, respectively, from Entries 2 and 3 in Table 48). The reason may be related to solubility differences. Since the equilibrium water-vapor content is greater in CO_2 than in N_2, perhaps the residual liquid water saturation in the core after injecting 10 PV of gas is lower for dry CO_2 injection than for dry N_2 injection. A higher endpoint gas mobility would then be associated with the lower residual water saturation (e.g., 2118 md/cp for CO_2 vs. 1430 md/cp for N_2). (Incidently, since the viscosity of compressed CO_2 is greater than compressed N_2, we might have expected the endpoint gas mobility to be less for CO_2 than for N_2.)

To explain why the endpoint water mobility appears to be greater for CO_2 than for N_2 (1250 md/cp vs. 480 md/cp), recall that gas solubility in water is greater for CO_2 than for N_2. Perhaps the residual gas saturation after injecting 10 PV of water is lower for CO_2 than for N_2. A higher endpoint water mobility would then be associated with the lower residual gas saturation. The latter explanation is not consistent with our tracer results, but our tracer studies are probably not precise enough to distinguish between saturation differences that are less than a few percent.

Table 50. Summary of Results During Injection of N_2 and Brine Before Gel Placement

Entry	Injectant	Flow Direction	Pore Volumes Injected	Fluid Mobility, md/cp	% of PV Open to Flow	α/α_o
1	Brine (no N_2 saturation)	horizontal	13	940	100	1.0
2	Dry N_2 (@ residual water)	horizontal	10	1430		
3	Brine (@ residual N_2)	horizontal	10	480	100	1.1
4	Brine (@ residual N_2)	vertical	14	328	99	1.4
5	Dry N_2 (@ residual water)	vertical	10	600		
6	Brine (@ residual N_2)	vertical	10	194	100	1.5

Total pore volumes injected: 47 PV for brine; 20 PV for N_2.

Experiments were also performed to assess the effects of core orientation on endpoint mobilities. When the core was oriented vertically (Entries 5 and 6), the endpoint mobilities for both N_2 and brine were noticably less than those when the core was oriented horizontally. The tracer studies indicated that the N_2 gas occupied a very small fraction of the pore volume and had a very small effect on the dispersivity of the core.

Effects of CO_2 and Water Injection After Gelation

This section will address the following question:

Is the permeability reduction (residual resistance factor) provided by gel sensitive to the volume of CO_2 or brine injected?

After performing the sequence described in Table 48, a resorcinol-formaldehyde gelant was placed in the core. The gelant composition was the same as that for the second entry in Table 38 (pH=8.3). Ten pore volumes of the gelant were injected using an injection rate of 15.7 ft/d. Then the core was shut in for 6 days. After the shut-in period, brine and CO_2 were injected using the sequence indicated in Table 51. In these experiments, the flow direction was vertical (in the top of the core and out the bottom).

Table 51. Summary of Results During Injection of CO_2 and Brine After Gel Placement

Entry	Injectant	Pore Volumes Injected	Residual Resistance Factor	% of PV Open to Flow	α/α_o (α_o=0.0473 cm)
1	Brine	2.3	29,000		
2	Dry CO_2	1			
3	Brine	11	550		
4	Dry CO_2	100	34.6		
5	Brine	100	412	58	194
6	Dry CO_2	10	34.4		
7	Brine	10	359	43	242
8	Dry CO_2	10	22.2		
9	Brine	10	350	41	225
10	Dry CO_2	10	18.2		
11	Brine	10	307	47	314

Total pore volumes injected: 143 PV for brine; 131 PV for CO_2.

The residual resistance factors observed during the five WAG cycles shown in Table 51 are in reasonable agreement with those observed earlier for the resorcinol-formaldehyde gel formed at pH=8.3 (see the data for Core 3 in Table 45). In Table 51, note that a WAG cycle with only one pore volume of CO_2 was sufficient to reduce the residual resistance factor for water from 29,000 to 550. During the subsequent WAG cycles, water residual resistance factors were reduced by 25%, 13%, 2.5%, and 12%, respectively. For the final three WAG cycles shown in Table 51, the analogous reductions in CO_2 residual resistance factors were 1%, 35%, and 18%, respectively.

Table 52 lists more detail about CO_2 and brine residual resistance factors associated with Entries 4 and 5 in Table 51. The first part of Table 52 shows that CO_2 residual resistance factors decreased from 57.2 to 34.6, as the number of pore volumes of CO_2 injected for this step increased from 10 to 100. One possible explanation for this decrease could be gel breakdown during CO_2 injection. Another explanation is that the large volume of continuous CO_2 injection gradually shrank the gel by extracting water. The latter explanation is more consistent with the behavior noted while injecting the subsequent 100 pore volumes of brine. As the second part of Table 52 shows, the brine residual resistance factor increased from 312 to 412, as the number of pore volumes of brine injected increased from 10 to 100. Perhaps this increase occurs because the gel is rehydrating and expanding during the prolonged period of brine injection.

Table 52. Residual Resistance Factors for Brine and Dry CO_2 vs. Pore Volumes Injected

Pore Volumes Injected	10	20	30	40	50	60	70	80	90	100
Residual Resistance Factor for Dry CO_2	57.2	56.0	48.2	43.6	42.0	39.9	38.3	40.6	35.7	34.6
Residual Resistance Factor for Brine	312	361	371	371	380	389	390	393	404	412

Close examination of our data reveals that residual resistance factors for both brine and CO_2 are not particularly sensitive to continuous injection of significant volumes of fluid. For a given injection rate, the rate of decline of residual resistance factors was generally less than 1% per pore volume of fluid injected. This insensitivity was also observed previously during studies of the other four gels. As was noted in Table 52, residual resistance factors can actually increase during prolonged brine injection.

Gel breakdown (i.e., irreversible loss of residual resistance factor) appears to be more sensitive to the process of switching from CO_2 injection to brine injection (and visa versa) than it is to continuous injection of either fluid. Recall from Table 51 that a WAG cycle with only one pore volume of CO_2 was sufficient to reduce the residual resistance factor for water by more than a factor of 50. Table 45 also shows the degrading effects of WAG cycles—especially during the first WAG cycle.

Conclusions

A second series of experiments were undertaken to assess how different gels reduce the permeability to water and compressed gases in Berea sandstone. This work complements that described in our Second Annual Report.[3] New results were reported for strong resorcinol-formaldehyde gels that were buffered and formed at pH values from 8.3 to 9.0. These properties were compared with those of four gels that were studied previously. The new results confirmed the conclusions reached in the previous study. First, all five gels can reduce water permeability in Berea sandstone to a greater extent than CO_2 permeability. Second, all five gels experienced some breakdown during a water-alternating-gas cycle. Third, for the polymer-based gels, an apparent shear-thinning behavior was observed during brine injection. Fourth, during CO_2 injection, the apparent rheology in porous media was more or less Newtonian for all five gels.

Using a resorcinol-formaldehyde gel that was buffered and formed at pH value 9.0, an experiment was performed at 900 psi using N_2 instead of CO_2. We noted (1) for both compressed CO_2 and compressed N_2, the gel can reduce brine permeability significantly more than gas permeability, and (2) multiple water-alternating-gas (WAG) cycles degrade the residual resistance factors to about the same extent for CO_2 as for N_2. The similarity in results suggests that the observed behavior is not sensitive to the type of gas used.

Most of our experiments were performed at 900 psi. However, two experiments were performed with CO_2 at 1500 psi—one using a resorcinol-formaldehyde gel (at pH=9) and the other using a Cr^{3+}(acetate)-HPAM gel. From these studies, we conclude that the overall behavior at 1500 psi (where CO_2 density is 0.641 g/cm^3) is not radically different from that at 900 psi (where CO_2 density is 0.156 g/cm^3).

During high-pressure visualization experiments, no significant macroscopic changes were observed for a resorcinol-formaldehyde gel or a Cr^{3+}(acetate)-HPAM gel when exposed to brine, CO_2, or oil (Soltrol 130®) at 1500 psi.

Additional studies were performed to assess the importance of certain variables on the results. Several observations were noted during experiments performed before gel placement. First, endpoint mobilities for CO_2 were not significantly different for horizontal versus vertical flow. Second, endpoint mobilities for brine were 26% less during vertical flow than during horizontal flow. Third, during the first 40 pore volumes of injection, the mobilities for wet CO_2 was the same as that for dry CO_2. Fourth, for the conditions tested, multiple WAG cycles did not appear to alter permeability or porosity of a Berea sandstone core.

Endpoint mobilities for N_2 and brine were found to be noticably less than those for the CO_2 experiments. These differences were discussed in light of differences in gas-water solubilities. Also, when the core was oriented vertically, the endpoint mobilities (both for N_2 and brine) were noticeably less than those when the core was oriented horizontally. The tracer studies indicated that the N_2 gas occupied a very small fraction of the pore volume and had a very small effect on the dispersivity of the core.

Studies were also performed during injection of brine and CO_2 after placement of a resorcinol-formaldehyde gel (formed at pH=8.3). The results suggest that gel breakdown in the core (i.e., permanent loss of residual resistance factor) is more severe during exposure to a WAG cycle than during prolonged injection of either brine or CO_2.

5. GEL PLACEMENT IN FRACTURED WELLS

Theoretical developments[2-5,19,20] and some field results[25,53-56] indicate that gel treatments could be particularly effective in reservoirs where fractures constitute the source of a severe fluid channeling problem. This section discusses gel placement in vertically fractured wells. More than one million wells have been intentionally fractured to stimulate oil and gas production.[57] Currently, 35% to 40% of newly drilled wells are hydraulically fractured. Many other wells have been fractured unintentionally during waterflooding operations. Furthermore, naturally fractured reservoirs are not uncommon.[58]

With the proper length and orientation, fractures can enhance productivity and/or injectivity without adversely affecting sweep efficiency.[59-66] Unfortunately, many circumstances exist where fractures can impair oil recovery. In reservoirs with water-drive or gas-drive recovery mechanisms, fractures may aggravate production of excess water or gas. In waterfloods or in enhanced recovery projects, fractures can impair sweep efficiency by allowing injected fluids to channel through the reservoir.

Vendors of gel materials commonly base their designs on an assumption of radial flow around the wellbore. At times this practice is used even though tracer studies indicate that fractures or formation parting is the source of a severe channeling problem.[67] The success rate for applications in fractured wells could be improved significantly if gel treatments were designed specifically to address channeling through fractures. In previous reports,[3-5] we introduced some basic concepts toward understanding gel placement in fractured wells. Refs. 4 and 5 presented basic equations to quantify the relative distances of gelant penetration into rock matrix adjacent to a fracture face in stratified reservoirs with no crossflow between layers. Ref. 3 used concepts from hydraulic fracturing to quantify gelant leakoff from a fracture face.

In this section, we discuss some idealized objectives for gel placement in fractured reservoirs. We also present some results from flow visualization studies in beadpacks that illustrate the importance of fluid properties during gelant placement in fractured systems.

Desired Placement Locations

Injection Wells. Where would we like a gel to be placed in a vertically fractured injector? Consider a fractured injection well, as shown in Fig. 20. The fracture may extend part or all of the way between the injection well and a nearby production well. Because of its orientation and conductivity, the fracture significantly reduces sweep efficiency. To improve sweep efficiency, we wish to reduce fracture conductivity using a gel. In one idealized scenario, the gel would completely fill the fracture and effectively negate the existence of the fracture. This scenario would increase sweep efficiency, but a significant reduction of injectivity would also occur. The injectivity loss associated with complete healing of the fracture may not be acceptable, especially in tight formations.

Hypothetically, a high injectivity could be maintained and sweep efficiency could be improved if the gel could be placed at the proper locations in the fracture. In fractured injection wells, we would prefer to plug that portion of the fracture farthest from the wellbore rather than the portion nearest the wellbore. To explain, the part of the fracture farthest from the wellbore is most likely to allow injected fluid (e.g., water) to bypass oil (see Fig. 20a). Thus, plugging this part is most likely to improve sweep efficiency. Also, if the near-wellbore part of the fracture remains open to flow, then injectivity could remain relatively high.

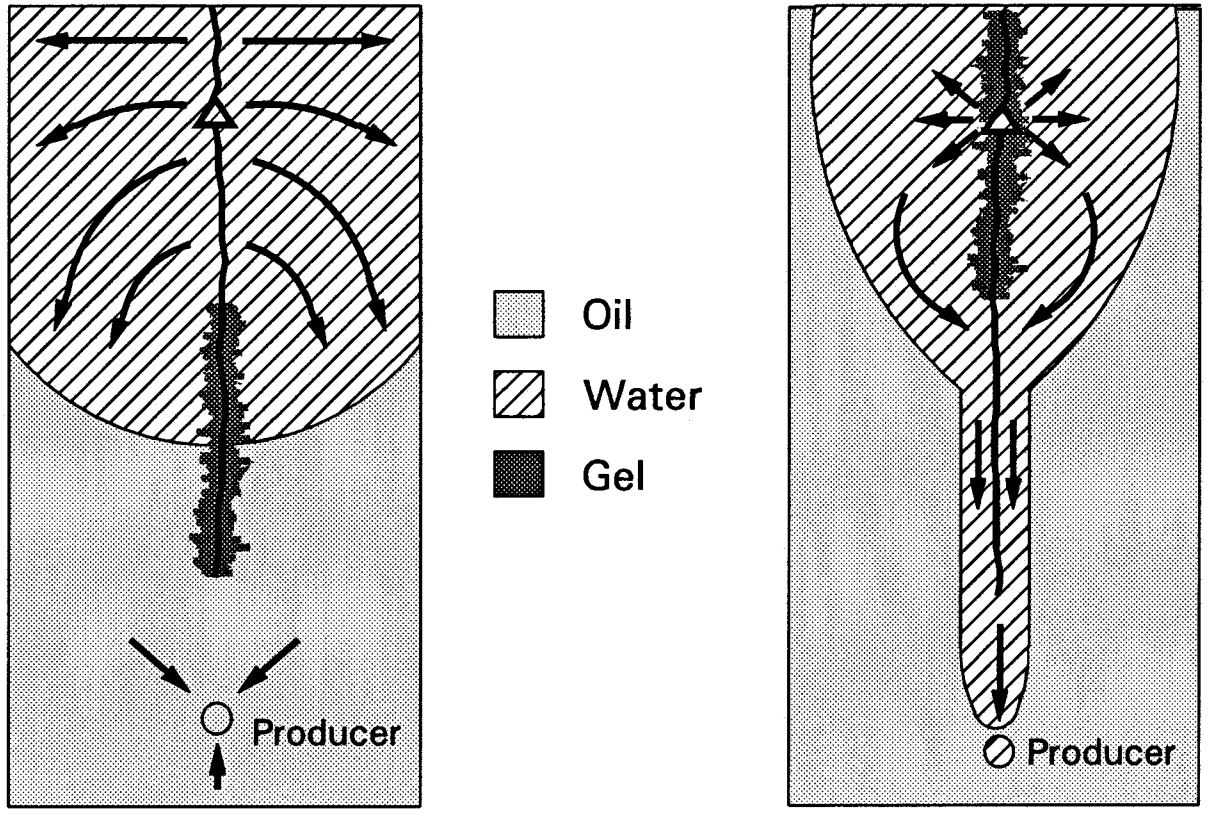

Fig. 20. Idealized gel placement in fractured injection wells.

In the contrasting scenario (Fig. 20b), the near-wellbore part of the fracture is plugged while leaving the deep portions of the fracture intact. In this situation, injectivity would be reduced to near the level associated with an unfractured injector. However, improvement in sweep efficiency would be minimal. Injected water would circumvent the fracture near the wellbore, but this region is the most likely to have already been swept to a low oil saturation. Farther from the wellbore, the water would re-enter the intact portion of the fracture and bypass unswept oil.

In stratified reservoirs where the fracture cuts multiple strata, we prefer the gel to plug or restrict flow in the most-permeable zones more than in the less-permeable zones. However, for injection wells, one could argue that reducing conductivity of the fracture is much more important than selectively plugging the matrix of different strata adjacent to the matrix.

Production Wells. In fractured production wells, the desired placement of gel varies with the situation. When the fracture channels water from deep within the reservoir (e.g., directly from a water injection well), then the gel should be placed deep in the fracture. In tight formations, the ideal case would place gel in the fracture far from the wellbore while leaving the fracture open near the well. Leaving the fracture open near the wellbore allows productivity to remain high (see Fig. 21).

If the fracture cuts a water-source zone (i.e., water enters the fracture from the matrix of a strata with a high water saturation), then, ideally, the gel would enter and plug the water-source zone all along the fracture. However, the gel (again, ideally) would not plug the oil-productive zones. A useful property in achieving this ideal is an ability of the gel to reduce water permeability much more than oil permeability.[5,22]

If the fracture allows water to cone or cusp into a producer from an underlying aquifer, then one of three objectives could be pursued. First, one could attempt to heal the fracture (illustrated in Figs. 22a and 22b). This action could increase the critical rate for water coning by two to three orders of magnitude.[5] However, it would also significantly reduce the well's productivity. An second objective could be to place the gel some distance into the rock matrix along the fracture face, while leaving the fracture open to flow. This course of action relies, again, on an ability of the gel to reduce water permeability much more than oil permeability. Ideally, this property, in concert with gravity, would prevent water in the aquifer from entering the fracture. In contrast, oil could still enter the fracture and flow to the production well. However, it is uncertain at this point whether bulk gels in fractures will exhibit disproportionate oil/water permeability to the same extent as observed in porous media. A third objective could be to place the gel only in the lower part of the fracture, as indicated in Fig. 23. Of course, one must exploit gravity during the gelant placement process for this scheme. If this placement can be achieved, then water production could be reduced substantially while maintaining high oil productivity.

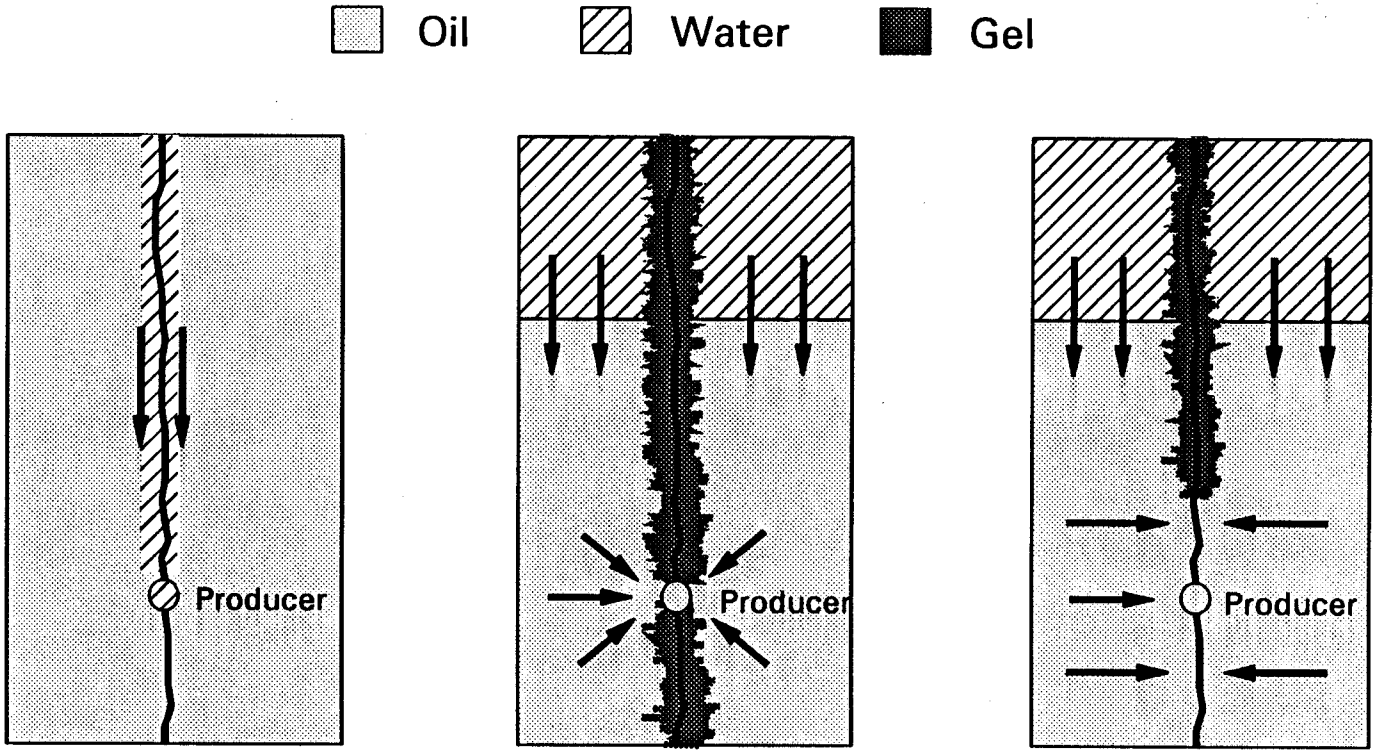

a. No gel: poor sweep, high productivity.

b. Gel plugs fracture: better sweep, but low productivity.

c. Gel plugs fracture, except near well: better sweep and high productivity.

Fig. 21. Idealized gel placement in fractured production wells.

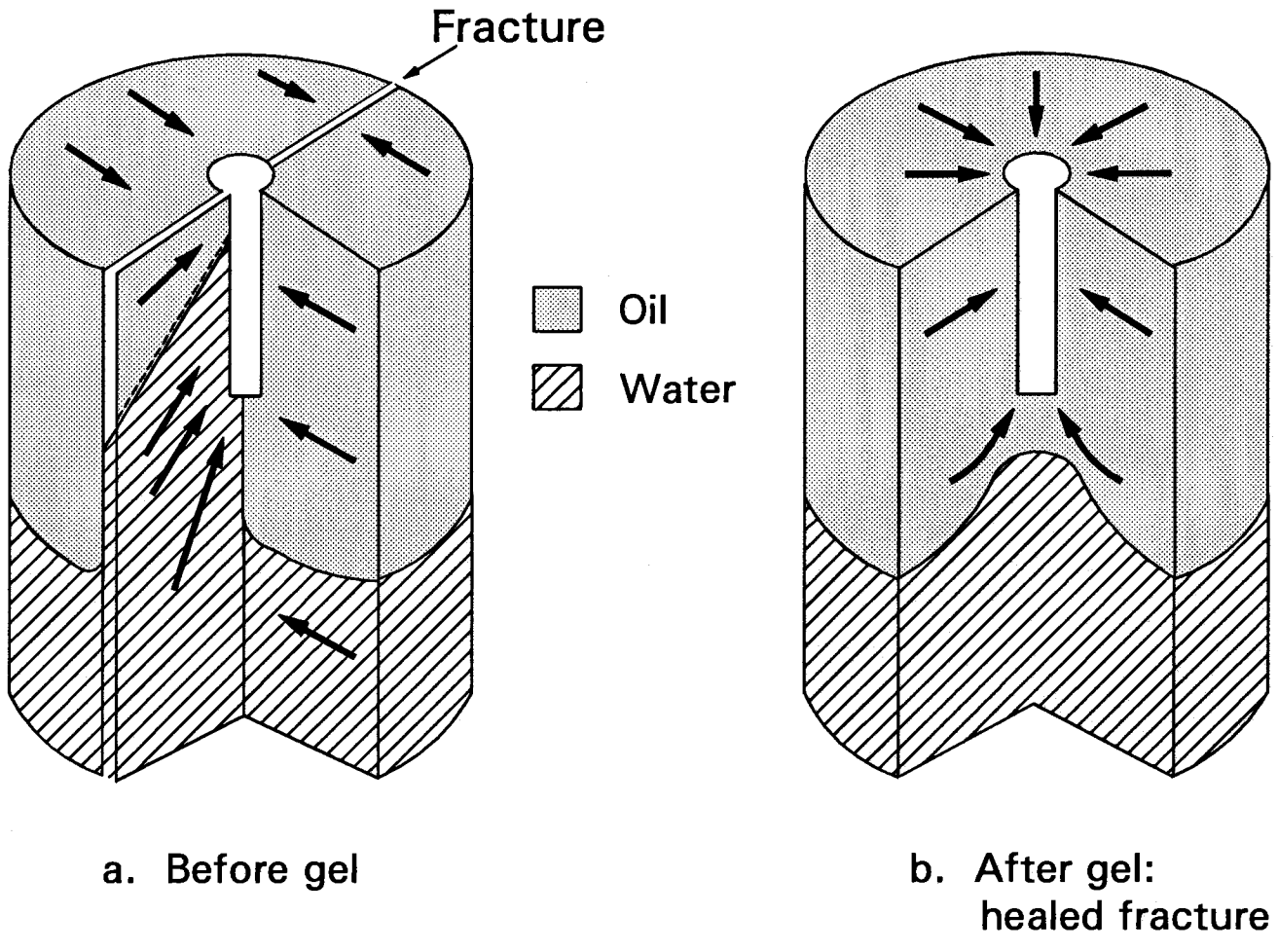

Fig. 22. Reduced coning by healing a fracture.

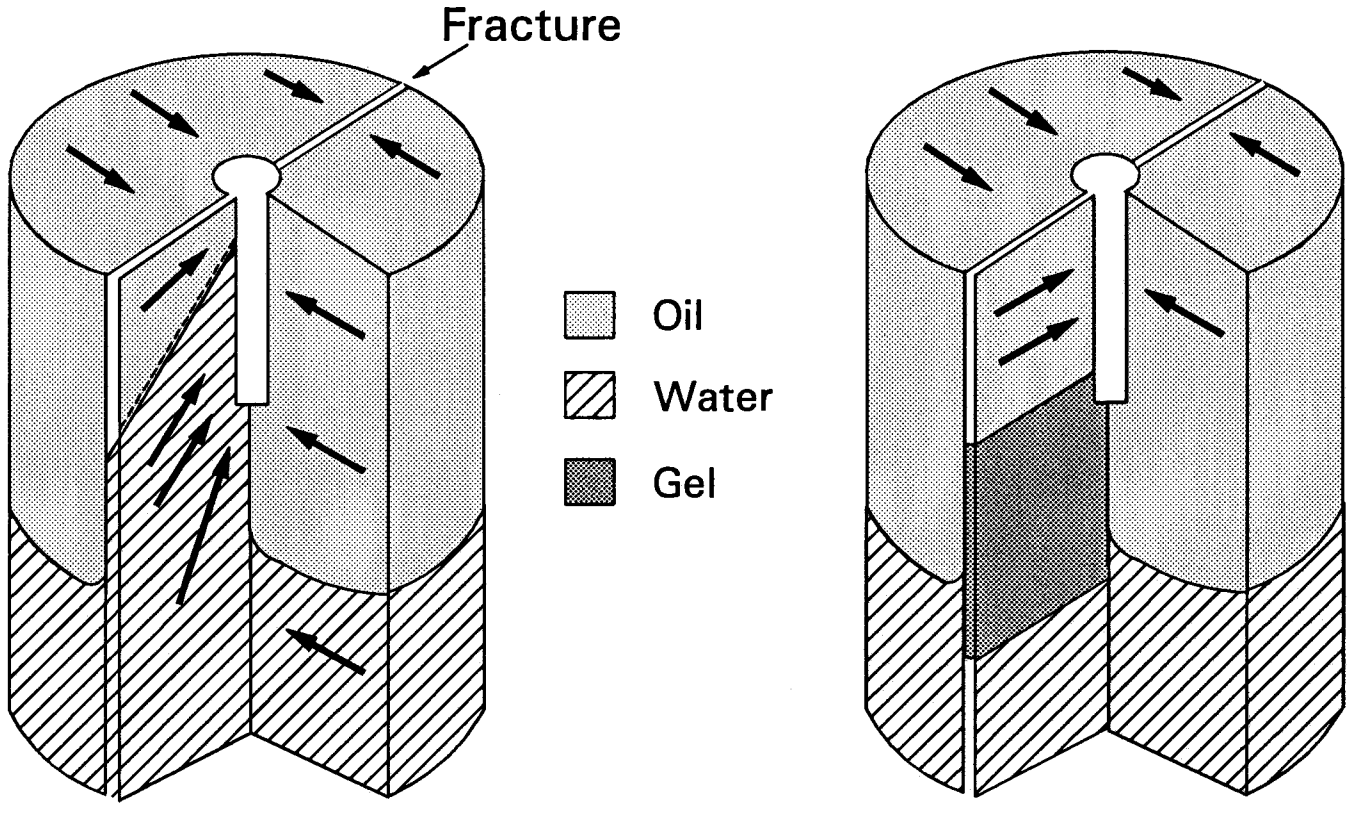

a. Before gel

b. After gel: partly healed fracture

Fig. 23. Reduced coning by partly healing a fracture.

Fractures Cutting Multiple Zones

Quantifying Gelant Leakoff. In the previous section, the ideal locations to place gels were considered qualitatively. Next, we will examine some obstacles in achieving these idealized gel placements. We especially want to quantify how far the gelant propagates along the length of the fracture and the distance that the gelant "leaks off" into the rock matrix along the fracture.

In a fracture that cuts multiple pay zones, the gelant will necessarily penetrate some distance into all open zones. The distance of penetration into a given zone has been quantified using different approaches.[3,4] One approach, based on concepts from hydraulic fracturing,[3,68,69] uses leakoff coefficients to quantify the distance of gelant penetration into the rock matrix. Three leakoff coefficients are commonly considered:[68,69] (1) a coefficient for viscous effects, C_v, (2) a coefficient for compressibility effects, C_c, and (3) a coefficient for filtration or "wall-building" effects, C_w.

Several factors act to minimize differences in the distance of gelant leakoff among strata of different permeability. First, the coefficients, C_v and C_c, are proportional to $\sqrt{k_m \phi_m}$, where k_m is the effective permeability of the matrix and ϕ_m is the matrix porosity.[68] This square-root dependence diminishes differences in leakoff distance among different strata. Second, if vertical pressure communication exists between adjacent strata, then crossflow of viscous gelants from high-permeability zones into low-permeability zones will further diminish differences in leakoff distances.[3,70] In fact, if the ratio of gelant viscosity to water viscosity is greater than the permeability contrast (ratio of permeabilities for adjacent zones), then the distance of gelant leakoff can be almost the same in adjacent strata.[70,71] Third, if the gelant contains particulate matter (e.g., fluid-loss additives or partially gelled material), then the "wall-building" coefficient, C_w, usually determines the distance of gelant leakoff.[68] The particulate matter forms a filter cake on the fracture face, thereby inhibiting leakoff. The thickness of the filter cake will increase with increasing level of leakoff and with increasing matrix permeability. This effect further reduces differences in leakoff distance among different strata. For filter cakes with effective permeabilities that are significantly less than the rock-matrix permeabilities, the distance of gelant leakoff can be almost the same in adjacent strata. Fig. 24 illustrates the leakoff distance (L_{p2}) in a low-permeability zone (Zone 2 with permeability, k_2, and porosity, ϕ_2) relative to the leakoff distance (L_{p1}) in an adjacent high-permeability zone (Zone 1 with permeability, k_1, and porosity, ϕ_1). The two curves in Fig. 24 bracket the range of L_{p2}/L_{p1} values as a function of permeability contrast. For cases where a fracture cuts multiple zones, Fig. 24 suggests that it may be difficult to place gelant in the most-permeable zones without significant gelant penetration into less-permeable zones.

Altering Flow Profiles at the Fracture Face. Once the gelant has been injected, the permeability reduction after gelation will play an important role in determining the degree of fluid diversion. Previous publications[21,23] revealed that for rocks with substantially different initial permeabilities, certain very "strong" gels can reduce the permeability to about the same final value—in the microdarcy range. This could be a useful property when treating certain special cases of fractured wells—in particular, wells with fractures that cut multiple zones that are separated by impermeable barriers. Conceptually, a thin "skin" of material with a uniform low permeability could improve the flow profile at the fracture face. More work will be needed to assess the value of this concept.

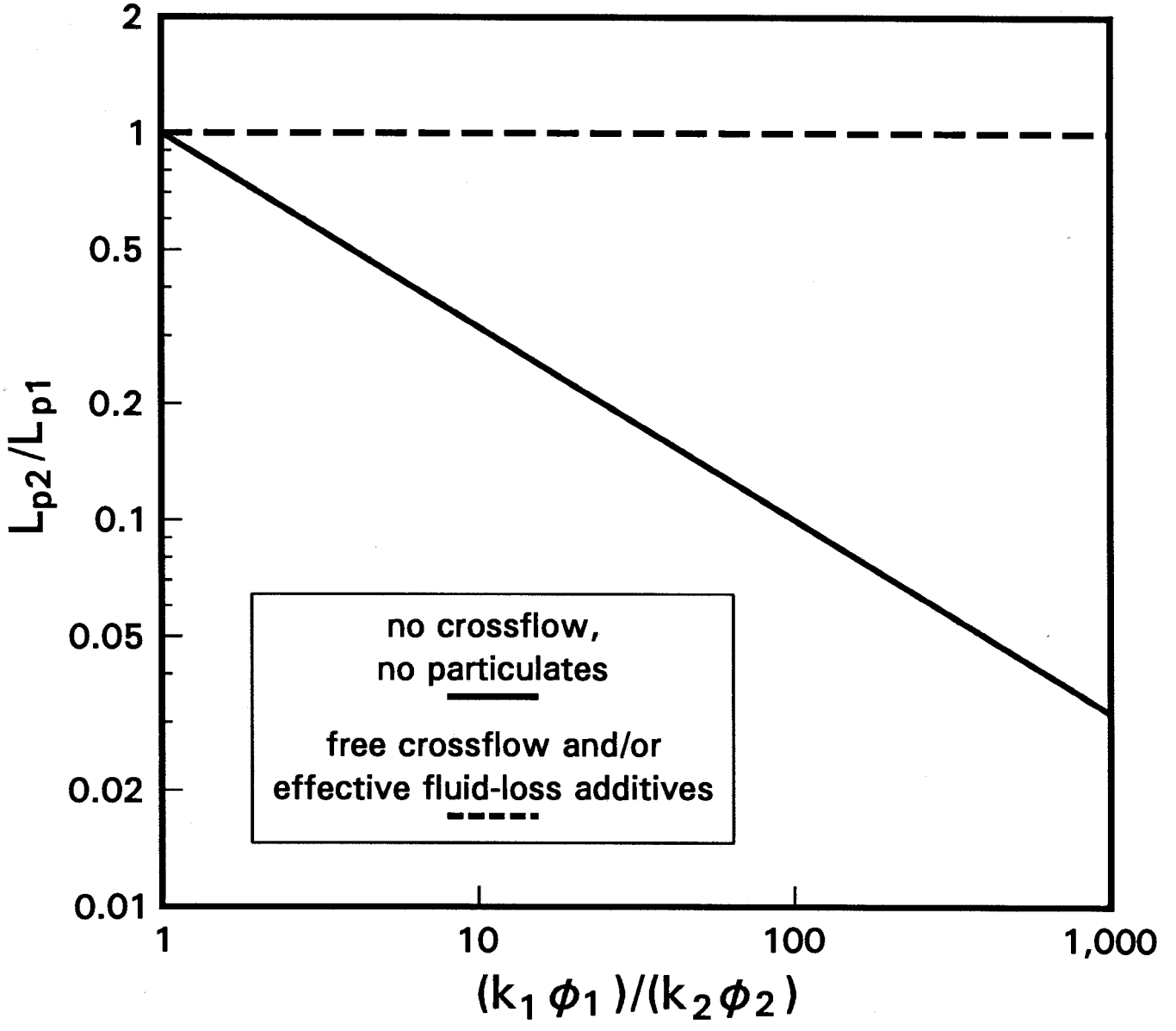

Fig. 24. Gelant leakoff distance in Zone 2 relative to that in Zone 1 as a function of permeability contrast.

Flow Visualization Experiments in Fractured Systems

To test some of our concepts regarding gelant placement in fractured systems, we performed several flow visualization experiments in a clear beadpack. The internal dimensions of the bead container were 238 cm x 12.5 cm x 1.25 cm. The container was constructed of transparent polycarbonate to allow flow visualization. Before placing beads in the pack, a "fracture" was laid along the bottom of the container. This "fracture" consisted of two layers of nylon mesh with 1000-μm openings. This nylon mesh was wrapped with one layer of nylon mesh that had 74-μm openings. The 74-μm nylon mesh was heat-sealed so that the 1000-μm nylon mesh was completely enclosed. Then small holes were made in the 74-μm mesh at both ends of the "fracture" near the injection and production ports. The 74-μm mesh was used to prevent glass beads from infiltrating the 1000-μm mesh. The dimensions of the "fracture" (including both nylon meshes) was 236 cm x 0.15 cm x 1.2 cm. In the bead container, an injection port was located next to one end of the fracture, while a production port was located next to the other end of the fracture (230 cm away).

After positioning the "fracture," the container was filled with 150-μm (nominal) glass beads. Without the fracture, beadpacks made from these beads had a permeability to water of about 13 darcies and a porosity of 0.38. The pore volume of the beadpack with the fracture was about 1500 ml. The fracture permeability was determined separately to be about 1000 darcies—77 times the permeability of the bead "matrix." All experiments described in this section were performed at room temperature. Also, a constant injection rate of 50 ml/hr was used during all experiments. The experiments were recorded on VHS video tape.

Dyed Water Displacing Clear Water. During tracer experiments, dyed water was injected to displace clear water from the beadpack with the fracture. In these studies, the tracer breakthrough at the production port occurred after injecting 75 ml ($\pm$10 ml) of dyed water (i.e., after injecting 0.05 pore volumes). Fig. 25a illustrates the location of the dyed fluid in the beadpack at the time when the dyed injectant reached the production port. As expected, most of the dyed injectant channeled through the fracture. However, some dyed water "leaked off" into the beadpack next to the fracture—especially near the injection port. Away from the injection port, slight variations in the fracture or the packing of the beads presumably were responsible for variations in leakoff along the fracture. Fig. 25 illustrates the displacement of clear water by dyed water at various throughput values between 0.05 and 0.88 pore volumes (PV).

Use of a Water-Like Gelant. Fig. 26 shows the results from a flow visualization experiment using a resorcinol-formaldehyde gelant. The gelant contained 3% resorcinol, 3% formaldehyde, 0.5% KCl, and 0.42% $NaHCO_3$ at pH=9. Prior to injecting the gelant, the beadpack was flushed with 20 liters of brine that contained 0.5% KCl, and 0.42% $NaHCO_3$ at pH=9. Fig. 26a illustrates the location of the gelant in the beadpack after injecting 150 ml (0.1 PV) of gelant. The resorcinol-formaldehyde gelant arrived at the production port after injecting 75 ml (0.05 PV) of gelant. Since the viscosity of the resorcinol-formaldehyde gelant was about the same as that for water, the breakthrough time was expected to be similar to that for injection of dyed water. After injecting the gelant, the beadpack was shut in for 26 hours to allow gelation to occur (gelation time was 4 hours). After gelation, dyed brine (containing 0.5% KCl and 0.42% $NaHCO_3$ at pH=9) was injected. Fig. 26 shows the results at various stages during this experiment. The postflush water broke through the gel bank immediately above the injection port. A detailed analysis revealed that this breakthrough was achieved by water channeling between the beadpack and the container wall in the region indicated in Fig. 26—i.e., the postflush did not form a channel by displacing gel from the beadpack. A comparison of Figs. 25 and 26 reveals that the sweep efficiency during water injection after the gel treatment was much greater than for the case where no gel was used. For the gel-treated system, the postflush arrived at the production port after injecting 1325 ml (0.88 PV) of dyed postflush brine.

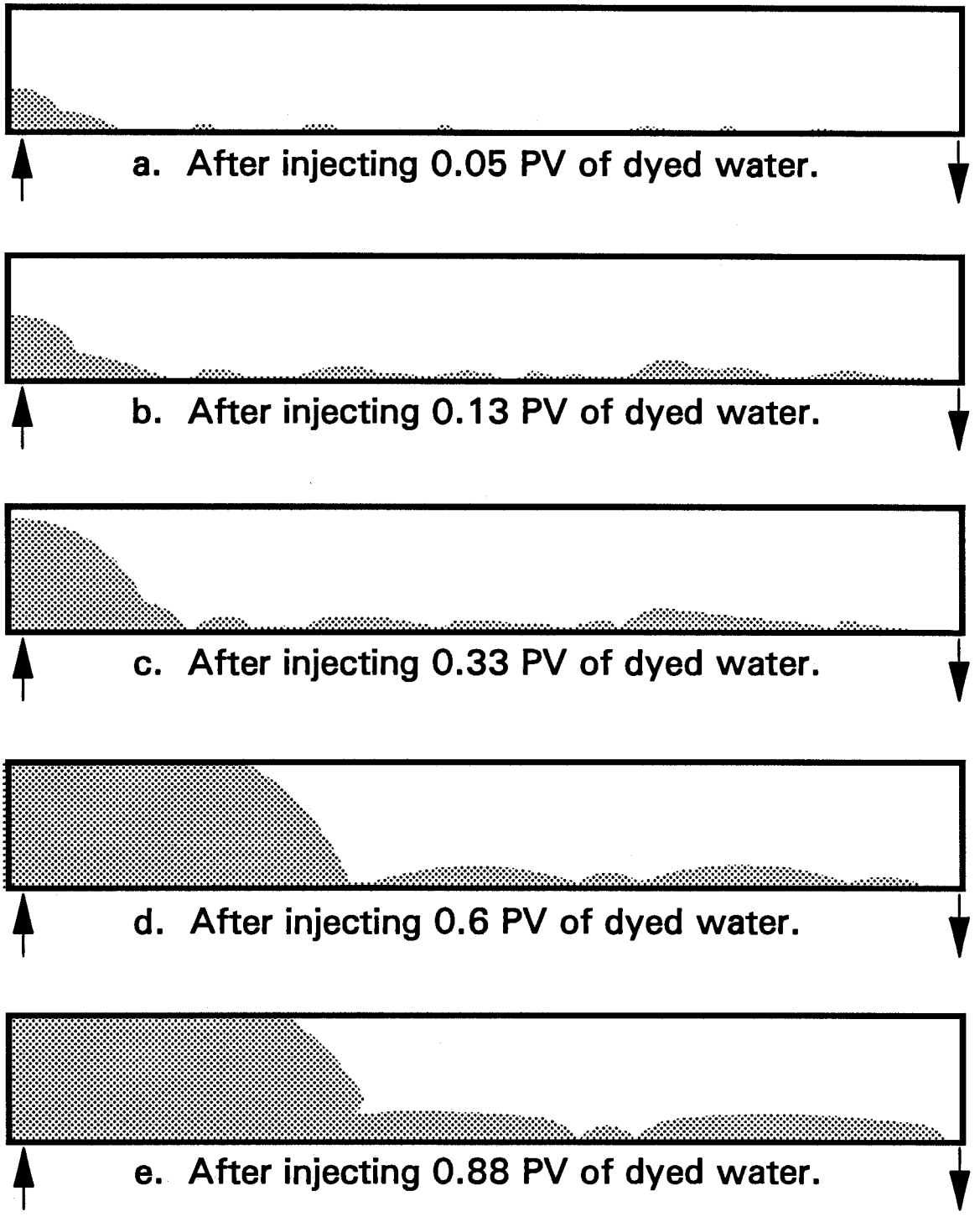

Fig. 25. Dyed water displacing clear water.

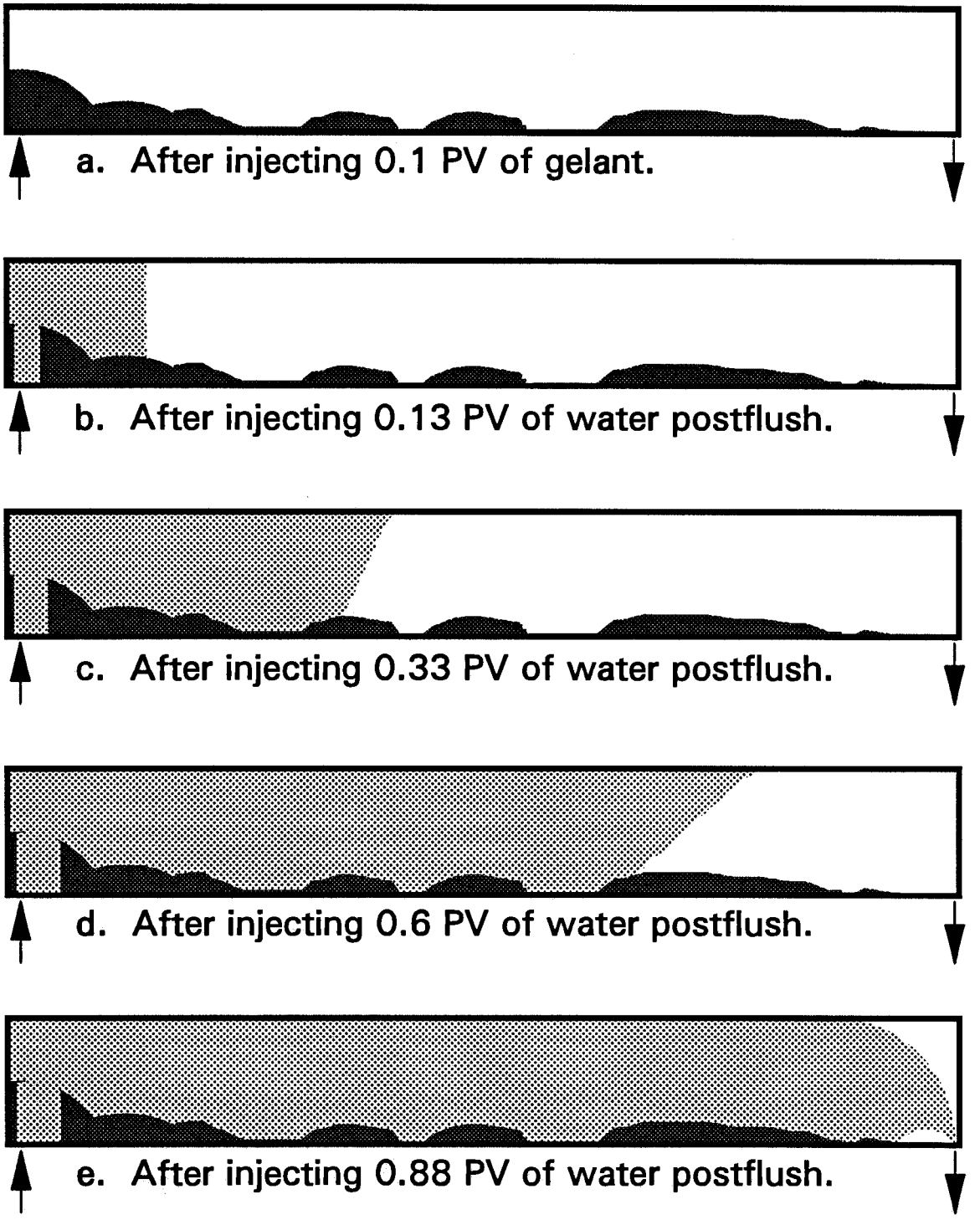

Fig. 26. Water postflush after placement of a resorcinol-formaldehyde gel.

Displacing a Water-Like Gelant with a Water Postflush Prior to Gelation. In the previous experiment when water was injected after gelation, the water fortuitously broke through the gel in a location that allowed sweep efficiency to be high during the water postflush. In a field application, we might not be so lucky. For an effective gel treatment, the conductivity of the fracture must be reduced and a viable flow path must remain open between the wellbore and mobile oil in the reservoir. If this flow path exists near the wellbore (as in our previous experiment), sweep efficiency could be improved significantly after the gel treatment. In contrast, the gel treatment will be ineffective if the fracture is reopened during subsequent water injection. With the use of very strong gels, it is not obvious that water injected after gelation will always force a pathway through gel in the matrix before reopening the healed fracture.

An experiment was performed using a brine postflush to displace a resorcinol-formaldehyde gelant away from the injection port prior to gelation. The procedures used during this experiment were exactly the same as those during the previous experiment except that 15 ml (0.01 PV) of brine was injected after the 150 ml (0.1 PV) gelant bank but before shut-in. This postflush displaced gelant from the first 42 cm of the fracture. This displacement provided a flow path that avoids the region of extensive gelant leakoff near the injection port. Figs. 27a and 27b show the gelant locations in the beadpack just before and just after the brine postflush, respectively.

After the brine postflush, the beadpack was shut in for 26 hours. After the shut-in period, dyed brine was injected. Figs. 27c through 27f show the results during this displacement. The dyed brine broke through the thin gel bank at a point about 40 cm from the injection port—corresponding to the greatest distance of penetration of brine postflush along the fracture before shut-in. After that point, the brine efficiently swept the beadpack, while the fracture remained plugged by the gel. The dyed brine arrived at the production port after injecting 1150 ml (0.77 PV). The only region that was not swept by the dyed brine was upstream of the point where the brine postflush broke through the gel bank.

Injection of Pre-Gelled Material. In another experiment, a pre-gelled resorcinol-formaldehyde gel was injected into a fresh beadpack. First, a formulation was prepared that contained 3% resorcinol, 3% formaldehyde, 0.5% KCl, and 0.42% $NaHCO_3$ at pH=9. Three days after gelation, the gel was sheared in a blender for one hour with an equal volume of brine (0.5% KCl, and 0.42% $NaHCO_3$ at pH=9). This suspension was then injected into a fresh, water-saturated beadpack. Fig. 28 shows the results obtained during this experiment. The gel formulation arrived at the production port after injecting 80 ml (0.053 PV). A total of 110 ml (0.073 PV) of gel formulation was injected (Fig. 28a). During injection of this gel, the injection pressure rapidly increased to 140 psi. In contrast, the injection pressure was very low throughout the previous experiments. After injecting the gel, dyed water was injected as illustrated in Fig. 28b. This water arrived at the production port after injecting only 100 ml (0.067 PV) of fluid. Thus, this pre-gelled material was not an effective diverting agent.

Injection of a Dyed Xanthan Solution. Another experiment involved injection of a dyed 2000-ppm xanthan solution to displace clear water from a fresh beadpack. Fig. 29 illustrates the position of the polymer-water front at various times during the displacement. Polymer solution arrived at the production port after injecting 1400 ml (0.93 PV). If the polymer solution had formed a gel at this point, the sweep efficiency during subsequent water injection would be the worst case imaginable. The most likely flow path between the injection and production ports would be through a reopened fracture. The "matrix" (beadpack) would have been totally plugged. On the other hand, Fig. 29 suggests that a traditional polymer flood could significantly improve sweep efficiency in a fractured system.

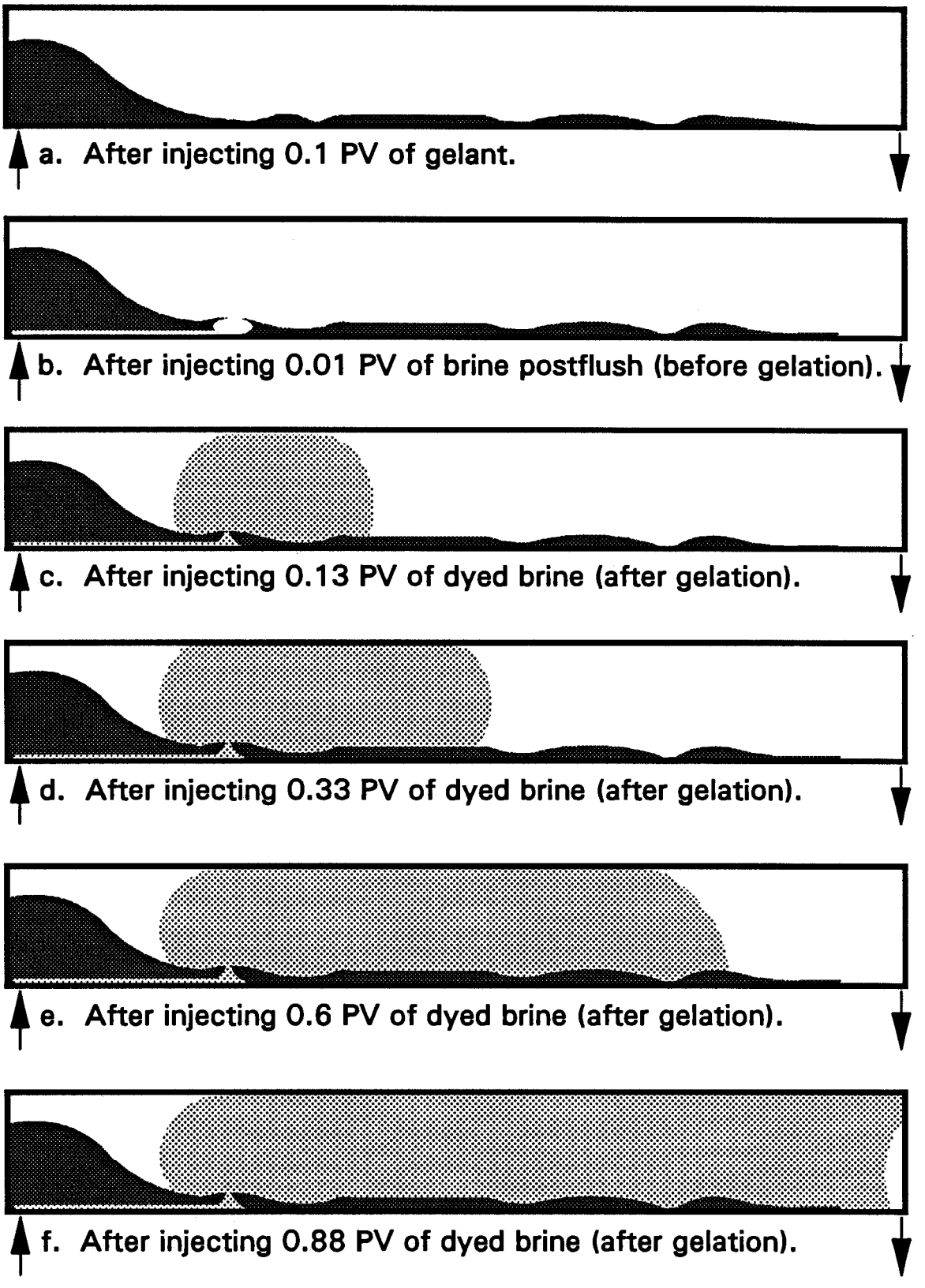

Fig. 27. Displacing a water-like gelant with a water postflush before gelation.

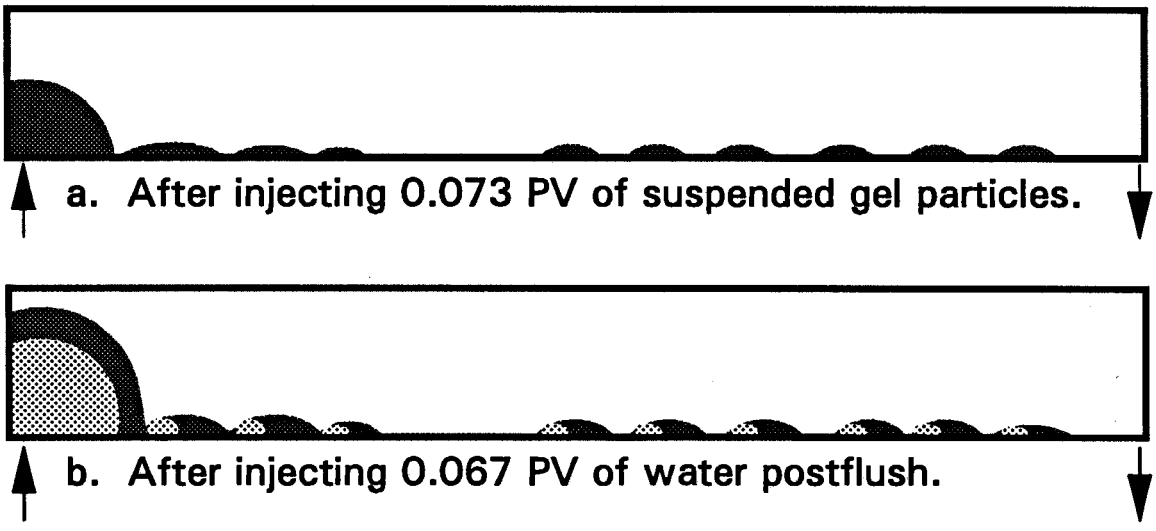

Fig. 28. Injection of a suspension of resorcinol-formaldehyde gel particles followed by water injection.

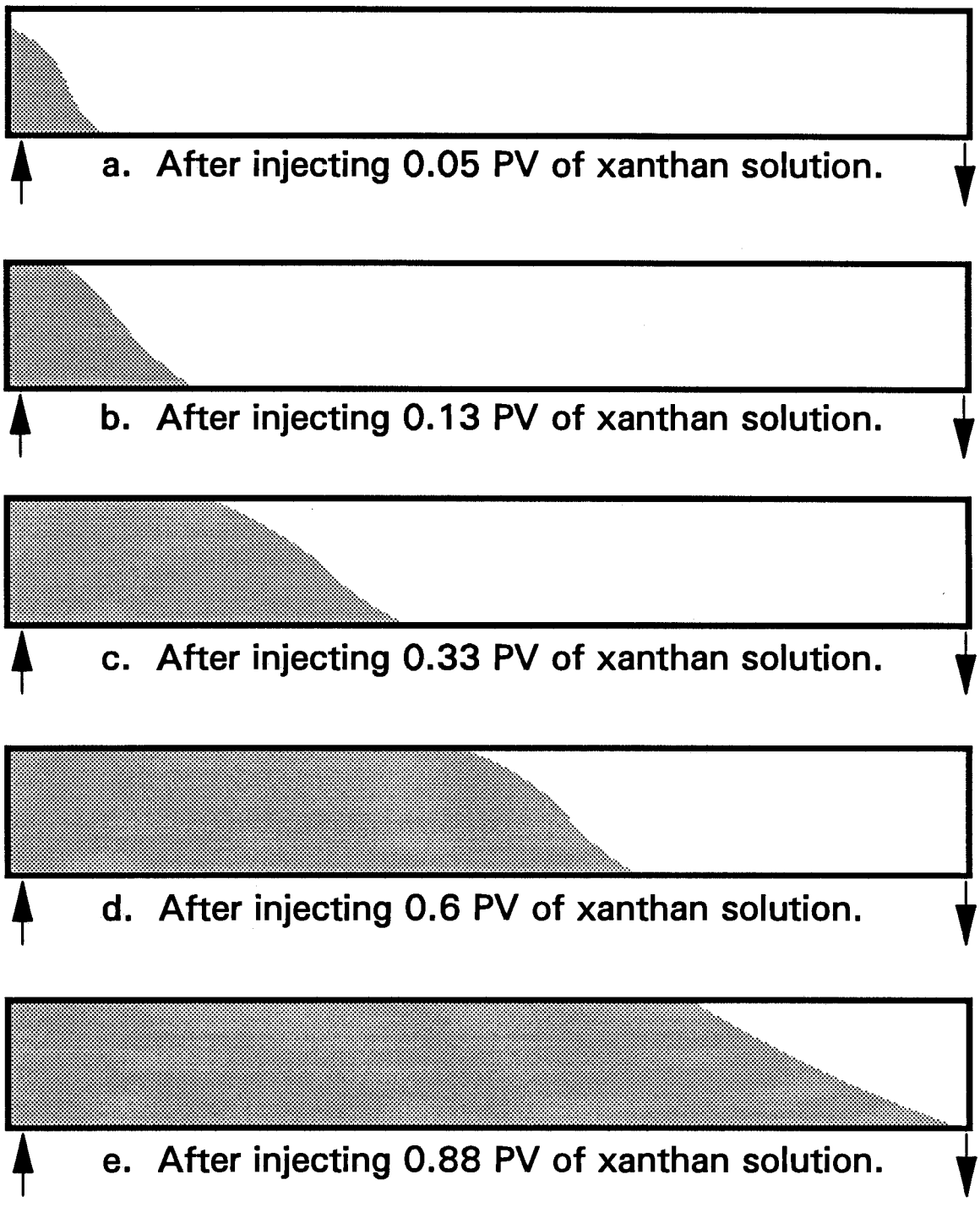

Fig. 29. Dyed 2000-ppm xanthan solution displacing clear water.

Injection of a Dyed Xanthan Solution with Suspended Particulate Matter. Analyses based on concepts from hydraulic fracturing suggest that leakoff from a fracture could be minimized by incorporating particulate matter ("fluid-loss agents") into the injected gelant (see pages 61-72 of Ref. 3). An important consideration when implementing this idea is that the particulate matter must remain suspended in the gelant during the process of gelant placement. In particular, the fluid-loss agent must not "screen out" and prematurely plug the fracture during gelant injection.

We performed an experiment using a 3% suspension of nominally 30-μm poly(styrenebutyl) methacrylate beads (Polysciences) in a dyed 2000-ppm xanthan solution. This suspension was injected to displace water from a fresh beadpack. Unfortunately, only 85 ml (0.057 PV) of suspension could be injected before the injection port was plugged. The methacrylate beads were clearly retained in the fracture (i.e., they did not penetrate into the beadpack "matrix"). However, after injecting 0.057 PV, the polymer-water front in the beadpack appeared identical to that observed previously using a xanthan solution without suspended beads (Fig. 29a). Therefore, the methacrylate beads were ineffective as fluid-loss agents during this experiment. When a water postflush was injected following the polymer bank, the postflush water arrived at the production port after injecting 60 ml (0.04 PV). Thus, the suspension was also ineffective as a diverting agent. Additional experiments will be needed to demonstrate the value of incorporating fluid-loss agents into gelants.

For the various cases considered above, Table 53 compares the pore-volume values when injectants arrived at the production port of our "fractured" beadpack. For the best gel treatments, the pore-volume values should be low in the "gelant" column and high in the last column.

Table 53. Pore-Volume Values when Injectants Arrived at the Production Port

Case	"Gelant" PV	Brine after "gelant" placement, PV
Dyed water displacing clear water (Fig. 25)	--	0.05
Resorcinol-formaldehyde gelant (Fig. 26)	0.050	0.88
Resorcinol-formaldehyde gelant with brine postflush before gelation (Fig. 27)	0.057	0.77
Suspension of pre-gelled resorcinol-formaldehyde (Fig. 28)	0.053	0.07
Dyed 2000-ppm xanthan solution displacing clear water (Fig. 29)	0.933	--
Xanthan solution with suspended methacrylate beads	--	0.04

Conclusions

For both injection wells and production wells, the ideal gel placement is such that the fracture is healed far from the wellbore but is open near the wellbore so that injectivity and productivity remain high. In fractured production wells with water coning problems, the gel ideally will plug the lower portion of the fracture while leaving the upper portion open for oil flow.

Flow visualization studies were performed to illustrate the importance of fluid properties during gelant placement in fractured systems. The most desirable gelant placements were obtained using a gelant with a water-like viscosity. Experiments using viscous xanthan solutions suggest that gelant placement using viscous gelants will be inferior to that for low-viscosity gelants. This result was somewhat unexpected based on concepts from hydraulic fracturing. More experiments should be performed to examine the relationship between fluid mobility ratio, fracture/matrix permeability contrast, and fluid leakoff from the fracture.

Although theoretical analyses indicate that incorporation of particulate matter ("fluid-loss" additives) should minimize gelant leakoff from a fracture, we have not yet been able to confirm these predictions using flow visualization experiments.

NOMENCLATURE

C_c = compressibility leakoff coefficient, ft/min$^{1/2}$ [m/s$^{1/2}$]
C_v = viscosity leakoff coefficient, ft/min$^{1/2}$ [m/s$^{1/2}$]
C_w = wall building (filter cake) leakoff coefficient, ft/min$^{1/2}$ [m/s$^{1/2}$]
F_r = resistance factor (brine mobility prior to gel placement divided by gelant mobility prior to gelation)
F_{rr} = residual resistance factor (mobility prior to gel treatment divided by mobility after gel treatment)
F_{rrCO2} = CO_2 residual resistance factor (CO_2 mobility prior to gel placement divided by CO_2 mobility after gel placement)
F_{rrN2} = N_2 residual resistance factor (N_2 mobility prior to gel placement divided by N_2 mobility after gel placement)
F_{rrgas} = gas residual resistance factor (gas mobility prior to gel placement divided by gas mobility after gel placement)
F_{rro} = oil residual resistance factor (oil mobility prior to gel placement divided by oil mobility after gel placement)
F_{rrw} = brine residual resistance factor (brine mobility prior to gel placement divided by brine mobility after gel placement)
k = formation permeability, md [μm^2]
k_i = effective permeability to water for Layer i, md [μm^2]
k_m = effective permeability to water for rock matrix, md [μm^2]
k_{ro} = oil relative permeability
k^o_o = endpoint oil permeability
k_{rw} = water relative permeability
k^o_w = endpoint water permeability
k_w = absolute permeability to water, md [μm^2]
L_{pi} = distance the chemical species has propagated in a linear core or from the face of a vertical fracture (into the rock matrix) in Layer i, ft [m]
PV = pore volume
r = correlation coefficient
S_{gel} = gel saturation
S_{or} = irreducible oil saturation
S_{wr} = irreducible water saturation
u = superficial or Darcy velocity or flux, ft/d [m/s]
V_p = apparent remaining pore volume, cm^3
V_{po} = initial pore volume of the core, cm^3
α = dispersivity at the given stage in the experiment, cm
α_o = initial dispersivity of the core, cm
γ = shear rate, s^{-1}
μ = effective viscosity of injected fluids, cp [mPa-s]
μ_o = oil viscosity, cp [mPa-s]
μ_w = viscosity of brine, cp [mPa-s]
ϕ = porosity
ϕ_i = effective aqueous-phase porosity in Layer i
ϕ_m = effective aqueous-phase porosity in rock matrix

REFERENCES

1. Schurz, G. *et al.*: "Polymer Augmented Waterflooding and Control of Reservoir Heterogeneity," *Proc.*, (paper NMT 890029) Petroleum Technology into the Second Century Symposium, Socorro, NM (1989) 263-75.

2. Seright, R.S. and Martin, F.D.: "Fluid Diversion and Sweep Improvement with Chemical Gels in Oil Recovery Processes," first annual report (DOE/BC/14447-8), U.S. DOE (June 1991).

3. Seright, R.S. and Martin, F.D.: "Fluid Diversion and Sweep Improvement with Chemical Gels in Oil Recovery Processes," second annual report (DOE/BC/14447-10), U.S. DOE (Nov. 1991).

4. Seright, R.S.: "Placement of Gels to Modify Injection Profiles," paper SPE/DOE 17332 presented at the 1988 SPE/DOE Enhanced Oil Recovery Symposium, Tulsa, April 17-20.

5. Liang, J., Lee, R.L., and Seright, R.S.: "Placement of Gels in Production Wells," paper SPE/DOE 20211 presented at the 1990 SPE/DOE Enhanced Oil Recovery Symposium, Tulsa, April 22-25.

6. King, J.A. and Fallgarter, W.S.: "Method of Increasing Oil Recovery," U.S. Patent 2,747,670 (May 29, 1956).

7. Nathan, C.C. and Perry, R.B.: "Treating Permeable Underground Formations," U.S. Patent 2,990,881 (July 4, 1961).

8. Routson, W.G.: "Method of Controlling Flow of Aqueous Fluids in Subterranean Formations," U.S. Patent 3,687,200 (Aug. 29, 1972).

9. Costerton, J.W. F. *et al.*: "Microbial Process for Selectively Plugging a Subterranean Formation," U.S. Patent 4,800,959 (Jan. 31, 1989).

10. Chang, P.W., Goldman, I.M., and Stingley, K.J.: "Laboratory Studies and Field Evaluation of a New Gelant for High-Temperature Profile Modification," paper SPE 14235 presented at the 1985 SPE Annual Technical Conference and Exhibition, Las Vegas, Sept. 22-25.

11. Avery, M.R., Burkholder, L.A., and Gruenenfelder, M.A.: "Use of Crosslinked Xanthan Gels in Actual Profile Modification Field Projects," paper SPE 14114 presented at the 1986 SPE International Meeting on Petroleum Engineering, Beijing, China, March 17-20.

12. McAuliffe, C.D.: "Oil-in-Water Emulsions and Their Flow Properties in Porous Media," *JPT* (June 1973) 727-33.

13. Varnon, J.E. *et al.*: "High Conformance Enhanced Oil Recovery Process," U.S. Patent 4,161,218 (July 17, 1979).

14. Bernard, G.G.: "Method for Water Flooding Heterogeneous Petroleum Reservoirs," U.S. Patent 3,530,937 (Sept. 29, 1970).

15. Harwell, J.H. and Scamehorn, J.F.: "Surfactant Enhanced Volumetric Sweep Efficiency," final report (DOE/BC/10845-15), U.S. DOE (Oct. 1989).

16. Smith, J.E.: "The Transition Pressure: A Quick Method for Quantifying Polyacrylamide Gel Strength," paper SPE 18739 presented at the 1989 SPE International Symposium on Oilfield Chemistry, Houston, Feb. 8-10.

17. Llave, F.M., Burchfield, T.E., and Dobson, R.E.: "A Novel Method of Developing In-Depth Permeability Modification Using Surfactant-Alcohol Blends," paper SPE 20484 presented at the 1990 SPE Annual Technical Conference and Exhibition, New Orleans, Sept. 23-26.

18. Fogler, H.S.: "Characterization and Modification of Fluid Conductivity in Heterogeneous Reservoirs to Improve Sweep Efficiency," *Enhanced Oil Recovery Progress Review*, **61**, U.S. DOE (Sept. 1990) 64-6.

19. Seright, R.S.: "Impact of Dispersion on Gel Placement for Profile Control," *SPERE* (Aug. 1991) 343-352.

20. Seright, R.S.: "Effect of Rheology on Gel Placement," *SPERE* (May 1991) 212-218; *Trans.*, AIME, **291**.

21. Seright, R.S.: "Impact of Permeability and Lithology on Gel Performance," paper SPE/DOE 24190 presented at the 1992 SPE/DOE Enhanced Oil Recovery Symposium, Tulsa, April 21-24.

22. Liang, J., Sun, H., and Seright, R.S.: "Reduction of Oil and Water Permeabilities Using Gels," paper SPE/DOE 24195 presented at the 1992 SPE/DOE Enhanced Oil Recovery Symposium, Tulsa, April 21-24.

23. Jurinak, J.J., Summers, L.E., and Bennett, K.E.: "Oilfield Application of Colloidal Silica Gel," paper SPE 18505 presented at the 1989 SPE International Symposium on Oilfield Chemistry, Houston, Feb. 8-10.

24. Sydansk, R.D.: "A New Conformance Improvement Treatment Chromium (III) Gel Technology," paper SPE/DOE 17329 presented at the 1988 SPE/DOE Enhanced Oil Recovery Symposium, Tulsa, April 17-20.

25. Sydansk, R.D. and Smith T.B.: "Field Testing of a New Conformance-Improvement Treatment-Chromium (III) Gel Technology," paper SPE/DOE 17383 presented at the 1988 SPE/DOE Enhanced Oil Recovery Symposium, Tulsa, April 17-20.

26. Sydansk, R.D.: "Acrylamide-Polymer/Chromium(III)-Carboxylate Gels for Near Wellbore Matrix Treatments," paper SPE/DOE 20214 presented at the 1990 SPE/DOE Enhanced Oil Recovery Symposium, Tulsa, April 22-25.

27. Perkins, T.K. and Johnston, O.C.: "A Review of Diffusion and Dispersion in Porous Media," *SPEJ* (March 1963) 70-84.

28. Seright, R.S. and Martin, F.D.: "Impact of Gelation pH, Rock Permeability, and Lithology on the Performance of a Monomer-Based Gel," paper SPE 20999 presented at the 1991 SPE International Symposium on Oilfield Chemistry, Anaheim, Feb. 20-22.

29. Shu, P.: "The Gelation Mechanism of Chromium(III)," *American Chemical Society Symposium Series* (1988) **33**, No. 1, 43-48.

30. Mumallah, N.A.: "Chromium (III) Propionate: A Crosslinking Agent for Water-Soluble Polymers in Hard Oilfield Brines," *SPERE* (Feb. 1988) 243-250.

31. Tackett, J.E.: "Characterization of Chromium(III) Acetate in Aqueous Solution," *Applied Spectroscopy* (1989) **43**, No. 3, 490-499.

32. Lockhart, T.P.: "Chemical and Structural Studies on Cr^{3+}/Polyacrylamide Gels," paper SPE 20998 presented at the 1991 SPE International Symposium on Oilfield Chemistry, Anaheim, Feb. 20-22.

33. Kolnes, J., Stavland, A, and Thorsen, S.: "The Effect of Temperature on the Gelation Time of Xanthan/Cr(III) Systems," paper SPE 21001 presented at the 1991 SPE International Symposium on Oilfield Chemistry, Anaheim, Feb. 20-22.

34. Willhite, G.P. *et al.*: "Gelled Polymer Systems for Permeability Modification in Petroleum Reservoirs," final report (DOE/ID/12846-6), U.S. DOE (Sept. 1991).

35. Garver, F.J., Sharma, M.M., and Pope, G.A.: "The Competition for Chromium Between Xanthan Biopolymer and Resident Clays in Sandstones," paper SPE 19632 presented at the 1989 SPE Annual Technical Conference and Exhibition, San Antonio, Oct. 8-11.

36. Kia, S.F., Fogler, H.S., and Reed, M.G.: "Effect of pH on Colloidally Induced Fines Migration," *J. Colloid & Interfac. Sci.* (1987) **118**, No. 1, 158-168.

37. Seright, R.S. and Martin, F.D.: "Effect of Cr^{3+} on the Rheology of Xanthan Formulations in Porous Media: Before and After Gelation," *In Situ* (1992) **16**, No.1, 1-16.

38. Avery, M.R. and Wells, T.A.: "Field Evaluation of a New Gelant for Water Control in Production Wells," paper SPE 18201 presented at the 1988 SPE Annual Technical Conference and Exhibition, Houston, Oct. 2-5.

39. Needham, R.B., Threlkeld, C.B., and Gall, J.W.: "Control of Water Mobility Using Polymers and Multivalent Cations," paper SPE 4747 presented at the 1974 SPE-AIME Improved Oil Recovery Symposium, Tulsa, April 22-24.

40. Sandiford, B.B. and Graham, G.A.: "Injection of Polymer Solutions in Producing Wells," AIChE Symposium Series, (1973) **69**, No. 127, 38.

41. Schneider, F.N. and Owens, W.W.: "Steady-State Measurements of Relative Permeability for Polymer/Oil Systems," *SPEJ* (Feb. 1982) 79.

42. Sparlin, D.D.: "An Evaluation of Polyacrylamides for Reducing Water Production," *JPT* (Aug. 1976) 906-914.

43. White, J.L., Goddard, J.E., and Phillips, H.M.: "Use of Polymers To Control Water Production in Oil Wells," *JPT* (Feb. 1973) 143-150.

44. Zaitoun, A. and Kohler N.: "Two-Phase Flow Through Porous Media: Effect of an Adsorbed Polymer Layer," paper SPE 18085 presented at the 1988 Annual Technical Conference and Exhibition, Houston, Oct. 2-5.

45. Zaitoun, A. and Kohler N.: "Thin Polyacrylamide Gels for Water Control in High-Permeability Production Wells" paper SPE 22785 presented at the 1991 Annual Technical Conference and Exhibition, Dallas, Oct. 6-9.

46. Willhite, G.P.: *Waterflooding,* SPE, Richardson, TX (1986) **3**, 21-24.

47. Jones, S.C. and Roszelle, W.O.: "Graphical Techniques for Determining Relative Permeability From Displacement Experiments," *JPT* (May 1978) 807-817.

48. Morrow, N.R., Lim, H.T., and Ward, J.S.: "Effect of Crude-Oil-Induced Wettability Changes on Oil Recovery," *SPEFE* (Feb. 1986) 89-103.

49. Jia, D., Buckley, J.S., Morrow, N.R.: "Control of Core Wettability With Crude Oil," paper SPE 21041 presented at the 1991 SPE International Symposium on Oilfield Chemistry, Anaheim, Feb. 20-22.

50. Jadhunandan, P.P.: "Effects of Brine Composition, Crude Oil, and Aging Conditions on Wettability and Oil Recovery," PhD dissertation, New Mexico Institute of Mining and Technology, Socorro, (1990).

51. Martin, F.D. and Kovarik, F.S.: "Chemical Gels for Diverting CO_2: Baseline Experiments," paper SPE 16728 presented at the 1987 Technical Conference and Exhibition, Dallas, Sept. 27-30.

52. Martin, F.D. *et al.*: "Gels for CO_2 Profile Modification," paper SPE/DOE 17330 presented at the 1988 SPE/DOE Symposium on Enhanced Oil Recovery, Tulsa, April 17-20.

53. Hessert, J.E. and Fleming, P.D.: "Gelled Polymer Technology for Control of Water in Injection and Production Wells," *Proc.*, Third Tertiary Oil Recovery Conf., Wichita (1979) 58-70.

54. DuBois, B.M.: "North Stanley Polymer Demonstration Project," third annual and final report, Contract No. BETC/RI-78/19, U.S. DOE (Nov. 1978).

55. Sydansk, R.D. and Moore, P.E.: "Production Responses in Wyoming's Big Horn Basin Resulting from Application of Acrylamide-Polymer/Cr^{III}-Carboxylate Gels," *Proc.* Sixth University of Wyoming Enhanced Oil Recovery Symposium (1990) Casper, May 3-4.

56. Moffitt, P.D.: "Long-Term Production Results of Polymer Treatments on Producing Wells in Western Kansas," paper SPE 22649 presented at the 1991 Technical Conference and Exhibition, Dallas, Oct. 6-9.

57. Veatch Jr., R.W., Moschovidis, Z.A., and Fast, C.R.: "An Overview of Hydraulic Fracturing," *Recent Advances in Hydraulic Fracturing*, Monograph Series, SPE, Richardson, TX (1989), **12**, 1.

58. Aguilera, R.: *Naturally Fractured Reservoirs*, PennWell Publishing, Tulsa (1980).

59. Crawford, P.B. and Collins, R.E.: "Estimated Effect of Vertical Fractures on Secondary Recovery," *Transactions*, AIME, **201** (1954) 192-196.

60. Dyes, A.B., Kemp, C.E., and Caudle, B.H.: "Effect of Fractures on Sweep-out Pattern," *Transactions*, AIME, **213** (1958) 245-249.

61. Bargas, C.L. and Yanosik, J.L.: "The Effects of Vertical Fractures on Areal Sweep Efficiency in Adverse Mobility Ratio Floods," paper SPE 17609 presented at the 1988 International Meeting on Petroleum Engineering, Tianjin, China, Nov. 1-4.

62. Donohue, A.T., Hansford, J.T., and Burton, R.A.: "The Effect of Induced Vertically-Oriented Fractures on Five-Spot Sweep Efficiency," *SPEJ* (Sept. 1968) 260-268.

63. Prats, M.: "Effect of Vertical Fractures on Reservoir Behavior—Incompressible Fluid Case," *SPEJ* (June, 1961) 105-118.

64. Prats, M., Hazebroek, P., and Strickler, W.R.: "Effect of Vertical Fractures on Reservoir Behavior—Compressible Fluid Case," *Transactions*, AIME (1962) **210**, 87-94.

65. Prats, M. and Levin, J.S.: "Effect of Vertical Fractures on Reservoir Behavior—Results on Oil and Gas Flow," *Transactions*, AIME (1963) **218**, 1119-1126.

66. Hartsock, J.H. and Slobod, R.L.: "The Effect of Mobility Ratio and Vertical Fractures on the Sweep Efficiency of a Five-Spot," *Prod. Monthly* (Sept. 1961) 2-7.

67. Hunter, B.L., Buell, R.S., and Abate, T.A.: "Application of a Polymer Gel System to Control Steam Breakthrough and Channeling," paper SPE/DOE 24031 presented at the 1992 SPE Western Regional Meeting, Bakersfield, March 30-April 1.

68. Penny, G.S. and Conway, M.W.: "Fluid Leakoff," *Recent Advances in Hydraulic Fracturing*, Monograph Series, SPE, Richardson, TX (1989) **12**, 147-176.

69. Ben-Naceur, K.: "Modeling of Hydraulic Fractures," *Reservoir Stimulation*, 2nd ed., Prentice Hall, Englewood Cliffs, NJ (1989) **12**, 3.1-3.31.

70. Sorbie, K.S. and Seright, R.S.: "Gel Placement in Heterogeneous Systems with Crossflow," paper SPE 24192 presented at the 1992 SPE/DOE Symposium on Enhanced Oil Recovery, Tulsa, OK, April 22-24.

71. Zapata, V.J. and Lake, L.W.: "A Theoretical Analysis of Viscous Crossflow," paper SPE 10111 presented at the 1981 SPE Annual Technical Conference and Exhibition, San Antonio, Oct. 5-7.

APPENDIX A

COREFLOOD DATA IN SANDSTONES AND LIMESTONES (SUPPLEMENT TO SECTION 2)

APPENDIX A

Table A-1. Residual Resistance Factors for Gel Formed From 4% Ludox SM® Colloidal Silica, 0.7% NaCl, pH=7.0, 41°C

Table A-1a. 4% Colloidal-Silica Gel in 13.4-md Indiana Limestone. ϕ=0.19.

Superficial velocity, ft/d	Pore volumes of brine injected	F_{rrw} in the second core segment	Pressure gradient, psi/ft
0.025	0.4	86	25
0.050	0.4	99	60
0.025	0.1	102	30
0.101	0.2	106	126
0.050	0.4	120	72
0.025	0.3	120	35
0.203	0.5	130	311
0.101	0.2	129	154
0.025	0.2	120	35
0.396	0.4	112	523
0.203	0.2	115	275
0.101	0.1	120	143
0.025	0.2	120	35
0.791	0.6	88	821
0.396	0.4	90	420
0.203	0.7	90	216
0.101	0.7	103	123
0.051	0.2	107	64
0.025	0.2	105	31
1.583	2.0	65	1214
0.791	0.8	74	690
0.396	0.2	78	364
0.203	0.2	85	204
0.101	0.2	91	108
0.025	0.2	100	29

Pore volumes of brine injected=10.0. Average F_{rrw}=102 & final k=130 μD.

Table A-1b. 4% Colloidal-Silica Gel in 546-md Berea Sandstone. ϕ=0.22.

Superficial velocity, ft/d	Pore volumes of brine injected	F_{rrw} in the second core segment	Pressure gradient, psi/ft
0.025	0.3	6000	29
0.051	0.4	6200	61
0.025	0.3	6100	30
0.101	0.4	6100	119
0.051	0.4	6250	62
0.025	0.3	6250	30
0.203	0.2	6000	236
0.101	0.3	6050	119
0.025	0.2	6100	29
0.396	4.1	165	13
0.203	0.2	145	6
0.101	0.2	131	3
0.025	0.2	140	1
0.791	0.5	121	19
0.396	0.8	91	7
0.203	1.4	66	3
0.101	0.6	51	1
1.583	1.1	57	17
0.791	1.1	53	8
0.396	0.3	53	4
0.203	0.8	43	2
0.101	0.2	30	1
3.165	1.0	40	25
1.583	0.6	40	12
0.791	1.5	35	5
0.396	2.0	30	2
0.203	0.5	24	1
6.331	8.9	21	25
3.165	1.5	21	13
1.583	0.7	21	7
0.791	1.9	18	3
0.396	1.6	15	1
0.203	0.3	12	0
15.827	5.0	18	55
6.331	5.3	18	22
3.165	1.5	24	15
1.583	1.0	21	7
0.791	1.3	16	3
0.396	2.2	12	1

Pore volumes of brine injected=51.1. When dp/dl < 400 psi/ft, average F_{rrw}=6100 & final k=90 μD.

Table A-1c. 4% Colloidal-Silica Gel in 67-md Berea Sandstone. ϕ=0.19.

Superficial velocity, ft/d	Pore volumes of brine injected	F_{rrw} in the second core segment	Pressure gradient, psi/ft
0.025	0.6	2300	91
0.050	0.6	1800	145
0.025	0.3	2200	87
0.101	0.4	1920	307
0.050	0.5	2300	185
0.025	0.3	2250	89
0.203	0.5	1575	505
0.101	0.2	1740	278
0.025	0.2	2180	86
0.396	0.5	1060	663
0.203	0.3	1240	398
0.101	0.3	1430	228
0.025	0.2	1750	69
0.791	0.5	693	886
0.396	0.3	870	545
0.203	0.2	1040	334
0.101	0.7	1300	208
0.025	0.4	1580	62
1.583	0.9	450	1126
0.791	0.8	610	763
0.396	0.4	770	482
0.203	1.8	1140	366
0.101	0.3	1300	208
0.025	0.2	1450	257
1.583	0.8	470	1176
0.791	0.5	645	806
0.396	0.6	850	532
0.203	0.8	1110	356
0.101	0.5	1330	212
0.051	0.2	1500	121
0.025	0.2	1530	60

Pore volumes of brine injected=15.0. Average F_{rrw}=1400 & final k=47 μD.

Table A-2. Residual Resistance Factors for Gel Formed From 0.4% Xanthan, 154-ppm Cr^{3+} (as $CrCl_3$), 0.05 M Acetate, 0.5% KCl, 41°C

Table A-2a. Buffered Cr^{3+}-Xanthan Gel in 840-md Berea Sandstone. ϕ=0.219.

Superficial velocity, ft/d	Pore volumes of brine injected	F_{rrw} in the second core segment	Pressure gradient, psi/ft
3.14	10.0	5.8	2
6.28	3.0	4.4	3
3.14	2.2	4.2	2
15.7	2.3	3.4	7
6.28	1.0	3.7	3
3.14	1.7	3.6	1
31.4	2.3	2.6	10
15.7	2.7	2.9	6
6.28	1.5	2.8	2
3.14	0.8	3.4	1

Pore volumes of brine injected=27.5. Maximum pressure gradient=10 psi/ft.
For the last four readings, the average F_{rrw}=2.9, and $F_{rrw}=3.6\ u^{-0.095}$ with r=0.853.

Table A-2b. Buffered Cr^{3+}-Xanthan Gel in 93-md Berea Sandstone. ϕ=0.181.

Superficial velocity, ft/d	Pore volumes of brine injected	F_{rrw} in the second core segment	Pressure gradient, psi/ft	F_{rrw} relation
0.025	0.3	430	13	
0.050	0.3	224	13	$F_{rrw} = 63.4\ u^{-0.42}$
0.025	0.1	300	9	
0.100	0.8	76	7	$F_{rrw} = 22.3\ u^{-0.54}$
0.050	0.5	114	7	
0.025	0.3	160	5	r = 0.999
0.201	1.1	35	7	$F_{rrw} = 16.0\ u^{-0.46}$
0.100	0.8	44	5	
0.050	0.6	65	4	r = 0.995
0.025	0.3	90	3	
0.393	0.9	23	10	$F_{rrw} = 12.8\ u^{-0.60}$
0.201	0.4	34	8	
0.100	0.8	48	6	r = 0.998
0.050	0.6	80	5	
0.025	0.4	120	3	

Table A-2b (continued). Buffered Cr^{3+}-Xanthan Gel in 93-md Berea Sandstone. ϕ=0.181.

Superficial velocity, ft/d	Pore volumes of brine injected	F_{rrw} in the second core segment	Pressure gradient, psi/ft	F_{rrw} relation
0.785	0.8	20	19	$F_{rrw} = 16.8\ u^{-0.67}$
0.393	0.6	31	14	
0.201	3.9	50	7	r = 0.999
1.570	1.4	13	25	
0.785	1.6	18	17	
0.393	0.5	21	10	$F_{rrw} = 15.2\ u^{-0.42}$
0.201	1.7	28	7	
0.100	0.4	37	5	r = 0.995
0.050	0.4	55	3	
0.025	0.3	75	2	
3.14	1.7	9.6	36	$F_{rrw} = 13.7\ u^{-0.38}$
1.57	0.7	10.2	19	
0.785	0.5	15.4	15	r = 0.968
0.393	2.4	20.0	9	
6.28	1.7	7.3	52	
3.14	1.2	8.3	33	$F_{rrw} = 10.2\ u^{-0.18}$
1.57	1.8	9.0	17	
0.785	2.5	11.5	6	r = 0.987
0.100	0.9	15.0	2	
15.7	2.5	5.5	103	
6.28	1.6	6.3	49	$F_{rrw} = 8.1\ u^{-0.14}$
3.14	1.3	6.8	26	
1.57	0.9	7.8	15	r = 0.997
0.785	1.1	8.3	8	
0.393	3.8	9.3	4	
0.201	0.7	11.9	3	(additional data)
0.100	1.0	14.6	2	$F_{rrw} = 8.6\ u^{-0.17}$
0.050	1.2	17.8	1	
0.025	0.3	13.0	0.4	r = 0.951

Pore volumes of brine injected=47.6. Maximum pressure gradient=103 psi/ft.

Table A-3. Residual Resistance Factors for Gel Formed From 1.39% Polyacrylamide (MARCIT), 212-ppm Cr^{3+} (as chromium acetate), 1.0% NaCl, 41°C

Table A-3a. Cr^{3+}(Acetate)-HPAM Gel in 746-md Berea Sandstone. ϕ=0.216.

Superficial velocity, ft/d	Pore volumes of brine injected	F_{rrw} in the second core segment	Pressure gradient, psi/ft
0.025	0.5	142,000	506
0.051	0.5	122,000	887
0.025	0.3	175,000	624
0.100	0.1	95,000	1354
0.051	0.5	146,000	1061
0.025	0.3	179,000	638

Pore volumes of brine injected=2.2. Maximum pressure gradient=1354 psi/ft.
For all six readings, the average F_{rrw}=143,000 ± 32,000.
Average permeability after gel=746/143,000=5.2 μD.
For the last three readings, $F_{rrw}=34{,}700\ u^{-0.46}$, with r=0.976.

Table A-3b. Cr^{3+}(Acetate)-HPAM Gel in 74-md Berea Sandstone. ϕ=0.19.

Superficial velocity, ft/d	Pore volumes of brine injected	F_{rrw} in the second core segment	Pressure gradient, psi/ft	F_{rrw} relation
0.025	0.6	2,100	75	
0.051	0.6	1,420	104	$F_{rrw} = 340\ u^{-0.48}$
0.025	0.3	2,000	72	
0.100	0.4	1,000	144	$F_{rrw} = 268\ u^{-0.57}$
0.051	0.6	1,510	111	
0.025	0.3	2,220	80	r=0.999
0.203	0.3	780	228	$F_{rrw} = 319\ u^{-0.57}$
0.101	0.8	1,220	177	
0.051	0.8	1,800	132	r=0.999
0.025	0.5	2,600	93	
0.396	1.2	570	323	
0.203	1.5	880	258	$F_{rrw} = 351\ u^{-0.56}$
0.101	0.4	1300	189	
0.051	0.4	1910	140	r=0.999
0.025	0.3	2700	97	

Table A-3b. (Continued)

Superficial velocity, ft/d	Pore volumes of brine injected	F_{rrw} in the second core segment	Pressure gradient, psi/ft	F_{rrw} relation
0.791	0.6	403	458	
0.396	1.0	550	313	$F_{rrw} = 353\ u^{-0.55}$
0.203	1.6	900	263	
0.101	0.4	1300	189	r=0.998
0.025	0.2	2600	93	
1.583	1.2	250	569	$F_{rrw} = 351\ u^{-0.56}$
0.791	0.4	305	347	
0.203	0.5	645	188	r=0.999
0.101	0.9	1100	160	
1.583	0.8	270	614	$F_{rrw} = 317\ u^{-0.54}$
0.791	0.9	340	386	
0.396	0.7	480	273	r=0.991
0.101	0.7	1150	167	
3.165	0.5	161	732	
1.583	0.7	180	409	$F_{rrw} = 264\ u^{-0.54}$
0.791	0.4	228	259	
0.396	0.4	338	192	r=0.990
0.101	1.0	840	122	
0.025	0.3	1980	71	
6.331	1.1	98	892	
3.165	1.0	110	500	
1.583	0.8	140	318	$F_{rrw} = 200\ u^{-0.53}$
0.791	1.2	200	227	
0.396	0.3	270	154	r=0.986
0.203	0.5	414	121	
0.101	0.7	720	104	
0.025	0.3	1740	63	

Pore volumes of brine injected=28.1. Maximum pressure gradient=892 psi/ft.
Based on last 8 points, $F_{rrw} = 200\ u^{-0.53}$. r=-0.986.

Table A-3c. Cr^{3+}(Acetate)-HPAM Gel in 10.7-md Indiana Limestone. ϕ=0.19.

Superficial velocity, ft/d	Pore volumes of brine injected	F_{rrw} in the second core segment	Pressure gradient, psi/ft	F_{rrw} relation
0.025	0.5	256	63	
0.051	0.3	210	106	$F_{rrw} = 54.6\ u^{-0.45}$
0.025	0.1	290	72	
0.101	0.9	158	158	$F_{rrw} = 59.5\ u^{-0.43}$
0.051	0.6	225	113	
0.025	0.3	290	72	r=0.994
0.203	0.4	121	243	$F_{rrw} = 64.3\ u^{-0.40}$
0.101	0.3	160	160	
0.025	0.2	278	69	r=0.999
0.396	0.3	83	325	$F_{rrw} = 58.4\ u^{-0.41}$
0.203	0.3	116	233	
0.101	0.1	152	152	r=0.999
0.025	0.2	263	65	
0.791	0.5	58	453	$F_{rrw} = 51.5\ u^{-0.43}$
0.396	0.2	75	293	
0.101	0.2	140	140	r=0.999
0.025	0.2	254	61	
1.583	0.4	41	641	
0.791	0.3	51	399	$F_{rrw} = 48.4\ u^{-0.44}$
0.396	0.3	70	274	
0.101	1.0	144	144	r=0.997
0.025	0.3	235	58	
3.165	1.1	30	938	
1.583	0.7	37	579	$F_{rrw} = 46.6\ u^{-0.42}$
0.791	0.6	49	383	
0.396	0.7	68	266	r=0.997
0.101	0.8	134	134	
0.025	0.3	214	53	

Pore volumes of brine injected=12.1. Maximum pressure gradient=938 psi/ft.
Based on all 28 points, $F_{rrw} = 49.7\ u^{-0.46}$. r=-0.991.

Table A-4. Residual Resistance Factors for Gel Formed From 1.39% Polyacrylamide (MARCIT), 636-ppm Cr^{3+} (as chromium acetate), 1.0% NaCl, 41°C

Table A-4a. Cr^{3+}(Acetate)-HPAM Gel in 662-md Berea Sandstone. ϕ=0.218.

Superficial velocity, ft/d	Pore volumes of brine injected	F_{rrw} in the second core segment	Pressure gradient, psi/ft
0.025	0.3	208,000	835
0.051	0.5	170,000	1393
0.025	0.3	182,000	731

Pore volumes of brine injected=1.1. Maximum pressure gradient=1393 psi/ft.
The average F_{rrw}=187,000 ± 20,000. Average permeability after gel=662/187,000=3.5 μD.

Table A-4b. Cr^{3+}(Acetate)-HPAM Gel in 65-md Berea Sandstone. ϕ=0.194.

Superficial velocity, ft/d	Pore volumes of brine injected	F_{rrw} in the second core segment	Pressure gradient, psi/ft
0.025	0.8	44,600	1824

Pore volumes of brine injected=0.8. Maximum pressure gradient=1824 psi/ft.
Permeability after gel=65/44,600=1.5 μD.

Table A-4b. Cr^{3+}(Acetate)-HPAM Gel in 11-md Indiana Limestone. ϕ=0.188.

Superficial velocity, ft/d	Pore volumes of brine injected	F_{rrw} in the second core segment	Pressure gradient, psi/ft
0.025	1.8	5,810	1404

Pore volumes of brine injected=1.8. Maximum pressure gradient=1404 psi/ft.
Permeability after gel=11/5,810=1.9 μD.

APPENDIX B

OIL AND WATER COREFLOOD DATA
(SUPPLEMENT TO SECTION 3)

APPENDIX B

Table B-1. Rock and Fluid Properties

Table B-1a. Rock and Fluid Properties of Core SSH-15

Core Properties	
Core type	Berea sandstone
Core length, cm	14.18
Cross-sectional area, cm^2	10.12
Initial pore volume, ml	35.49
Porosity	0.247
Absolute permeability to brine, md	803
Fluid Properties	
Brine	0.5% KCl
Brine viscosity at 41°C, cp	0.57
Oil	Moutray
Oil viscosity at 41°C, cp	7.6

Table B-1b. Rock and Fluid Properties of Core SSH-17

Core Properties	
Core type	Berea sandstone
Core length, cm	14.29
Cross-sectional area, cm^2	10.12
Initial pore volume, ml	34.69
Porosity	0.24
Absolute permeability to brine, md	795
Fluid Properties	
Brine	0.5% KCl
Brine viscosity at 41°C, cp	0.57
Oil	Soltrol-130
Oil viscosity at 41°C, cp	1.05

Table B-1c. Rock and Fluid Properties of Core SSH-22

Core Properties	
Core type	Berea sandstone
Core length, cm	14.63
Cross-sectional area, cm^2	10.12
Initial pore volume, ml	36.52
Porosity	0.247
Absolute permeability to brine, md	809
Fluid Properties	
Brine	0.5% KCl
Brine viscosity at 41°C, cp	0.57
Oil	Soltrol-130
Oil viscosity at 41°C, cp	1.05

Table B-1d. Rock and Fluid Properties of Core SSH-23

Core Properties	
Core type	Berea sandstone
Core length, cm	13.97
Cross-sectional area, cm^2	10.12
Initial pore volume, ml	36.57
Porosity	0.259
Absolute permeability to brine, md	815
Fluid Properties	
Brine	0.5% KCl
Brine viscosity at 41°C, cp	0.57
Oil	Moutray
Oil viscosity at 41°C, cp	4.07

Table B-1e. Rock and Fluid Properties of Core SSH-26

Core Properties	
Core type	Berea sandstone
Core length, cm	14.43
Cross-sectional area, cm^2	10.12
Initial pore volume, ml	37.68
Porosity	0.258
Absolute permeability to brine, md	742
Fluid Properties	
Brine	1% NaCl
Brine viscosity at 41°C, cp	0.67
Oil	Soltrol-130
Oil viscosity at 41°C, cp	1.05

Table B-1f. Rock and Fluid Properties of Core SSH-27

Core Properties	
Core type	Berea sandstone
Core length, cm	13.95
Cross-sectional area, cm^2	10.12
Initial pore volume, ml	36.19
Porosity	0.256
Absolute permeability to brine, md	765
Fluid Properties	
Brine	1% NaCl
Brine viscosity at 41°C, cp	0.67
Oil	Soltrol-130
Oil viscosity at 41°C, cp	1.05

Table B-1g. Rock and Fluid Properties of Core SSH-31

Core Properties	
Core type	Berea sandstone
Core length, cm	13.95
Cross-sectional area, cm^2	10.12
Initial pore volume, ml	34.3
Porosity	0.243
Absolute permeability to brine, md	718
Fluid Properties	
Brine	1% NaCl
Brine viscosity at 41°C, cp	0.67
Oil	Soltrol-130
Oil viscosity at 41°C, cp	1.05

Table B-1h. Rock and Fluid Properties of Core SSH-32

Core Properties	
Core type	Berea sandstone
Core length, cm	13.95
Cross-sectional area, cm^2	10.12
Initial pore volume, ml	32.49
Porosity	0.236
Absolute permeability to brine, md	767
Fluid Properties	
Brine	0.7% NaCl
Brine viscosity at 41°C, cp	0.65
Oil	Soltrol-130
Oil viscosity at 41°C, cp	1.05

Table B-1i. Rock and Fluid Properties of Core SSH-33

Core Properties	
Core type	Berea sandstone
Core length, cm	14.28
Cross-sectional area, cm^2	10.12
Initial pore volume, ml	34.73
Porosity	0.24
Absolute permeability to brine, md	788
Fluid Properties	
Brine	0.7% NaCl
Brine viscosity at 41°C, cp	0.65
Oil	Soltrol-130
Oil viscosity at 41°C, cp	1.05

Table B-2. Results of Oil/Water Experiments

Table B-2a. Endpoint Permeabilities Prior to Gel Treatment, SSH-15

Waterflood		
	S_{or}	k_w^o
Step 6	0.26	155
Step 8	0.24	146
Step 9 (Flow reversed)	0.17	252
Step 10 (Flow reversed)	0.13	269
Oilflood		
	S_{wr}	k_o^o
Step 4	0.25	1745
Step 8	0.28	1626
Step 9 (Flow reversed)	0.31	1530
Step 10 (Flow reversed)	0.35	1311

Table B-2b. Endpoint Permeabilities Prior to Gel Treatment, SSH-17

Waterflood		
	S_{or}	k_w^o
Step 6	0.28	186
Step 8	0.29	177
Step 9 (Flow reversed)	0.32	173
Step 10 (Flow reversed)	0.34	165
Oilflood		
	S_{wr}	k_o^o
Step 4	0.34	719
Step 8	0.32	708
Step 9 (Flow reversed)	0.31	730
Step 10 (Flow reversed)	0.30	700

Table B-2c. Endpoint Permeabilities Prior to Gel Treatment, SSH-22

Waterflood		
	S_{or}	k_w^o
Step 6	0.31	187
Step 8	0.34	184
Step 9 (Flow reversed)	0.33	215
Step 10 (Flow reversed)	0.33	196
Oilflood		
	S_{wr}	k_o^o
Step 4	0.27	674
Step 8	0.26	736
Step 9 (Flow reversed)	0.25	782
Step 10 (Flow reversed)	0.27	801

Table B-2d. Endpoint Permeabilities Prior to Gel Treatment, SSH-23

Waterflood		
	S_{or}	k_w^o
Step 6	0.23	235
Step 8	0.21	318
Step 9 (Flow reversed)	0.20	402
Step 10 (Flow reversed)	0.18	401
Oilflood		
	S_{wr}	k_o^o
Step 4	0.32	944
Step 8	0.30	837
Step 9 (Flow reversed)	0.26	936
Step 10 (Flow reversed)	0.29	882

Table B-2e. Endpoint Permeabilities Prior to Gel Treatment, SSH-26

Waterflood		
	S_{or}	k_w^o
Step 6	0.27	184
Step 8	0.28	169
Step 9 (Flow reversed)	0.28	172
Step 10 (Flow reversed)	0.29	168
Oilflood		
	S_{wr}	k_o^o
Step 4	0.33	582
Step 8	0.32	604
Step 9 (Flow reversed)	0.32	611
Step 10 (Flow reversed)	0.31	579

Table B-2f. Endpoint Permeabilities Prior to Gel Treatment, SSH-27

Waterflood		
	S_{or}	k_w^o
Step 6	0.30	151
Oilflood		
	S_{wr}	k_o^o
Step 4	0.30	573

Table B-2g. Endpoint Permeabilities Prior to Gel Treatment, SSH-31

Waterflood		
	S_{or}	k_w^o
Step 6	0.27	220
Oilflood		
	S_{wr}	k_o^o
Step 4	0.29	589

Table B-2h. Endpoint Permeabilities Prior to Gel Treatment, SSH-32

Waterflood		
	S_{or}	k_w^o
Step 6	0.28	239
Oilflood		
	S_{wr}	k_o^o
Step 4	0.26	616

Table B-2i. Endpoint Permeabilities Prior to Gel Treatment, SSH-33

Waterflood		
	S_{or}	k_w^o
Step 6	0.34	133
Oilflood		
	S_{wr}	k_o^o
Step 4	0.29	634

Table B-3. Summary of Residual Resistance Factors After Gel Treatments

Table B-3a. Residual Resistance Factors for Brine (F_{rrw}) and Moutray Crude (F_{rro}), SSH-15 3% resorcinol, 3% formaldehyde, 0.5% KCl, 0.05M $NaHCO_3$, pH=6.5

	Flux, ft/d	F_{rrw}	F_{rro}
1st waterflood after gel treatment (Step 13)	0.025	1772	--
	0.050	1197	--
	0.025	1274	--
	0.100	678	--
	0.025	887	--
	0.200	510	--
	0.025	853	--
1st oilflood after gel treatment (Step 15a)	2.334	--	26
2nd waterflood after gel treatment (Step 15c)	0.778	180	--
2nd oilflood after gel treatment (Step 16a)	2.023	--	29
3rd waterflood after gel treatment (Step 16c)	0.622	241	--

Table B-3b. Residual Resistance Factors for Brine (F_{rrw}) and Soltrol-130 (F_{rro}), SSH-17
3% resorcinol, 3% formaldehyde, 0.5% KCl, 0.05M $NaHCO_3$, pH=6.5

	Flux, ft/d	F_{rrw}	F_{rro}
1st waterflood after gel treatment (Step 13)	0.025	84	--
	0.050	94	--
	0.025	94	--
	0.100	92	--
	0.025	135	--
	0.200	110	--
	0.025	141	--
	0.400	61	--
	0.025	69	--
	0.778	58	--
	0.025	74	--
	1.556	51	--
	0.025	72	--
	2.023	48	--
	0.025	60	--
	2.334	49	--
	0.025	58	--
1st oilflood after gel treatment (Step 15a)	20.23	--	11
2nd waterflood after gel treatment (Step 15c)	2.334	40	--
2nd oilflood after gel treatment (Step 16a)	20.23	--	12
3rd waterflood after gel treatment (Step 16c)	2.334	41	--

Table B-3c. Residual Resistance Factors for Brine (F_{rrw}) and Soltrol-130 (F_{rro}), SSH-22 0.4% xanthan (Flocon 4800®), 154-ppm Cr^{3+} (as $CrCl_3$), 0.5% KCl, pH=4.0

	Flux, ft/d	F_{rrw}	F_{rro}
1st waterflood after gel treatment (Step 13)	0.023	42	--
	0.047	32	--
	0.023	38	--
	0.093	25	--
	0.023	36	--
	0.187	18	--
	0.023	28	--
	0.373	16	--
	0.023	26	--
	0.747	13	--
	0.023	20	--
	1.494	13	--
	0.023	28	--
	2.987	11	--
	0.023	28	--
	5.974	9	--
	0.023	25	--
	11.948	7	--
	0.023	16	--
	23.897	5	--
	0.023	13	--
	46.673	5	--
	0.023	13	--

Table B-3c (continued). Residual Resistance Factors for Brine (F_{rrw}) and Soltrol-130 (F_{rro}), SSH-22 0.4% xanthan (Flocon 4800®), 154-ppm Cr^{3+} (as $CrCl_3$), 0.5% KCl, pH=4.0

	Flux, ft/d	F_{rrw}	F_{rro}
1st oilflood after gel treatment (Step 15a)	46.673	--	5
	23.337	--	4
	11.668	--	5
	5.864	--	5
	3.112	--	5
	1.556	--	5
	0.778	--	5
	0.389	--	6
2nd waterflood after gel treatment (Step 15c)	31.116	6	--
	23.337	6	--
	11.668	6	--
	5.834	7	--
	3.112	8	--
	1.556	10	--
	0.778	13	--
	0.389	17	--
	0.187	18	--
	0.093	21	--
	0.047	25	--
	0.023	30	--

Table B-3c (continued). Residual Resistance Factors for Brine (F_{rrw}) and Soltrol-130 (F_{rro}), SSH-22 0.4% xanthan (Flocon 4800®), 154-ppm Cr^{3+} (as $CrCl_3$), 0.5% KCl, pH=4.0

	Flux, ft/d	F_{rrw}	F_{rro}
2nd oilflood after gel treatment (Step 16a)	46.673	--	4
	23.337	--	4
	11.668	--	4
	5.864	--	5
	3.112	--	5
	1.556	--	4
	0.778	--	4
	0.389	--	4
3rd waterflood after gel treatment (Step 16c)	31.116	6	--
	23.337	6	--
	12.448	6	--
	6.224	6	--
	3.112	7	--
	1.556	8	--
	0.778	9	--
	0.389	9	--
	0.187	10	--
	0.093	11	--
	0.047	12	--

Table B-3d. Residual Resistance Factors for Brine (F_{rrw}) and Moutray (F_{rro}), SSH-23 0.4% xanthan (Flocon 4800®), 154-ppm Cr^{3+} (as $CrCl_3$), 0.5% KCl, pH=4.0

	Flux, ft/d	F_{rrw}	F_{rro}
1st waterflood after gel treatment (Step 13)	0.025	183	--
	0.05	122	--
	0.025	134	--
	0.10	94	--
	0.025	128	--
	0.199	64	--
	0.025	95	--
	0.398	52	--
	0.025	85	--
	0.778	41	--
	0.025	79	--
	1.556	33	--
	0.025	71	--
	3.112	29	--
	0.025	67	--
	6.223	28	--
	0.025	67	--
	12.446	20	--
	0.025	60	--
	23.337	16	--
	0.025	49	--
	46.673	12	--
	0.025	38	--

Table B-3d (continued). Residual Resistance Factors for Brine (F_{rrw}) and Moutray (F_{rro}), SSH-23 0.4% xanthan (Flocon 4800®), 154-ppm Cr^{3+} (as $CrCl_3$), 0.5% KCl, pH=4.0

	Flux, ft/d	F_{rrw}	F_{rro}
1st oilflood after gel treatment (Step 15a)	12.446	--	10
	6.223	--	11
	3.112	--	12
	1.556	--	13
	0.778	--	15
	0.389	--	17
	0.187	--	18
	0.093	--	19
	0.047	--	20
2nd waterflood after gel treatment (Step 15c)	23.337	22	--
	12.446	23	--
	6.223	25	--
	3.112	26	--
	1.556	29	--
	0.778	31	--
	0.389	34	--
	0.187	37	--
	0.093	41	--
	0.047	44	--
	0.023	52	--

Table B-3d (continued). Residual Resistance Factors for Brine (F_{rrw}) and Moutray (F_{rro}), SSH-23 0.4% xanthan (Flocon 4800®), 154-ppm Cr^{3+} (as $CrCl_3$), 0.5% KCl, pH=4.0

	Flux, ft/d	F_{rrw}	F_{rro}
2nd oilflood after gel treatment (Step 16a)	12.446	--	12
	6.223	--	13
	3.112	--	14
	1.556	--	15
	0.778	--	17
	0.389	--	18
	0.187	--	19
	0.093	--	19
	0.047	--	20
	0.023	--	25
3rd waterflood after gel treatment (Step 16c)	12.446	28	--
	6.223	31	--
	3.112	35	--
	1.556	39	--
	0.778	44	--
	0.389	49	--
	0.187	54	--
	0.093	61	--
	0.047	69	--
	0.023	86	--

Table B-3e. Residual Resistance Factors for Brine (F_{rrw}) and Soltrol-130 (F_{rro}), SSH-26 1.39% polyacrylamide (MARCIT®), 636-ppm Cr^{3+} (as acetate), 1% NaCl, pH=6.0

	Flux, ft/d	F_{rrw}	F_{rro}
1st waterflood after gel treatment (Step 13)	0.008	40,000	--
1st oilflood after gel treatment (Step 15a)	0.023	--	1823
	0.047	--	2241
	0.023	--	1517
	0.093	--	1948
	0.047	--	2260
	0.023	--	1850
	0.187	--	1370
	0.093	--	1080
	0.047	--	1209
	0.023	--	1152
	0.389	--	1139
	0.187	--	1060
	0.093	--	1121
	0.047	--	1053
	0.023	--	1037
	0.653	--	876
	0.389	--	1088
	0.187	--	1088
	0.093	--	1076
	0.047	--	1046
	0.023	--	946
2nd waterflood after gel treatment (Step 15c)	0.014	12,314	--

Table B-3e (continued). Residual Resistance Factors for Brine (F_{rrw}) and Soltrol-130 (F_{rro}), SSH-26 1.39% polyacrylamide (MARCIT®), 636-ppm Cr^{3+} (as acetate), 1% NaCl, pH=6.0

	Flux, ft/d	F_{rrw}	F_{rro}
2nd oilflood after gel treatment (Step 16a)	4.667	--	132
	3.112	--	133
	1.556	--	138
	0.778	--	144
	0.389	--	146
	0.187	--	148
	0.093	--	149
	0.047	--	167
	0.023	--	173
3rd waterflood after gel treatment (Step 16c)	0.023	2175	--
3rd oilflood after gel treatment (Step 17a)	6.223	--	93
	3.112	--	95
	1.556	--	103
	0.778	--	104
	0.389	--	106
	0.187	--	103
	0.093	--	108
	0.047	--	100
	0.023	--	101
	0.047	--	101
	6.223	--	84
4th waterflood after gel treatment (Step 17c)	0.366	637	--
	0.187	820	--
	0.093	1136	--
	0.047	1477	--
	0.023	2073	--
	For 4th waterflood, $F_{rrw}=409\ u^{-0.43}$; r=0.999.		

Table B-3f. Residual Resistance Factors for Brine (F_{rrw}) and Soltrol-130 (F_{rro}), SSH-27 0.7% polyacrylamide (MARCIT®), 318-ppm Cr^{3+} (as acetate), 1% NaCl, pH=6.0

	Flux, ft/d	F_{rrw}	F_{rro}
1st waterflood after gel treatment (Step 13)	0.023	4750	--
	0.047	3421	--
	0.023	4979	--
	0.093	2441	--
	0.047	3287	--
	0.023	4595	--
	For last 3 readings of 1st waterflood, $F_{rrw}=829\ u^{-0.45}$; r=1.		
1st oilflood after gel treatment (Step 15a)	46.673	--	13
	23.337	--	13
	12.446	--	14
	6.223	--	11
	3.112	--	12
	1.556	--	12
	0.778	--	12
	0.389	--	21
	0.187	--	25
	0.093	--	40
	0.047	--	44
2nd waterflood after gel treatment (Step 15c)	3.112	89	--
	1.556	102	--
	0.778	124	--
	0.389	151	--
	0.187	184	--
	0.093	233	--
	0.047	281	--
	0.023	359	--
	For 2nd waterflood, $F_{rrw}=117\ u^{-0.29}$; r=0.998.		

Table B-3f (continued). Residual Resistance Factors for Brine (F_{rrw}) and Soltrol-130 (F_{rro}), SSH-27 0.7% polyacrylamide (MARCIT®), 318-ppm Cr^{3+} (as acetate), 1% NaCl, pH=6.0

	Flux, ft/d	F_{rrw}	F_{rro}
2nd oilflood after gel treatment (Step 16a)	46.673	--	9
	23.337	--	9
	12.446	--	10
	6.223	--	12
	3.112	--	11
	1.556	--	11
	0.778	--	16
	0.389	--	22
	0.187	--	37
3rd waterflood after gel treatment (Step 16c)	15.558	15	--
	12.446	15	--
	6.223	18	--
	3.112	21	--
	1.556	24	--
	0.778	29	--
	0.389	41	--
	0.187	54	--
	0.093	64	--
	0.047	82	--
	0.023	182	--
	15.558	17	--
	For 3rd waterflood, $F_{rrw}=33\ u^{-0.33}$; r=0.97 (all readings).		

Table B-3f (continued). Residual Resistance Factors for Brine (F_{rrw}) and Soltrol-130 (F_{rro}), SSH-27 0.7% polyacrylamide (MARCIT®), 318-ppm Cr^{3+} (as acetate), 1% NaCl, pH=6.0

	Flux, ft/d	F_{rrw}	F_{rro}
3rd oilflood after gel treatment (Step 17a)	46.673	--	4
	23.337	--	4
	12.446	--	4
	6.223	--	5
	3.112	--	6
	1.556	--	7
	0.778	--	11
4th waterflood after gel treatment (Step 17c)	46.473	5	
	15.558	5	--
	12.446	7	--
	6.223	6	--
	3.112	7	--
	1.556	9	--
	0.778	10	--
	0.389	12	--
	0.187	15	--
	0.093	14	--
	0.047	16	--
	For 4th waterflood, $F_{rrw}=8.5\ u^{-0.18}$; r=0.98.		

Table B-3g. Residual Resistance Factors for Brine (F_{rrw}) and Soltrol-130 (F_{rro}), SSH-31 1.39% polyacrylamide (MARCIT®), 212-ppm Cr^{3+} (as acetate), 1% NaCl, pH=6.0

	Flux, ft/d	F_{rrw}	F_{rro}
1st waterflood after gel treatment (Step 13)	0.023	52954	--
1st oilflood after gel treatment (Step 15a)	9.335	--	53
	12.446	--	44
	17.144	--	36
	23.337	--	29
	12.446	--	34
	6.223	--	41
	3.112	--	49
	1.556	--	56
	0.778	--	60
	1.389	--	64
	0.187	--	61
	0.093	--	64
	0.047	--	64
	0.023	--	61
	23.337	--	29
2nd waterflood after gel treatment (Step 15c)	0.187	2200	--
	0.156	2498	--
	0.093	3212	--
	0.093	3233	--
	0.047	4508	--
	0.047	4517	--
	0.023	6375	--
	For 2nd waterflood, $F_{rrw}=972\ u^{-0.50}$; r=0.999.		

Table B-3g (continued). Residual Resistance Factors for Brine (F_{rrw}) and Soltrol-130 (F_{rro}), SSH-31 1.39% polyacrylamide (MARCIT®), 212-ppm Cr^{3+} (as acetate), 1% NaCl, pH=6.0

	Flux, ft/d	F_{rrw}	F_{rro}
2nd oilflood after gel treatment (Step 16a)	35.005	--	18
	23.337	--	19
	12.446	--	22
	6.223	--	25
	3.112	--	28
	1.556	--	30
	0.778	--	32
	0.389	--	32
	0.187	--	29
	0.093	--	28
	0.047	--	25
	0.023	--	15
	23.337	--	19
3rd waterflood after gel treatment (Step 16c)	1.167	332	--
	0.778	389	--
	0.389	520	--
	0.389	536	--
	0.389	548	--
	0.187	752	--
	0.093	1129	--
	0.093	1158	--
	0.047	1601	--
	0.047	1623	--
	0.023	2443	--
	0.778	511	--
	For 3rd waterflood, $F_{rrw}=357\ u^{-0.49}$; r=0.99.		

Table B-3g (continued). Residual Resistance Factors for Brine (F_{rrw}) and Soltrol-130 (F_{rro}), SSH-31 1.39% polyacrylamide (MARCIT®), 212-ppm Cr^{3+} (as acetate), 1% NaCl, pH=6.0

	Flux, ft/d	F_{rrw}	F_{rro}
3rd oilflood after gel treatment (Step 17a)	46.773	--	11
	23.337	--	12
	12.446	--	13
	6.223	--	15
	3.113	--	15
	1.556	--	16
	0.778	--	16
	0.389	--	16
	0.187	--	16
	0.093	--	15
	0.047	--	13
	46.673	--	11
4th waterflood after gel treatment (Step 17c)	12.446	33	--
	6.223	37	--
	3.112	49	--
	1.556	65	--
	0.778	102	--
	0.389	171	--
	0.187	238	--
	0.093	368	--
	0.047	514	--
	0.023	1260	--
	6.223	49	--
	For 4th waterflood, $F_{rrw}=105\ u^{-0.55}$; r=0.986.		

Table B-3h. Residual Resistance Factors for Brine (F_{rrw}) and Soltrol-130 (F_{rro}), SSH-32
10% colloidal silica, 0.7% NaCl, pH=8.2

	Flux, ft/d	F_{rrw}	F_{rro}
1st waterflood after gel treatment (Step 13)	0.023	3206	--
	0.047	2558	--
	0.023	2536	--
	0.093	4121	--
	0.047	4154	--
	0.023	4605	--
	0.156	2986	--
	0.140	2914	--
	0.156	1974	--
	0.187	1439	--
	0.187*	47	--
	0.093	45	--
	0.047	56	--
	0.389	39	--
	0.187	38	--
	0.093	37	--
	0.047	41	--
	0.778	34	--
	0.389	33	--
	0.187	33	--
	0.093	32	--
	0.047	32	--
	1.556	29	--

* After injected 15 pore volumes of brine (0.7% NaCl) through

Table B-3h (continued). Residual Resistance Factors for Brine (F_{rrw}) and Soltrol-130 (F_{rro}), SSH-32 10% colloidal silica, 0.7% NaCl, pH=8.2

	Flux, ft/d	F_{rrw}	F_{rro}
1st waterflood after gel treatment (Step 13)	0.778	28	--
	0.389	28	--
	0.187	27	--
	6.223	27	--
	3.112	26	--
	1.556	27	--
	0.778	26	--
	0.389	26	--
1st oilflood after gel treatment (Step 15a)	35.005	--	24
	23.337	--	23
	12.446	--	23
	6.223	--	23
	3.112	--	23
	1.556	--	23
	0.778	--	23
	0.389	--	24
	0.187	--	24
	0.093	--	24
	0.047	--	24
	23.337	--	23

Table B-3h (continued). Residual Resistance Factors for Brine (F_{rrw}) and Soltrol-130 (F_{rro}), SSH-32 10% colloidal silica, 0.7% NaCl, pH=8.2

	Flux, ft/d	F_{rrw}	F_{rro}
2nd waterflood after gel treatment (Step 15c)	23.337	14	--
	12.446	14	--
	6.223	15	--
	3.112	15	--
	1.556	15	--
	0.778	15	--
	0.389	14	--
	0.187	14	--
	0.093	14	--
	0.047	15	--
	23.337	11	--
2nd oilflood after gel treatment (Step 16a)	46.673	--	10
	23.337	--	10
	12.446	--	9
	6.223	--	9
	3.112	--	9
	1.556	--	9
	0.778	--	9
	0.389	--	9
	46.473	--	10

Table B-3h (continued). Residual Resistance Factors for Brine (F_{rrw}) and Soltrol-130 (F_{rro}), SSH-32 10% colloidal silica, 0.7% NaCl, pH=8.2

	Flux, ft/d	F_{rrw}	F_{rro}
3rd waterflood after gel treatment (Step 16c)	46.673	10	--
	23.337	9	--
	12.446	10	--
	6.223	10	--
	3.112	11	--
	1.556	13	--
	0.778	14	--
	0.389	14	--
	0.187	13	--
	46.673	10	--
3rd oilflood after gel treatment (Step 17a)	46.673	--	6
	23.337	--	6
	12.446	--	6
	6.223	--	6
	3.112	--	6
	1.556	--	6
	0.778	--	5
	0.389	--	5
	46.473	--	6

Table B-3h (continued). Residual Resistance Factors for Brine (F_{rrw}) and Soltrol-130 (F_{rro}), SSH-32 10% colloidal silica, 0.7% NaCl, pH=8.2

	Flux, ft/d	F_{rrw}	F_{rro}
4th waterflood after gel treatment (Step 17c)	46.673	7	--
	23.337	7	--
	12.446	7	--
	6.223	8	--
	3.112	8	--
	1.556	9	--
	0.778	9	--
	0.389	9	--
	0.187	8	--
	0.093	8	--
	46.673	8	--

Table B-3i. Residual Resistance Factors for Brine (F_{rrw}) and Soltrol-130 (F_{rro}), SSH-33
10% colloidal silica, 0.7% NaCl, pH=8.2

	Flux, ft/d	F_{rrw}	F_{rro}
1st waterflood after gel treatment (Step 13)	0.023	1626	--
	0.047	1200	--
	0.023	1187	--
	0.093	1808	--
	0.047	2211	--
	0.023	2548	--
	0.187	114	--
	0.093	223	--
	0.047	258	--
	0.023	550	--
	0.389	18	--
	0.187	14	--
	0.093	11	--
	0.047	12	--
	0.778	11	--
	0.389	11	--
	0.187	9	--
	0.093	7	--
	1.556	9	--
	0.778	9	--
	0.389	11	--
	0.187	7	--
	0.093	8	--

Table B-3i (continued). Residual Resistance Factors for Brine (F_{rrw}) and Soltrol-130 (F_{rro}), SSH-33 10% colloidal silica, 0.7% NaCl, pH=8.2

	Flux, ft/d	F_{rrw}	F_{rro}
1st waterflood after gel treatment (Step 13)	0.047	8	--
	3.112	8	--
	1.556	9	--
	0.778	9	--
	0.389	8	--
	0.187	8	--
	0.093	7	--
	6.223	8	--
	1.556	8	--
	0.389	8	--
	0.093	7	--
	12.446	8	--
	3.112	8	--
	0.778	9	--
	0.187	7	--
	23.337	8	--
	6.223	8	--
	1.556	8	--
	0.389	9	--
	23.337	8	--
	23.337*	8	--

* After injected 15 pore volumes of brine (0.7% NaCl) through.

Table B-3i (continued). Residual Resistance Factors for Brine (F_{rrw}) and Soltrol-130 (F_{rro}), SSH-33 10% colloidal silica, 0.7% NaCl, pH=8.2

	Flux, ft/d	F_{rrw}	F_{rro}
1st oilflood after gel treatment (Step 15a)	38.894	--	16
	23.337	--	16
	12.446	--	16
	6.223	--	17
	3.112	--	16
	1.556	--	16
	0.778	--	17
	0.389	--	17
	0.187	--	17
	0.093	--	17
	23.337	--	16
2nd waterflood after gel treatment (Step 15c)	23.337	9	--
	12.446	9	--
	6.223	10	--
	3.112	15	--
	1.556	19	--
	0.778	22	--
	0.389	19	--
	0.187	17	--
	12.446	11	--
	3.112	12	--
	0.778	12	--
	0.187	13	--
	0.093	13	--
	0.047	13	--
	23.337	10	--

Table B-3i (continued). Residual Resistance Factors for Brine (F_{rrw}) and Soltrol-130 (F_{rro}), SSH-33 10% colloidal silica, 0.7% NaCl, pH=8.2

	Flux, ft/d	F_{rrw}	F_{rro}
2nd oilflood after gel treatment (Step 16a)	46.673	--	12
	23.337	--	11
	12.446	--	11
	6.223	--	11
	3.112	--	11
	1.556	--	11
	0.778	--	12
	0.389	--	13
	0.187	--	14
	0.093	--	13
	23.337	--	12
3rd waterflood after gel treatment (Step 16c)	23.337	7	--
	12.446	7	--
	6.223	8	--
	3.112	8	--
	1.556	12	--
	0.778	15	--
	0.389	12	--
	0.187	14	--
	0.093	12	--
	0.047	12	--
	23.337	9	--

Table B-4 Summary of Relative Dispersivities from Water- and Oil-Tracer Studies

Table B-4a. Relative Dispersivities from Water-Tracer Studies,
Core SSH-15 (Oil phase: Moutray Crude, Gelant: Resorcinol-Formaldehyde)

Tracer Study	α/α_o (10/90)	α/α_o (20/50)
After 1st waterflood (Step 7)	15	18
After 2nd waterflood (Step 8)	10	16
After 3rd waterflood (Step 9)	4	4
After 4th waterflood (Step 10)	3	3

Table B-4b. Relative Dispersivities from Water-Tracer Studies,
Core SSH-17 (Oil phase: Soltrol-130, Gelant: Resorcinol-Formaldehyde)

Tracer Study	α/α_o (10/90)	α/α_o (20/50)
After 1st waterflood (Step 7)	14	35
After 2nd waterflood (Step 8)	14	32
After 3rd waterflood (Step 9)	23	64
After 4th waterflood (Step 10)	24	67
1st waterflood after gel treatment (Step 14)	48	41
2nd waterflood after gel treatment (Step 15d)	138	93

Table B-4c. Relative Dispersivities from Water-Tracer Studies,
Core SSH-22 (Oil phase: Soltrol-130, Gelant: Cr^{3+}-Xanthan)

Tracer Study	α/α_o (10/90)	α/α_o (20/50)
After 1st waterflood (Step 7)	40	69
After 2nd waterflood (Step 8)	36	61
After 3rd waterflood (Step 9)	51	81
After 4th waterflood (Step 10)	44	70
1st waterflood after gel treatment (Step 14)	91	60
2nd waterflood after gel treatment (Step 15d)	92	65
3rd waterflood after gel treatment (Step 16d)	81	62

Table B-4d. Relative Dispersivities from Water-Tracer Studies,
Core SSH-23 (Oil phase: Moutray Crude, Gelant: Cr^{3+}-Xanthan)

Tracer Study	α/α_o (10/90)	α/α_o (20/50)
After 1st waterflood (Step 7)	14	36
After 2nd waterflood (Step 8)	9	20
After 3rd waterflood (Step 9)	10	17
After 4th waterflood (Step 10)	6	9
1st waterflood after gel treatment (Step 14)	62	57
2nd waterflood after gel treatment (Step 15d)	80	84

Table B-4e. Relative Dispersivities from Water-Tracer Studies,
Core SSH-26 (Oil phase: Soltrol-130, Gelant: Cr^{3+}(Acetate)-HPAM; 1.39% HPAM, 636-ppm Cr^{3+})

Tracer Study	α/α_o (10/90)	α/α_o (20/50)
After 1st waterflood (Step 7)	25	56
After 2nd waterflood (Step 8)	18	39
After 3rd waterflood (Step 9)	20	42
After 4th waterflood (Step 10)	19	46
4th waterflood after gel treatment (Step 17d)	552	159

Table B-4f. Relative Dispersivities from Oil-Tracer Studies,
Core SSH-26 (Oil phase: Soltrol-130, Gelant: Cr^{3+}(Acetate)-HPAM; 1.39% HPAM, 636-ppm Cr^{3+})

Tracer Study	α/α_o (10/90)	α/α_o (20/50)
After 1st oilflood (Step 5)	2	2
After 2nd oilflood (Step 8)	3	2
After 3rd oilflood (Step 9)	3	2
After 4th oilflood (Step 10)	3	2
1st oilflood after gel treatment (Step 15b)	77	84
2nd oilflood after gel treatment (Step 16b)	80	83
3rd oilflood after gel treatment (Step 17b)	186	174

Table B-4g. Relative Dispersivities from Water-Tracer Studies,
Core SSH-27 (Oil phase: Soltrol-130, Gelant: Cr^{3+}(Acetate)-HPAM; 0.7% HPAM, 318-ppm Cr^{3+})

Tracer Study	α/α_o (10/90)	α/α_o (20/50)
After 1st waterflood (Step 7)	21	60
2nd waterflood after gel treatment (Step 15d)	123	90
3rd waterflood after gel treatment (Step 16d)	71	95
4th waterflood after gel treatment (Step 17d)	46	80

Table B-4h. Relative Dispersivities from Oil-Tracer Studies,
Core SSH-27 (Oil phase: Soltrol-130, Gelant: Cr^{3+}(Acetate)-HPAM; 0.7% HPAM, 318-ppm Cr^{3+})

Tracer Study	α/α_o (10/90)	α/α_o (20/50)
After 1st oilflood (Step 5)	2	2
1st oilflood after gel treatment (Step 15b)	26	21
2nd oilflood after gel treatment (Step 16b)	19	22
3rd oilflood after gel treatment (Step 17b)	7	7

Table B-4i. Relative Dispersivities from Water-Tracer Studies,
Core SSH-31 (Oil phase: Soltrol-130, Gelant: Cr^{3+}(Acetate)-HPAM; 1.39% HPAM, 212-ppm Cr^{3+})

Tracer Study	α/α_o (10/90)	α/α_o (20/50)
After 1st waterflood (Step 7)	21	51
2nd waterflood after gel treatment (Step 15d)	--	--
3rd waterflood after gel treatment (Step 16d)	483	327
4th waterflood after gel treatment (Step 17d)	299	156

Table B-4j. Relative Dispersivities from Oil-Tracer Studies,
Core SSH-31 (Oil phase: Soltrol-130, Gelant: Cr^{3+}(Acetate)-HPAM; 1.39% HPAM, 212-ppm Cr^{3+})

Tracer Study	α/α_o (10/90)	α/α_o (20/50)
After 1st oilflood (Step 5)	2	1
1st oilflood after gel treatment (Step 15b)	63	60
2nd oilflood after gel treatment (Step 16b)	38	41
3rd oilflood after gel treatment (Step 17b)	30	33

Table B-4k. Relative Dispersivities from Water-Tracer Studies,
Core SSH-32 (Oil phase: Soltrol-130, Gelant: 10% Colloidal Silica)

Tracer Study	α/α_o (10/90)	α/α_o (20/50)
After 1st waterflood (Step 7)	25	56
1st waterflood after gel treatment (Step 14)	--	570
2nd waterflood after gel treatment (Step 15d)	48	29
3rd waterflood after gel treatment (Step 16d)	51	21
4th waterflood after gel treatment (Step 17d)	37	24

Table B-4l. Relative Dispersivities from Oil-Tracer Studies,
Core SSH-32 (Oil phase: Soltrol-130, Gelant: 10% Colloidal Silica)

Tracer Study	α/α_o (10/90)	α/α_o (20/50)
After 1st oilflood (Step 5)	0.7	0.4
1st oilflood after gel treatment (Step 15b)	206	79
2nd oilflood after gel treatment (Step 16b)	14	7
3rd oilflood after gel treatment (Step 17b)	6	4

Table B-4m. Relative Dispersivities from Water-Tracer Studies,
Core SSH-33 (Oil phase: Soltrol-130, Gelant: 10% Colloidal Silica)

Tracer Study	α/α_o (10/90)	α/α_o (20/50)
After 1st waterflood (Step 7)	88	73
1st waterflood after gel treatment (Step 14)	--	1598
2nd waterflood after gel treatment (Step 15d)	--	938
3rd waterflood after gel treatment (Step 16d)	273	163

Table B-4n. Relative Dispersivities from Oil-Tracer Studies,
Core SSH-33 (Oil phase: Soltrol-130, Gelant: 10% Colloidal Silica)

Tracer Study	α/α_o (10/90)	α/α_o (20/50)
After 1st oilflood (Step 5)	1	0.9
1st oilflood after gel treatment (Step 15b)	148	123
2nd oilflood after gel treatment (Step 16b)	44	50

APPENDIX C

GAS AND WATER COREFLOOD DATA (SUPPLEMENT TO SECTION 4)

APPENDIX C

Table C-1. CO_2 and Water Residual Resistance Factors for Resorcinol-Formaldehyde Gel (formed at pH=8.3), 900 psi

Table C-1a. Resorcinol-Formaldehyde Gel
F_{rrw} Data During First Brine Injection After Gelation, 41°C, 900 psi

Superficial Velocity, ft/d	Pore Volumes of Brine Injected	F_{rrw} in the Second Core Segment	Pressure Gradient, psi/ft
0.201	0.3	26,100	775
0.100	0.7	23,000	340
0.050	1.0	22,600	167
0.100	0.9	21,000	310
0.201	0.4	20,400	604
0.393	2.9	16,000	965

Pore volumes of brine injected=6.2. Maximum pressure gradient=965 psi/ft.
Average F_{rrw}=21,600.

Table C-1b. Resorcinol-Formaldehyde Gel
F_{rrCO2} Data During First CO_2 Injection After Gelation, 41°C, 900 psi

Superficial Velocity, ft/d	Pore Volumes of CO_2 Injected	F_{rrCO2} in the Second Core Segment	Pressure Gradient, psi/ft
0.393	1.0	1100	37
0.785	0.8	580	39
0.785	4.3	287	19
3.14	2.1	168	45
6.28	1.9	123	66
15.7	1.9	105	139
6.28	2.5	68	36
3.14	2.4	76	20
1.57	2.9	103	14
0.393	1.7	154	5

Pore volumes of CO_2 injected=21.5. Maximum pressure gradient=139 psi/ft.
Average F_{rrCO2}=101 (last 5 readings).

Table C-1c. Resorcinol-Formaldehyde Gel
F_{rrw} Data During Second Brine Injection After Gelation, 41°C, 900 psi

Superficial Velocity, ft/d	Pore Volumes of Brine Injected	F_{rrw} in the Second Core Segment	Pressure Gradient, psi/ft
0.393	0.8	773	45
0.785	4.3	518	60
1.57	1.1	556	129
3.14	1.5	496	230
6.28	3.4	531	492
3.14	1.4	531	246
1.57	1.3	620	144
0.785	4.9	620	72
0.393	1.3	548	32

Pore volumes of brine injected=20. Maximum pressure gradient=492 psi/ft.
Average F_{rrw}=570 (last 5 readings).

Table C-1d. Resorcinol-Formaldehyde Gel
F_{rrCO2} Data During Second CO_2 Injection After Gelation, 41°C, 900 psi

Superficial Velocity, ft/d	Pore Volumes of CO_2 Injected	F_{rrCO2} in the Second Core Segment	Pressure Gradient, psi/ft
1.57	0.9	259	34
3.14	3.7	93	25
6.28	2.8	69	37
15.7	5.0	46	62
6.28	1.8	54	29
3.14	2.2	59	16
1.57	1.6	82	10

Pore volumes of CO_2 injected=18. Maximum pressure gradient=62 psi/ft.
Average F_{rrCO2}=60 (last 4 readings).

Table C-1e. Resorcinol-Formaldehyde Gel
F_{rrw} Data During Third Brine Injection After Gelation, 41°C, 900 psi

Superficial Velocity, ft/d	Pore Volumes of Brine Injected	F_{rrw} in the Second Core Segment	Pressure Gradient, psi/ft
1.57	1.6	416	96
3.14	1.4	372	172
6.28	1.7	381	353
15.7	1.7	377	874
6.28	2.0	416	386
3.14	1.7	405	187
1.57	1.1	404	94

Pore volumes of brine injected=11.2. Maximum pressure gradient=874 psi/ft.
Average F_{rrw}=400 (last 4 readings).

Table C-1f. Resorcinol-Formaldehyde Gel
F_{rrCO2} Data During Third CO_2 Injection After Gelation, 41°C, 900 psi

Superficial Velocity, ft/d	Pore Volumes of CO_2 Injected	F_{rrCO2} in the Second Core Segment	Pressure Gradient, psi/ft
1.57	4.7	108	14
3.14	3.9	74	20
6.28	3.2	56	30
15.7	3.3	51	68
6.28	2.0	43	23
3.14	1.8	54	14
1.57	2.2	80	11

Pore volumes of CO_2 injected=21.1. Maximum pressure gradient=68 psi/ft.
Average F_{rrCO2}=57 (last 4 readings).

Table C-1g. Resorcinol-Formaldehyde Gel
F_{rrw} Data During Fourth Brine Injection After Gelation, 41°C, 900 psi

Superficial Velocity, ft/d	Pore Volumes of Brine Injected	F_{rrw} in the Second Core Segment	Pressure Gradient, psi/ft
1.57	1.7	398	92
3.14	1.8	354	164
6.28	1.4	354	328
15.7	2.3	342	791
6.28	1.5	354	328
3.14	2.5	354	164
1.57	1.4	394	91

Pore volumes of brine injected=12.6. Maximum pressure gradient=791 psi/ft.
Average F_{rrw}=361 (last 4 readings).

Table C-2. N_2 and Water Residual Resistance Factors for Resorcinol-Formaldehyde Gel (formed at pH=9), 900 psi

Table C-2a. Resorcinol-Formaldehyde Gel
F_{rrw} Data During First Brine Injection After Gelation, 41°C, 900 psi

Superficial Velocity, ft/d	Pore Volumes of Brine Injected	F_{rrw} in the Second Core Segment	Pressure Gradient, psi/ft
0.201	2.6	11,400	754
0.100	1.0	10,700	353
0.201	2.2	9,080	601

Pore volumes of brine injected=5.8. Maximum pressure gradient=754 psi/ft.
Average F_{rrw}=10,400.

Table C-2b. Resorcinol-Formaldehyde Gel
F_{rrN2} Data During First N_2 Injection After Gelation, 41°C, 900 psi

Superficial Velocity, ft/d	Pore Volumes of N_2 Injected	F_{rrN2} in the Second Core Segment	Pressure Gradient, psi/ft
1.57	5.0	257	45
3.14	1.7	145	50
6.28	2.1	213	145
15.7	3.7	152	264
6.28	2.1	119	82
1.57	4.2	106	18

Pore volumes of N_2 injected=18.8. Maximum pressure gradient=264 psi/ft.
Average F_{rrN2}=126 (last 3 readings).

Table C-2c. Resorcinol-Formaldehyde Gel
F_{rrw} Data During Second Brine Injection After Gelation, 41°C, 900 psi

Superficial Velocity, ft/d	Pore Volumes of Brine Injected	F_{rrw} in the Second Core Segment	Pressure Gradient, psi/ft
0.201	0.3	840	56
1.57	1.2	710	370
3.14	1.5	610	634
6.28	1.6	460	950
1.57	1.1	490	253
0.393	2.6	610	79

Pore volumes of brine injected=8.3. Maximum pressure gradient=950 psi/ft.
Average F_{rrw}=520 (last 3 readings).

Table C-2d. Resorcinol-Formaldehyde Gel
F_{rrN2} Data During Second N_2 Injection After Gelation, 41°C, 900 psi

Superficial Velocity, ft/d	Pore Volumes of N_2 Injected	F_{rrN2} in the Second Core Segment	Pressure Gradient, psi/ft
3.14	3.8	152	53
6.28	3.1	76	53
15.7	2.9	62	108
31.4	4.1	53	185

Pore volumes of N_2 injected=13.9. Maximum pressure gradient=185 psi/ft.
Average F_{rrN2}=64 (last 3 readings).

Table C-2e. Resorcinol-Formaldehyde Gel
F_{rrw} Data During Third Brine Injection After Gelation, 41°C, 900 psi

Superficial Velocity, ft/d	Pore Volumes of Brine Injected	F_{rrw} in the Second Core Segment	Pressure Gradient, psi/ft
0.785	0.6	1790	462
1.57	1.1	710	370
3.14	1.6	420	438
6.28	2.1	340	697
3.14	0.8	376	389
1.57	1.5	580	301
0.785	4.6	640	165

Pore volumes of brine injected=12.3. Maximum pressure gradient=697 psi/ft.
Average F_{rrw}=484 (last 4 readings).

Table C-2f. Resorcinol-Formaldehyde Gel
F_{rrN2} Data During Third N_2 Injection After Gelation, 41°C, 900 psi

Superficial Velocity, ft/d	Pore Volumes of N_2 Injected	F_{rrN2} in the Second Core Segment	Pressure Gradient, psi/ft
3.14	3.9	76	26
6.28	3.6	43	30
15.7	1.8	29	50
31.4	2.4	24	84
15.7	5.9	65	114
6.28	2.0	94	65
3.14	2.3	61	21

Pore volumes of N_2 injected=21.9. Maximum pressure gradient=114 psi/ft.
Average F_{rrN2}=61 (last 4 readings).

Table C-2g. Resorcinol-Formaldehyde Gel
F_{rrw} Data During Fourth Brine Injection After Gelation, 41°C, 900 psi

Superficial Velocity, ft/d	Pore Volumes of Brine Injected	F_{rrw} in the Second Core Segment	Pressure Gradient, psi/ft
1.57	1.8	610	317
3.14	2.4	440	454
6.28	1.9	320	665
3.14	1.9	420	434

Pore volumes of brine injected=8.0. Maximum pressure gradient=665 psi/ft.
Average F_{rrw}=370 (last 2 readings).

Table C-3. CO_2 and Water Residual Resistance Factors for Resorcinol-Formaldehyde Gel (formed at pH=9), 1500 psi

Table C-3a. Resorcinol-Formaldehyde Gel
F_{rrw} Data During First Brine Injection After Gelation, 41°C, 1500 psi

Superficial Velocity, ft/d	Pore Volumes of Brine Injected	F_{rrw} in the Second Core Segment	Pressure Gradient, psi/ft
0.025	0.7	54,000	316
0.051	0.5	29,000	345
0.203	0.5	27,800	1319
0.101	0.7	19,500	461
0.025	0.3	11,600	68

Pore volumes of brine injected=2.7. Maximum pressure gradient=1319 psi/ft.
Average F_{rrw}=19,600 (last 3 readings).

Table C-3b. Resorcinol-Formaldehyde Gel
F_{rrCO2} Data During First CO_2 Injection After Gelation, 41°C, 1500 psi

Superficial Velocity, ft/d	Pore Volumes of CO_2 Injected	F_{rrCO2} in the Second Core Segment	Pressure Gradient, psi/ft
0.79	0.6	123	9
1.58	0.4	70	10
3.16	1.2	40	12
6.33	1.1	26	16
15.83	1.5	17	25
31.65	4.8	12	36
15.83	3.6	13	20
6.33	1.7	16	10
3.16	1.4	23	7
1.58	1.2	19	3
0.79	0.7	19	1

Pore volumes of CO_2 injected=18.2. Maximum pressure gradient=36 psi/ft.
Average F_{rrCO2}=17 (last 6 readings).

Table C-3c. Resorcinol-Formaldehyde Gel
F_{rrw} Data During Second Brine Injection After Gelation, 41°C, 1500 psi

Superficial Velocity, ft/d	Pore Volumes of Brine Injected	F_{rrw} in the Second Core Segment	Pressure Gradient, psi/ft
0.396	0.7	146	14
0.79	1.2	38	7
1.58	1.4	30	11
3.16	1.6	20	15
6.33	0.8	20	29
15.83	2.3	19	70
6.33	0.8	20	29
3.16	2.5	23	17
1.58	1.3	25	9
0.396	2.3	26	2

Pore volumes of brine injected=14.9. Maximum pressure gradient=70 psi/ft.
Average F_{rrw}=23 (last 5 readings).

Table C-3d. Resorcinol-Formaldehyde Gel
F_{rrCO2} Data During Second CO_2 Injection After Gelation, 41°C, 1500 psi

Superficial Velocity, ft/d	Pore Volumes of CO_2 Injected	F_{rrCO2} in the Second Core Segment	Pressure Gradient, psi/ft
3.16	1.2	42	12
6.33	1.6	25	15
15.83	2.1	15	22
31.65	3.0	9	28
15.83	1.8	11	17
6.33	1.0	14	8
3.16	1.5	21	6
1.58	0.7	17	3

Pore volumes of CO_2 injected=12.9. Maximum pressure gradient=28 psi/ft.
Average F_{rrCO2}=14 (last 5 readings).

Table C-3e. Resorcinol-Formaldehyde Gel
F_{rrw} Data During Third Brine Injection After Gelation, 41°C, 1500 psi

Superficial Velocity, ft/d	Pore Volumes of Brine Injected	F_{rrw} in the Second Core Segment	Pressure Gradient, psi/ft
0.79	0.7	105	19
1.58	2.3	21	8
3.16	1.0	18	13
6.33	0.7	17	24
15.83	1.5	16	58
6.33	0.6	16	23
3.16	0.5	17	13
1.58	1.3	24	9

Pore volumes of brine injected=8.6. Maximum pressure gradient=58 psi/ft.
Average F_{rrw}=18 (last 4 readings).

Table C-3f. Resorcinol-Formaldehyde Gel
F_{rrCO2} Data During Third CO_2 Injection After Gelation, 41°C, 1500 psi

Superficial Velocity, ft/d	Pore Volumes of CO_2 Injected	F_{rrCO2} in the Second Core Segment	Pressure Gradient, psi/ft
1.58	1.0	57	8
3.16	1.2	32	9
6.33	2.9	19	11
15.83	4.2	11	17
31.65	2.0	9	28
15.83	3.1	9	14
6.33	1.4	13	8
3.16	1.0	11	3
1.58	0.5	13	2

Pore volumes of CO_2 injected=17.3. Maximum pressure gradient=28 psi/ft.
Average F_{rrCO2}=11 (last 5 readings).

Table C-3g. Resorcinol-Formaldehyde Gel
F_{rrw} Data During Fourth Brine Injection After Gelation, 41°C, 1500 psi

Superficial Velocity, ft/d	Pore Volumes of Brine Injected	F_{rrw} in the Second Core Segment	Pressure Gradient, psi/ft
1.58	1.1	47	17
3.16	2.1	16	12
6.33	1.6	14	21
15.83	1.4	15	56
6.33	1.6	18	27
3.16	2.0	22	16
1.58	0.6	27	10

Pore volumes of brine injected=10.4. Maximum pressure gradient=56 psi/ft.
Average F_{rrw}=20 (last 4 readings).

Table C-4. CO_2 and Water Residual Resistance Factors for Cr^{3+}(Acetate)-Polyacrylamide Gel (formed at pH=5.9), 1500 psi

Table C-4a. Cr^{3+}(Acetate)-Polyacrylamide Gel
F_{rrw} Data During First Brine Injection After Gelation, 41°C, 1500 psi

Superficial Velocity, ft/d	Pore Volumes of Brine Injected	F_{rrw} in the Second Core Segment	Pressure Gradient, psi/ft	F_{rrw} Relation
0.396	0.4	9,440	1055	
0.203	0.7	20,000	1146	
0.101	0.5	32,800	935	$F_{rrw} = 4970\ u^{-0.72}$
0.051	0.2	48,000	691	
0.025	0.2	55,200	390	$r = 0.96$
0.101	1.1	25,600	730	
0.396	1.2	7,200	805	
1.58	0.4	960	429	
3.16	0.7	528	472	
6.33	0.9	320	572	
15.83	1.5	160	715	
6.33	1.1	212	379	
3.16	2.1	320	286	
1.58	0.7	520	232	
0.79	0.5	880	196	
0.396	3.1	1,392	156	$F_{rrw} = 780\ u^{-0.68}$
0.203	4.1	4,040	231	
0.396	0.3	1,040	116	$r = 0.975$
0.79	0.6	840	188	
1.58	0.3	536	239	
3.16	1.0	344	307	
6.33	0.8	224	400	
15.83	1.2	125	558	

Pore volumes of brine injected=23.6.
For the first 7 readings, maximum pressure gradient=1146 psi/ft, and $F_{rrw} = 4970\ u^{-0.72}$.
For the last 13 readings, $F_{rrw} = 780\ u^{-0.68}$.

Table C-4b. Cr^{3+}(Acetate)-Polyacrylamide Gel
F_{rrCO2} Data During First CO_2 Injection After Gelation, 41°C, 1500 psi

Superficial Velocity, ft/d	Pore Volumes of CO_2 Injected	F_{rrCO2} in the Second Core Segment	Pressure Gradient, psi/ft
3.16	3.7	283	118
6.33	2.7	175	146
15.83	3.3	110	229
6.33	2.3	197	96
3.16	1.6	137	57

Pore volumes of CO_2 injected=13.6. Maximum pressure gradient=229 psi/ft.
Average F_{rrCO2}=148 (last 3 readings).

Table C-4c. Cr^{3+}(Acetate)-Polyacrylamide Gel
F_{rrw} Data During Second Brine Injection After Gelation, 41°C, 1500 psi

Superficial Velocity, ft/d	Pore Volumes of Brine Injected	F_{rrw} in the Second Core Segment	Pressure Gradient, psi/ft	F_{rrw} Relation
1.58 0.396 1.58	0.2 0.4 1.0	640 1,680 520	286 188 232	$F_{rrw} = 821\ u^{-0.77}$ r = 0.986
3.16	1.4	240	214	
6.33	1.2	188	336	
15.83 6.33 1.58	2.4 1.5 2.4	115 176 344	514 315 154	$F_{rrw} = 427\ u^{-0.48}$ r = 0.999

Pore volumes of brine injected=10.5. Maximum pressure gradient=514 psi/ft.
$F_{rrw} = 427\ u^{-0.48}$ (last 3 readings).

Table C-4d. Cr^{3+}(Acetate)-Polyacrylamide Gel
F_{rrCO2} Data During Second CO_2 Injection After Gelation, 41°C, 1500 psi

Superficial Velocity, ft/d	Pore Volumes of CO_2 Injected	F_{rrCO2} in the Second Core Segment	Pressure Gradient, psi/ft
1.58	1.3	343	71
3.16	1.3	197	82
6.33	1.3	125	104
15.83	5.1	60	125
6.33	1.2	70	59
3.16	1.9	57	24
1.58	0.6	69	14

Pore volumes of CO_2 injected=12.7. Maximum pressure gradient=125 psi/ft.
Average F_{rrCO2}=64 (last 4 readings).

Table C-4e. Cr^{3+}(Acetate)-Polyacrylamide Gel
F_{rrw} Data During Third Brine Injection After Gelation, 41°C, 1500 psi

Superficial Velocity, ft/d	Pore Volumes of Brine Injected	F_{rrw} in the Second Core Segment	Pressure Gradient, psi/ft	F_{rrw} Relation
1.58	1.0	240	107	
3.16	1.0	100	89	
6.33	4.7	80	143	
15.83	2.7	56	250	$F_{rrw} = 177\ u^{-0.43}$
6.33	1.5	74	132	
3.16	0.7	104	93	$r = 0.991$
1.58	0.3	152	68	

Pore volumes of brine injected=11.9. Maximum pressure gradient=250 psi/ft.
$F_{rrw} = 177\ u^{-0.43}$ (last 4 readings).

Table C-4f. Cr^{3+}(Acetate)-Polyacrylamide Gel
F_{rrCO2} Data During Third CO_2 Injection After Gelation, 41°C, 1500 psi

Superficial Velocity, ft/d	Pore Volumes of CO_2 Injected	F_{rrCO2} in the Second Core Segment	Pressure Gradient, psi/ft
1.58	1.4	137	29
3.16	1.5	77	32
6.33	1.5	51	43
15.83	2.1	34	71
6.33	1.6	33	27
3.16	1.8	34	14
1.58	0.7	34	7

Pore volumes of CO_2 injected=10.6. Maximum pressure gradient=71 psi/ft.
Average F_{rrCO2}=34 (last 4 readings).

Table C-4g. Cr^{3+}(Acetate)-Polyacrylamide Gel
F_{rrw} Data During Fourth Brine Injection After Gelation, 41°C, 1500 psi

Superficial Velocity, ft/d	Pore Volumes of Brine Injected	F_{rrw} in the Second Core Segment	Pressure Gradient, psi/ft	F_{rrw} Relation
1.58	1.0	212	95	
3.16	1.2	56	57	
6.33	1.4	40	71	
15.83	2.0	29	129	$F_{rrw} = 93.7\ u^{-0.43}$
6.33	4.4	42	74	
3.16	2.0	54	49	$r = 0.996$
1.58	0.5	80	36	

Pore volumes of brine injected=12.5. Maximum pressure gradient=129 psi/ft.
$F_{rrw} = 94\ u^{-0.43}$ (last 4 readings).

*U.S.GPO:1992-661-026/60044